Distribution Agreement

In presenting this thesis or dissertation as a partial fulfillment of the requirements for an advanced degree from Emory University, I hereby grant to Emory University and its agents the non-exclusive license to archive, make accessible, and display my thesis or dissertation in whole or in part in all forms of media, now or hereafter known, including display on the world wide web. I understand that I may select some access restrictions as part of the online submission of this thesis or dissertation. I retain all ownership rights to the copyright of the thesis or dissertation. I also retain the right to use in future works (such as articles or books) all or part of this thesis or dissertation.

Signature:

_____ _____

Yuxin Duan Date

Ultrasensitive Tension Sensors with Catalytic Amplification Reactions: From Fundamental Development to Clinical Applications

By

Yuxin Duan

Doctor of Philosophy

Chemistry

Khalid Salaita

Advisor

Yonggang Ke

Co-Advisor

Vincent Conticello

Committee Member

Accepted:

Kimberly Jacob Arriola, Ph.D, MPH

Dean of the James T. Laney School of Graduate Studies

Date

Ultrasensitive Tension Sensors with Catalytic Amplification Reactions: From Fundamental Development to Clinical Applications

By

Yuxin Duan

B.S., Peking University, 2017

Advisor: Khalid Salaita, Ph.D.; Yonggang Ke, Ph.D.

An abstract of
A dissertation submitted to the Faculty of the
James T. Laney School of Graduate Studies of Emory University
in partial fulfillment of the requirements for the degree of
Doctor of Philosophy
in Chemistry
2022

Abstract

Ultrasensitive Tension Sensors with Catalytic Amplification Reactions: From Fundamental Development to Clinical Applications

By

Yuxin Duan

Cells transmit piconewton forces to their receptors to mediate essential biological processes such as coagulation and immune recognition. A major challenge is that cell-generated forces are infrequent, transient, and difficult to detect. In this dissertation, we introduce the development and application of ultrasensitive tension sensors using a number of mechanically triggered catalytic amplification reactions. These ultrasensitive tension sensors and assays, once optimized, allow one to detect cell forces without the need for microscopy instrumentation. Chapter 1 of this dissertation introduces the current state of mechanobiology, as well as methods to detect cellular forces and catalytic amplification reactions. Chapter 2 describes the development and application of the mechanically triggered hybridization chain reaction (mechano-HCR). Building on the work, Chapter 3 summarizes the mechano-Cas12a assisted tension sensor which offers greater amplification and hence improves sensitivity compared to mechano-HCR. We show that both of these catalytic amplification assays provide tools to detect receptor mediated forces generated by fibroblasts, platelets, and T cells in a high-throughput manner. We further show that cellular forces may be used as a diagnostic marker for predicting post-surgery bleeding risk and for personalized tailoring of anti-coagulant drugs. Finally, Chapter 5 summarizes the work in this dissertation and discusses its future outlook.

Ultrasensitive Tension Sensors with Catalytic Amplification Reactions: From Fundamental Development to Clinical Applications

By

Yuxin Duan

B.S., Peking University, 2017

Advisor: Khalid Salaita, Ph.D.; Yonggang Ke, Ph.D.

A dissertation submitted to the Faculty of the
James T. Laney School of Graduate Studies of Emory University
in partial fulfillment of the requirements for the degree of
Doctor of Philosophy
in Chemistry
2022

Acknowledgements

I've always dreamt of becoming a scientist. None-of this wonderful dream could ever be slightly realized without the support and love from my family, friends, and mentors.

First, I'd like to thank my amazing advisors Dr. Khalid Salaita and Dr. Yonggang Ke for their invalueable gudiances and supports. I'm trully lucky to be able to work with both of them during my PhD. In the past five years, they've transformed me from an naïve undergraduate into a sophisticated researcher. Khalid's innovative way of thinking and his passionate for science has inspired me to design and conquer my research project. His cretique in the first two years have also motivated me to become a better scientist. Yonggang has been a great support in getting through the difficult time of the research and finding critical ways to dig deeper in my research. They not only support me on my research but has been always supportive on my life as an international student. I would not have made this progress without them. I also thank my committee members, Dr. Vincent Conticello who has provided me precious advice and motivate me to think more about my research.

I would also like to thank the current members and alumnis of the Salaita lab and Ke lab for their support and kindness over the past few years. You've made this challenging and sometimes frustrating journey colorful and fun. (Kim, Jing, Victor Ma, Jessica, Josh, Han, Roxy, Aaron, Jiahui, Rong, Alisina, Dale, Brendan, and Yixiao, Anna, Allison, Hiroaki, Alex, Rachel, Aysha, Arventh, Radhika, Yuesong, Selma, Thea, Steven, Sarah, Yusha, Shuhong, Tharindu, Jhordan, Krista, Joseph, Hus, Luna, Tianyi, Pengfei, Dongfang, Luyao, Shuang, Kun, Travis, Victor Pan, Yunlong, Qinyi) I thank Joshua Brockman and Travis Meyer for their mentorship at the beginging of my PhD years. You brought me intor the world of DNA tension probes and DNA origami. I thank Hanquan who is so kind to me and has always been a great collaborator. I thank

Yuesong who has been not only a great help to my research but also an amazing roommate. I thank Roxy, Alisina, Hiroaki, Rachel, Aysha for your amazing collaboration and insights on research. I thank Selma for her great support, discussion and friendship. I'd also like to thank my other friends Bo, Yunlong, Zhiyao who has been my friends since graduate school and accompany me travelling through not only the PhD but also many places in US. I also thank Qinyi, Sa, Xinlin for the party and karaoke we've gone to.

I would like to thank my wonderful collaborators outside the lab. I thank Dr. Roman Sniecinski and Fania Szlam for their priceless help and great discussion in my MCATS study. I thank Dr. Renhao Li, Dr. Wenchun Chen and Dr. Brian Petrich for providing insightful advice on platelets. I also appreciate Dr. Dr. Josh Hihath, Dr. Liwei Hui, Dr. Haitao Liu for their collaborations.

Finally, I would like to give my thanks to my family. I thank my mom and dad who has provided me everything and loved me so much. I thank them for supporting me under any situation. I thank my sister for all the support and love. I won't be who I am without them. They own this degree as well.

Table of Content

Table of Figures

List of Tables

List of Abbreviations

Abbreviation	Full Name
pN	piconewton
ECM	extracellular matrix
TM	transmembrane
RGD	peptide arginine-glycine-aspartic acid
FA	focal adhesions
VWF	Willebrand Factor
BC	bent closed
EC	extended closed
EO	extended open
GT	Glanzmann's thrombasthenia
CPB	cardiopulmonary bypass
CAD	coronary artery disease
HIT	heparin induced thrombocytopenia
SRA	serotonin release assay
AFM	Atomic force microscopy

WLC	worm-like-chain
GFP	green fluorescent protein
TGT	tension gauge tether
SLB	supported lipid bilayers
MFM	molecular force microscopy
DNA-PAINT	DNA-Points Accumulation for Imaging in Nanoscale Topography
MTFM	molecular tension fluorescence microscopy
ELISA	enzyme-linked immunoassay
PCR	polymerase chain reaction
RCA	rolling circle amplification
RICM	reflection interference contrast microscopy
TIRF	total internal reflection fluorescence
MCR	mechanically induced catalytic amplification reaction
FISH	fluorescence in situ hybridization
HCR	hybridization chain reaction

HPLC	high-performance liquid chromatography
SPR	surface plasmon resonance
SERS	surface-enhanced Raman scattering
CRISPR	clustered regularly interspaced short palindromic repeats
Cas	CRISPR-associated proteins
Cpf1	CRISPR-Cas12a
gRNA	guide RNA
crRNA	CRISPR RNA
AIOD-CRISPR	all-in-one dual CRISPR–Cas12a
CaT-SMelor	CRISPR–Cas12a-mediated and aTF-mediated small molecule detector
aTF	transcription factors
LOD	limit of detection
MCATS	Mechano-Cas12a Assisted Tension Sensor
Mechano-HCR	mechanically triggered hybridization chain reaction

I	initiator
H1	hairpin 1
H2	hairpin 2
IC_{50}	half maximal inhibitory concentration
RT	room temperature
SRRF	super-resolution radial fluctuations
MLC	Myosin light chain
COX	cyclooxygenase
S/N	Signal to noise ratio
FRET	Fluorescence Resonance Energy Transfer
PGE-1	prostaglandin E1
MEF	Mouse embryonic fibroblasts
SUB	Small unilamellar vesicles
cRGDfk	cyclo-Arg-Gly-Asp-Phe-Lys
BHQ2	Black hole quencher 2
GP	glycoprotein
TEG	thromboelastography
PFA	Platelet Function Analyzer

NA	numerical aperture
DMEM	Dulbecco's Modified Eagle Medium
Ex	excitation
Em	emission
S.E.M.	Standard error of the mean
S.D.	Standard deviation
LatB	Latrunculin B
APC	antigen-presenting cells
pMHC	peptide-bound major histocompatibility complexes
RT-MCATS	reversible tension probe MCATS
APTES	(3-Aminopropyl) triethoxysilane
ADP	Adenosine 5‘-diphosphate

Chapter 1. Introduction of Mechanotransduction, Receptor Force Detection Methods and Catalytic Amplification Reactions.

Partially adapted from Duan, Y.; Glazier, R.; Bazrafshan, A.; Hu, Y.; Rashid, A; Petrich, B; Ke, Y; Salaita, K Mechanically-triggered Hybridization Chain Reaction. *Angew. Chemie.,* **2021** 60(36):19974-81 DOI:10.1002/anie.202107660 Adapted with permission.

1.1 Introduction of Mechanobiology and Receptor Mediated Forces

Cells dynamically generate mechanical forces through the polymerization/depolymerization of their cytoskeletal proteins and the activity of motor proteins. These forces are transmitted across the plasma membrane receptors, such as the integrin adhesion receptors, to mediate processes including cell migration, immune recognition, and coagulation (**Figure 1.1**).[1-5] Interestingly, adhesion receptors not only transmit forces, but also detect the magnitude of tension corresponding to the physical cues presented by other cells and the extracellular matrix.[6] Such forces are highly transient, sparse, and relatively weak at the piconewton (pN) scale, and for reference, ~ 7 pN applied over a distance of 1 nm is approximately 1 kcal/mol, which is diminishingly small and difficult to detect and investigate. Not only is measuring such force of fundamental importance to understanding mechanisms of mechanotransduction, mechanics has also been shown as a diagnostic marker of cell state in a variety of pathologies.[7-9] For example, Sniadecki and colleagues found that the magnitude of traction forces generated by platelets from patients suffering from trauma was predictive of bleeding risk.[7] Diminished platelet contractile forces are also reported by Lam and colleagues in patients suffering from chronic bleeding symptoms.[8] Thus, the development of molecular technologies to detect the pN forces transmitted by adhesion receptors can provide robust tools for clinical assays. In this chapter, we aim to introduce cell receptor mediated forces, more specifically, the force exerted by integrin receptors and their ligand. In addition, we will introduce the tools that have been developed to study receptor forces. Next, we will discuss the use of catalytic amplification reactions in assays that have historically been used to transform modern biology. Last, we will briefly discuss the aim and scope of this dissertation.

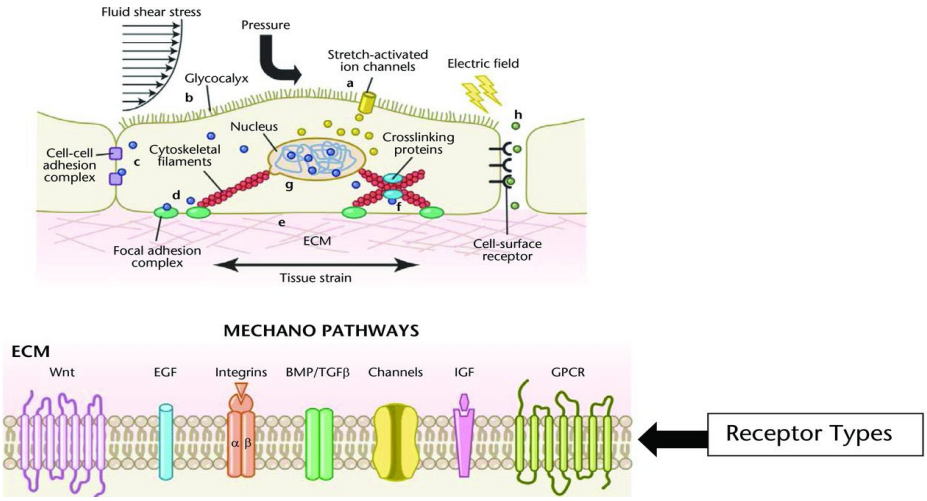

Figure 1.1: Examples of mechanotransduction affecting various biological processes. Reprinted from Ref. 5 with permission of the publisher.

1.2 Mechanotransduction Mediated by Integrin Receptors

1.2.1 General background of integrin mediated mechanotransduction

Integrins are a type of transmembrane protein that are required for cell adhesion by binding and responding to the extracellular matrix (ECM). They are heterodimers that consist of an alpha and a beta subunit. Each subunit consists of an extracellular domain, a single-pass transmembrane (TM) domain, and a cytoplasmic tail of approximately 20~70 amino acids. In humans, integrins are comprised of 9 types of β subunits and 24 types of α subunits.[10] Even though integrins are highly diverse, at least 8 integrins bind to fibronectin. And one ligand that integrins can generally recognize is the short peptide arginine-glycine-aspartic acid (RGD) motif, which is found in ECM proteins such as fibronectin and fibrinogen. Integrins display multiple conformations with different affinity to the ligand. These receptors constantly change conformation upon binding to the ligand.

Integrins, however, not only bind to their ligands on ECM proteins but also actively signal. The integrin signal can be initiated either by "inside out" – when cellular proteins binding on the intercellular part of integrins (cytoplasmic tail) or "outside in" when ECM ligands binding to extracellular part of integrins (ectodomains). When activated and bound to its ligand, integrins experience conformational change and are extended. The activated integrins then cluster and recruit multiple proteins such as talin, vinculin and paxillin to form focal adhesions (FA). Cell utilizes these FAs that transmit forces at the level of piconewtons (pN) to sense their environment and activate pathways such as phosphorylation of myosin light chain which can further stabilize the FAs (**Figure 1.2**).[11] The FAs can then support actin stress fiber formation and further trigger signaling pathways. Then, cells hydrolyze ATP for actin filament cross-linking and myosin motor activity and apply forces to surroundings through integrins. Therefore, integrins play an essential role in mechanotransduction in various cell types and mediate multiple processes such as cell adhesion, and coagulation.

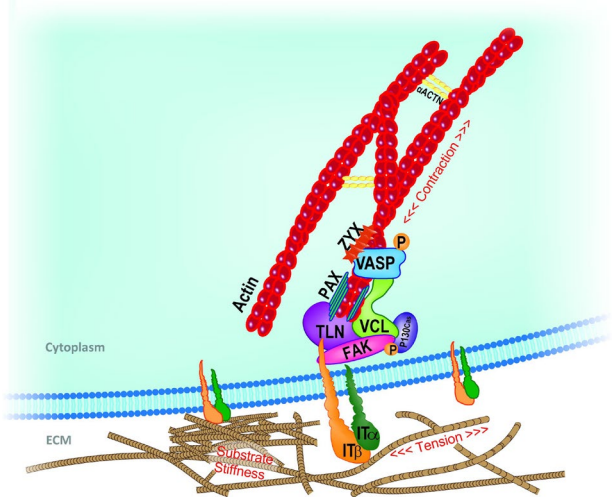

Figure 1.2. Representation of integrin-mediated mechanotransduction at focal adhesions (FA). Reprinted from Ref. 11 with permission of the publisher. ACTN, actinin; FAK, focal adhesion kinase; IT, integrin; PAX, paxillin; TLN, talin; VASP, vasodilator-stimulated phosphoprotein; VCL, vinculin; ZYX**,** zyxin**.**

1.2.2 Platelet integrins and integrin tension in platelet function

Platelets are anucleated blood cells derived from megakaryocyte that participate in many fundamental physiological and pathological processes—such as coagulation, immune response, and cancer metastasis.[12] As a central part of the hemostatic system, platelets form the initial plug to stop the bleeding when an injury occurs in a vessel. Two subgroups of integrins (β1 and β3) with five total integrins are presented in platelets. Among them, three β1 integrins (α2β1, α5β1, and α6β1) aid platelet adhesion to the extracellular matrix proteins collagen[13], fibronectin[14], and laminin[15], respectively. Two β3 integrins (αvβ3 and αIIbβ3) exist on platelets. However, different from fibroblasts, the density of integrin αvβ3 on platelets is very low and its function in platelets is poorly understood.[16, 17] On the contrary, αIIbβ3, also known as the glycoprotein IIbβ3a (CD41/CD61), is the dominant integrin on platelets and is essential for platelet function. Integrin αIIbβ3a can bind to RGD ligands containing protein such as fibrinogen, fibrin, von Willebrand factor (vWF), and fibronectin. Platelets contract through GPIIbβ3a-fibronogin interactions which provides strength and stability to platelet aggregates against shear flow and during consolidation of fibrin-rich blood clots.

Platelet function in coagulation can be divided into three sequential parts: adhesion, activation, and aggregation.[18] Bio-mechanical components play important roles in all the steps.[19] One vital element of platelet adhesion is the transient binding of GPIb to von Willebrand Factor (VWF). GPIb has been regarded as a blood flow sensor as forces transmit through VWF-GP1b would trigger platelet activation cascades (Ca^{2+} influx, P selectin enhanced expression and filopodia formation). Then reinforcement of stable platelet adhesion and platelets aggregation is mediated by the interaction of the integrin GP IIb/IIIa, with fibrinogen and VWF. Integrin αIIbβ3a has three

conformations: bent closed (BC), extended closed (EC) and extended open (EO). (**Figure 1.3**) BC conformed GP αIIbβ3a has low affinity against fibrinogen and the activation cascades would switch BC into EC conformation and allow engagement to its ligand. Finally, the biomechanical signal would trigger mechanical signaling and the maturation of αIIbβ3a, leading to platelet aggregation. [19, 20]

Because of the importance of platelet function in coagulation, impaired platelet function reduces the efficacy of blood clots and can result in profound coagulopathy. For example,

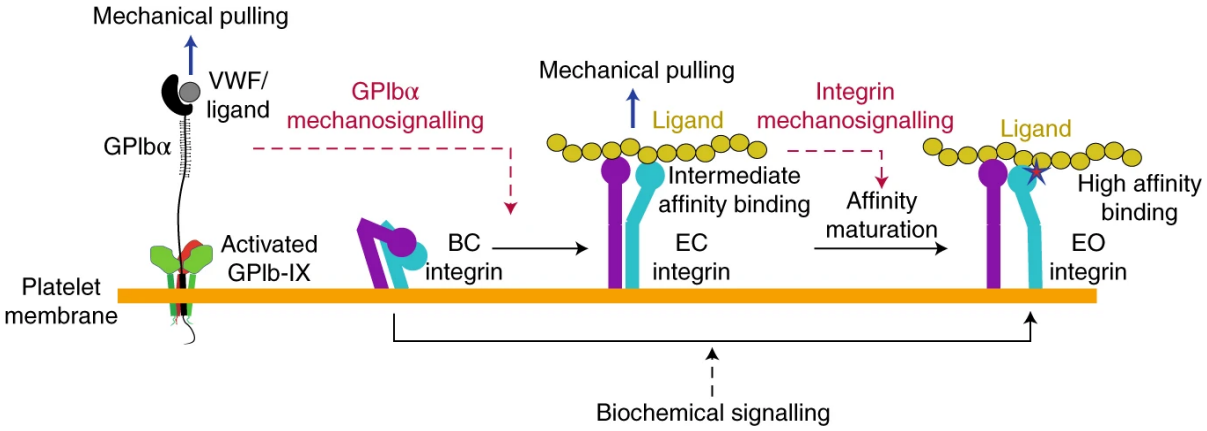

Figure 1.3. Schematic representation of the platelet mechanosensing process. Reprinted from Ref. 19 with permission of the publisher. Integrin αIIBβ3, α (purple) and β (turquoise) subunit, exhibits BC, EC and EO conformation at different stage of platelets activation.

Glanzmann's thrombasthenia (GT) is a rare bleeding disorder that arises from disrupted GP αIIbβ3a synthesis and function.[21] This disruption will impair platelet function, including adhesion, activation, and aggregation. Conversely, inappropriate platelet activity can result in thrombus formation where it is not needed. This impedes normal blood flow, resulting in complications such as stroke, and myocardial infarction. Considering the close relationship between platelet traction and its functionality, monitoring platelet function through platelet force is therefore of great interest to clinicians in both the treatment of bleeding and prevention of pathological clotting. Two

major past studies using micropillar arrays to detect platelet forces have shown that platelet forces can be used to detect underlying genetic clotting disorders such as Wisckott Aldrich Syndrome, and May Hegglin Disorder, and for detecting trauma-induced coagulopathy for patients that required an emergency room visit (Figure 1.4). [7, 8, 22] An area that could specifically benefit from a more accurate platelet function test is guiding the transfusion of platelets in bleeding patients, particularly these undergoing cardiac surgery with cardiopulmonary bypass (CPB). Unfortunately, preoperative platelet aggregometry has been shown to have a low positive predictive value for platelet transfusions in cardiac surgical patients (44%).[23] A recent meta-analysis of viscoelastic testing in cardiac surgery concluded that it was not associated with a reduction in the exposure to blood products.[24] Better identification of platelet dysfunction, independent of platelet count, may help clinicians identify patients that could benefit from medications, such as desmopressin, and prevent unnecessary platelet transfusions.

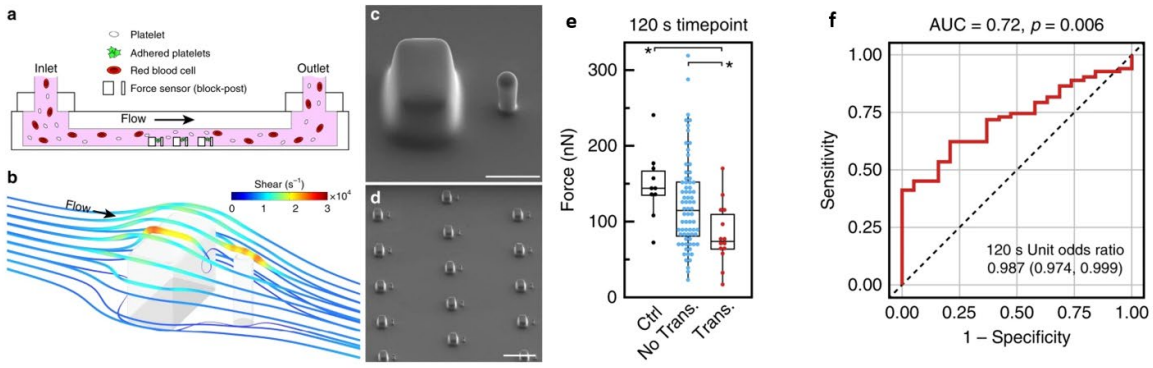

Figure 1.4. Schematic, model and SEM images showing a using micropillar arrays to detect platelet forces. (a-d) Schematic, model and SEM images of a micropillar array to detect platelet forces. (e-f) Platelets forces decreased significantly after trauma and can be used to predict blood transfusion need. Reprinted from Ref. 8 with permission of the publisher.

Another interesting area is the risk stratification of patients on antiplatelet medications. Platelet function testing for guiding antiplatelet medication currently suffers from a similar lack of

sensitivity. Ideally, patients with coronary artery disease (CAD) could have their agent or dose tailored to their level of medication responsiveness to balance the risks of bleeding and thrombosis. Unfortunately, several large clinical trials have failed to show benefit in using platelet aggregometry for this purpose.[25, 26] High-throughput measurements of platelet forces with high sensitivity may provide the method to identify patients with diverse responses to antiplatelets medication and improve the benefit/risk for patients.

Measuring platelet forces is particularly important in the diagnosis of platelet function-related diseases such as heparin induced thrombocytopenia (HIT). Although HIT is relatively rare, there are consistently about 20,000 cases annually in the United States with about a 10% overall mortality rate.[27] Because of the severity of the disease, testing for HIT is frequent among hospitalized patients. However, the testing of HIT is also difficult, requiring a screening test to detect HIT antibodies which is then often followed by a serotonin release assay (SRA) for confirmation. The SRA test involves radioactive agents and typically requires several days to perform, forcing clinicians to place patients on alternate anticoagulants with increased bleeding risk while waiting for results. Therefore, a rapid and robust platelets function based on platelet forces test may open the door for better HIT diagnostics.

1.3 Methods in Cellular Force Detection

Historically, traction force microscopy, micropillar arrays and AFM are typically used in biological research to measure the forces exerted by cells.(**Figure 1.5**)[28, 29] AFM is very sensitive but highly serial – measuring forces applied by single receptors, one at a time. In contrast, traction force microscopy and micropillar arrays allows for whole cell imaging of forces, but the techniques can only detect forces with nN force resolution and hence low magnitudes of forces or forces transmitted by a low copy number of receptors are difficult to measure.[30] To address this gap in capabilities, researchers have developed molecular based tension probes beginning with a genetically encoded tenson sensor. [31] In this sensor, cellular forces would separate a fluorescent protein FRET pair (mTFP1 and Venus) that was linked to vinculin. Next, Salaita lab and others developed DNA based tension sensors which offer the pN sensitivity of single molecule force spectroscopy methods with the throughput of traction force microscopy; and thus allowing researchers to map and quantify cell forces with molecular resolution.[32] Moreover, DNA offers unique advantages when used as molecular force probes. For example, DNA based tension probes

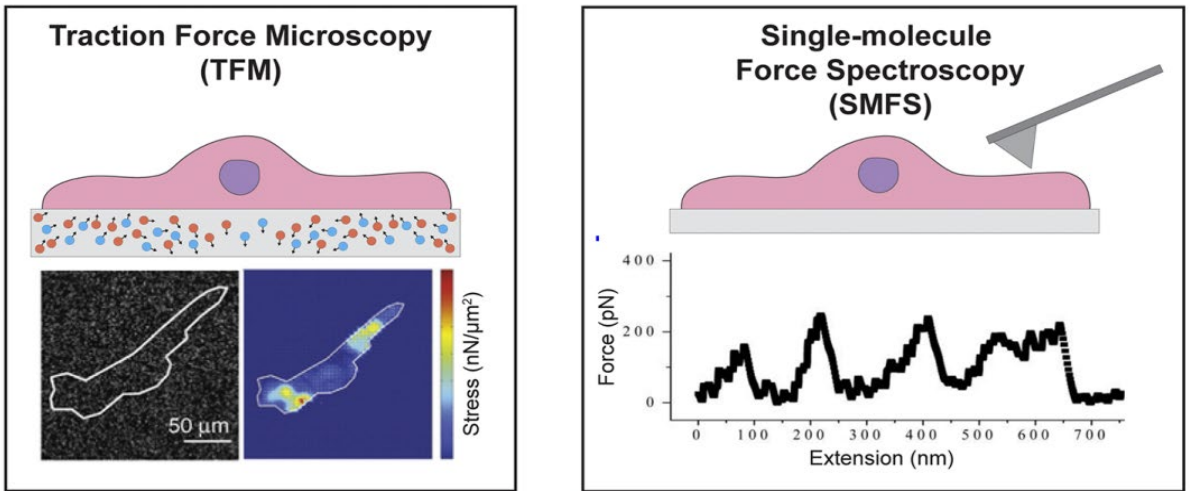

Figure 1.5. Schematic of traction force microscopy and single-molecule force spectroscopy. Reprinted from Ref. 30 with permission of the publisher.

are highly tunable because of Watson-Crick base paring principle and can withstand multiple force threshold for different purposes. Second, the development of bioconjugation chemistry enables labelling of DNA with a diverse of target molecules including ligands and fluorophores. Third, the development of DNA nanotechnology allows unprecedented complexity when using the DNA tension probes for diverse purposes.

1.3.1 DNA based tension probes

DNA as the main material that carries our genetic information, is promising to be used as tools for biophysical studies. Other than the advantages we've discussed previously, it has been extensively studied of its properties under mechanical forces. Because DNA is an elastic polymer, its behavior under forces is typically described using a worm-like-chain (WLC) model. The characterization of DNA with optical tweezer, AFM, magnetic tweezers build the foundation to use DNA as a molecular tension probe. Based on the mechanical properties of DNA molecules, DNA-based force probes have been developed to study the forces mediated by cellular receptors. There are mainly two types of DNA tension probes – reversible DNA probes and irreversible DNA probes that are based on DNA hairpin and DNA duplex structures, respectively.

1.3.1.1 Reversible DNA tension probes

In the reversible DNA tension probe design, DNA hairpin is flanked by a dye-quencher pair and labeled with a ligand that binds to targeted receptors and a functional group for surface immobilization. (**Figure 1.6**) Once the receptor forces are applied on the DNA hairpin probes and the force is greater than the $F_{1/2}$ (force threshold) of the DNA hairpin probes, mechanical melting will occur, producing up to 100-fold enhancement of the fluorescent signal. By varying the hairpin sequence and different length of stem regions of the hairpin, our lab has produced a small library

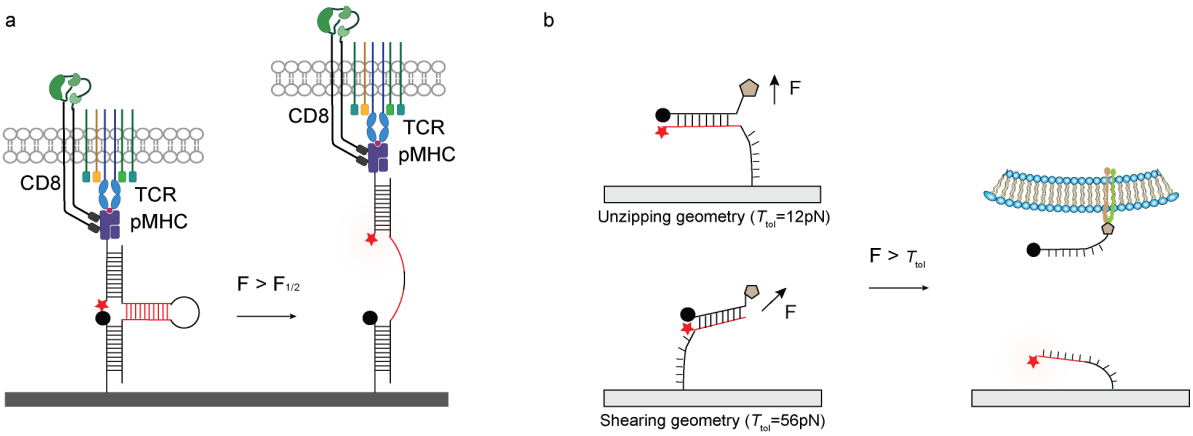

Figure 1.6. Schematic of reversible DNA probes and irreversible DNA probes in unzipping and shearing geometry. (a) Reversible tension probes. (b) irreversible tension probe in unzipping and shearing geometry

of DNA hairpin tension probes that have $F_{1/2}$ ranging from 2.1 pN to 19pN. [32] Because of their exceptional temporal resolution and low force threshold, reversible DNA tension probes have been used to study a variety of mechanotransduction pathways, ranging from T cell[33] and B cell antigen recognition[34] to cell adhesion[32] and platelet activation.[35, 36] However, one limitation of the reversible hairpin probes is that it is not suitable for receptors that exert stronger forces.

1.3.1.2 Irreversible DNA tension probes

Irreversible DNA tension probes typically consist of a DNA duplex structure. Wang and Ha first reported modulating of the tension mediated by receptor-ligand binding with tension gauge tether (TGT).[37] TGTs can be designed with two geometries - unzipping and shearing with different tension tolerance T_{tol} (depending on the positioning of the anchor and ligand on the same or different end of DNA) (**Figure 1.6b**). The T_{tol} is defined as the amount of force that leads to rupture of a DNA duplex within 2 sec. Based on previous literature [37-40], the rupture force of different TGTs can be estimated using the following equation:

$$F = 2f_c \left[\chi^{-1} \tanh\left(\chi \frac{L}{2}\right) + 1\right]$$

where f_c is the rupture force for a single bond (f_c = 3.9 pN), L is the number of DNA base pairs between the two anchor points, and χ^{-1} represents the finite length where the force is distributed (χ^{-1}= 6.8).[38]

Compared to reversible DNA probes, TGTs can detect a bigger range of force. However, TGTs are typically ruptured after the mechanical event, making it an irreversible probe that record tension history. To counteract this, Salaita lab introduced a reversible TGT by hybridizing a DNA duplex probe on a single-stranded strand that is anchored to the surface. (**Figure 1.7**) By employing irreversible tension probes, researchers have uncovered integrin receptor forces are essential for cardiomyocyte maturation and platelets activation.[35, 41]

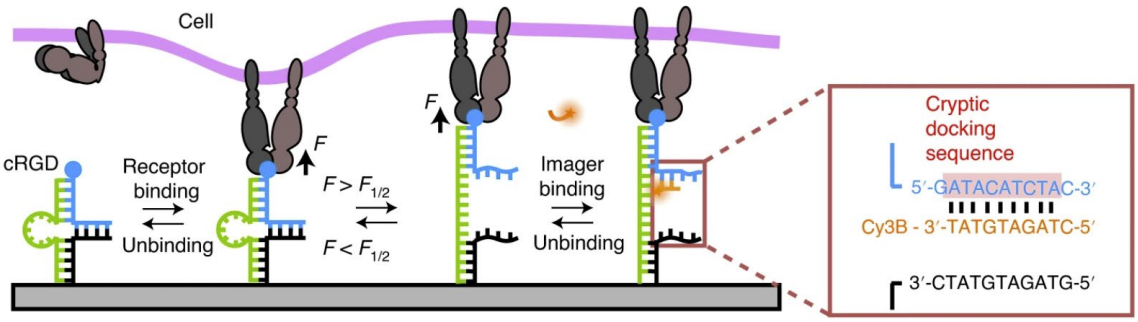

Figure 1.7. Schematic of a reversible TGT probe used in tension-PAINT This probe composed of a ligand (blue) and an anchor (black) strand held together using a loop strand (green) and increase the resolution of tension detection to nm level. Reprinted from Ref. 45 with permission of the publisher.

1.3.1.3 Other Development and Limitations of the DNA Tension Probes

Based on the DNA tension probe design described above, more developments have taken place. For example, DNA origami structures with multiple reversible DNA probes were developed to study the relationship between the receptor forces and receptor clustering.[42] DNA tension probes were also designed to be used with supported lipid bilayers (SLB) to mimic the receptor forces on cell membrane.[43] Further development was made by anchor DNA tension probe on cell membrane with cholesterol to study the forces at the cell-cell junction. Later, molecular force microscopy (MFM) was invented by coupling fluorescence polarization microscopy with DNA hairpin probes to study the orientation of receptor forces.[6] MFM successfully reported that lateral forces is involved during platelets activation. Other developments such as employing PNA to increase DNA probe stability show promise in study cancer cell mechanics.[44] By combining DNA-Points

Accumulation for Imaging in Nanoscale Topography (DNA-PAINT) with DNA tension probes, researchers push the spatial resolution of DNA tension probes to tens nm level.[45] (**Figure 1.7**)

Even with many advances in DNA tension probe, there is still one major limitation of DNA tension probes - the quantification of DNA tension probe signal requires high-end microscopes equipped with high NA objectives and single photon counting EMCCDs. This is because the receptor-mediated forces are highly transient (~msec to 10's of sec), weak (~pN), and fairly rare events (compared to ligand-receptor binding). The density of mechanical events is typically ~100 events/μm^2.[33, 46] Given the size of a typical mammalian cell of 100's of μm^2, at best each cell can generate a fluorescence signal corresponding to ~10^3-10^4 fluorophores, which is difficult to quantify. Therefore, the instrumentation requirement hinders the widespread adoption of molecular tension probes to the broad cell biology and clinical chemistry community. In this dissertation, we will describe the methods we developed to solve this challenge.

1.4 Catalytic Amplification Reactions

Limited signal in bioanalytical chemistry is typically addressed by using enzymes such as horseradish peroxidase[47], DNA polymerases to amplify the signal in assays such as ELISA and PCR.[48, 49] These types of catalytic amplification assays have transformed modern biology and are the cornerstone of the vast majority of clinical diagnostics. Developing amplification reactions that can boost the tension probe signal generated by receptor forces is therefore highly desirable for mechanobiology and may open the door toward new areas, such as "mechanopharmacology" and "mechanodiagnostics" that can be personalized using primary cells derived from patients.

In the past, researchers have tried to combine amplification reactions with DNA tension probes to overcome this challenge. Ma et al. combines rolling circle amplification (RCA) with irreversible tension probes to create mechanically induced catalytic amplification reaction (MCR) that can amplify the receptor mediated tension signal and test the activity of mechanomodulatory drug and integrin antibodies.[50] (**Figure 1.8**) However, because the enzyme being used in the reaction is not compatible with cell cultural medium, MCR can't be applied to live cell experiments. Also, the fast quantification of the tension signal requires FISH and dehybridization of fluorescent strand from surface which not only increased reaction time but also lead to error during the procedures.

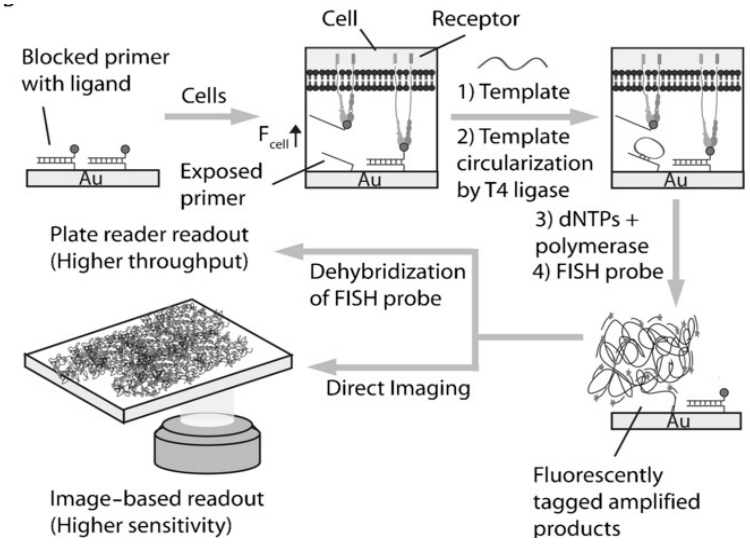

Figure 1.8. Schematic of MCR. Reprinted from Ref. 50 with permission of the publisher.

Comparing with traditional amplification reactions such as PCR or RCA, newly developed amplification assays such as the hybridization chain reaction and Cas12a nuclease reaction have better specificity and is more versatile in reaction conditions, making them great candidate in our development of ultrasensitive tension sensors with catalytic amplification reactions.

1.4.1 Hybridization chain reaction

HCR is an isothermal and enzyme-free dynamic DNA nanotechnology originally developed by Pierce and colleagues.[51] In HCR, two partially self-complementary hairpin oligonucleotides are designed with a large kinetic barrier to hybridization. The assembly of the two hairpins requires opening of one of the hairpins by a toehold mediated displacement reaction with a short DNA strand called the initiator (*I*) to propagate the formation of the nicked DNA polymers. (**Figure 1.2**) Because the reaction happens spontaneously until all materials are exhausted, the average weight of HCR product is typically inversely proportional to the amount of initiators in the system even though the length of products is heterogeneous.

Building on the basic principle of HCR, a variety of new developments have been made by Tan and others for HCR. For example, new activation and controlling methods of HCR such as photoactivation[52], pH control[53] and proximity-dependent activation[54] have been reported. More complexed systems such as branched HCR[55] or controlled HCR have also been developed by designing mismatch or multiple toehold on the sequence.[55, 56] Those developments enable more precise control over the HCR product and can achieve higher orders of amplifications.

While many HCR techniques are designed with fluorophore labelled DNA or intercalating dyes for detection. New development such as FRET HCR has been developed by positioning dyes at specific locations on hairpins to allow FRET when polymerized.[57] There have also been reports using chemiluminescence[58], colorimetry,[59] surface plasmon resonance (SPR),[60] and surface-enhanced Raman scattering (SERS)[61] for detection of HCR products.

Because of isothermal and enzyme-free conditions of HCR, it is widely used in detection of nucleic acid such as DNA or mRNA. For example, HCR has been used to detect different mRNA in the

early development of chicken embryo. [62] Otherwise, HCR can also be used to detect proteins. By employing antibody or aptamer labeled DNA, HCR can sensitively detect target proteins for applications such as immunohistochemistry[63] or cancer detection[64].

Inspired by the versality and specificity of HCR, we developed an HCR based tension detection method that enables real-time, live-cell detection of mechanical tension which will be introduced in Chapter 2.

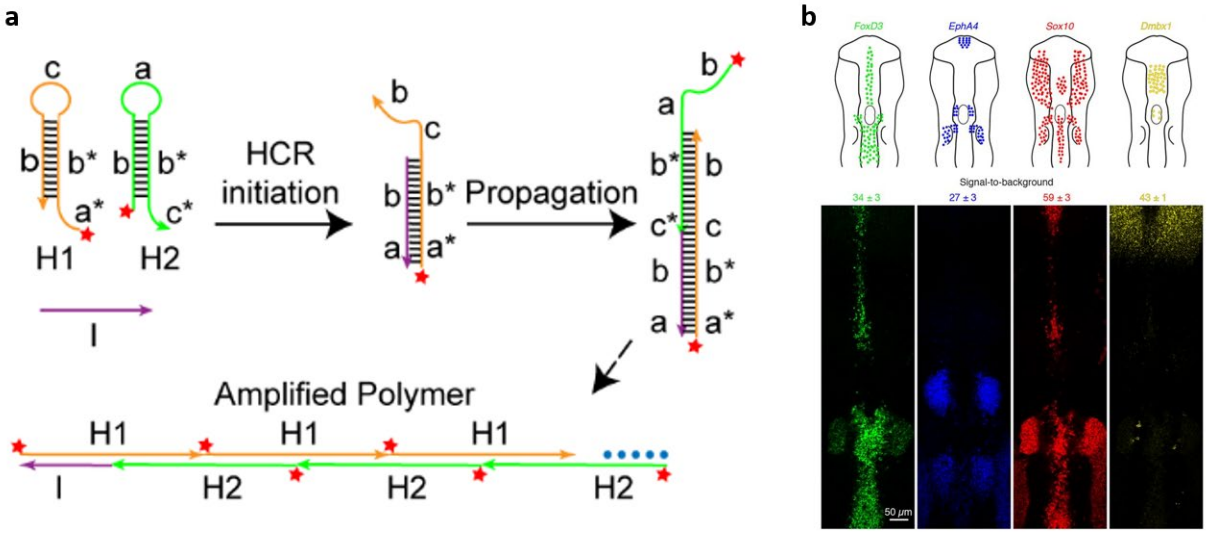

Figure 1.9 Schematic of HCR and its application in mRNA detection in chicken embryo development. (a) Schematic of HCR mechanisms. (b) using HCR to detect mRNA in chicken embryo. Reprinted from Yuxin Duan et al. *Mechanically-triggered Hybridization Chain Reaction* and Ref. 62 with permission of the publisher.

1.4.2 CRISPR-Cas12a nuclease reaction

The discovery and development of clustered regularly interspaced short palindromic repeats (CRISPR) and CRISPR-associated proteins (Cas) system have gained great popularity in the field of genome editing, and more recently in molecular diagnostics.[65, 66] The fast and isothermal features of CRISPR-Cas system make it a prodigious candidate for nucleic acid detecting assay.

One notable Cas enzyme used in diagnostics is CRISPR-Cas12a (Cpf1) enzyme which is a class 2 type V-A enzyme that is loaded with single-stranded guide RNA (gRNA) or CRISPR RNA (crRNA).[67] The crRNA-loaded Cas12a can be activated using two different approaches. The first is by binding to a complementary target double stranded DNA (activator) containing a PAM sequence (TTTV for LbCas12a). Double stranded DNA lacking the PAM is a poor activator of Cas12a. Alternatively, Cas12a can be activated by binding to a complementary target single stranded activator DNA. In this case, the PAM sequence is not required to potently activate the nuclease. Regardless of the type of activator (ssDNA or dsDNA), upon activation of the Cas12a, the enzyme undergoes a conformation change that unleashes its indiscriminate cleavage activity which hydrolyzes any ssDNA in proximity.[67] The nuclease activity of Cas12a is robust, highly efficient with $k_{cat}/K_m \sim 10^6$-10^7 $M^{-1}s^{-1}$, and thus has been used for a number of diagnostic assays.

For example, SARS-CoV-2 DETECTR assay where Cas12a is guided to dsDNA targets by a crRNA triggers an indiscriminate cleavage of ssDNA reporter labeled with a quencher and a fluorophore, leading to a production of massive fluorescent signal. (**Figure 1.10**) As a result, DETECTR shows attomolar sensitivity and a 95% positive and a 100% negative predictive agreement relative to the RT–qPCR assay.[68] Other Cas12a based assay such as HOLMES and AIOD-CRISPR (for all-in-one dual CRISPR–Cas12a) assay also show high sensitivity and specific towards SARS-Cov-2 detection.[69] Besides infectious disease detection, Cas12a has also been used in detection of miR-21[70] and mutations in the epidermal-growth-factor-receptor gene[49].

Other than nucleic acid, researchers has also developed two strategies for detection of proteins and small molecules. In CaT-SMelor (CRISPR–Cas12a-mediated and aTF-mediated small molecule detector), immobilized bacterial allosteric transcription factors(aTF)–dsDNA complexes will experience a conformational change when aTF binds to target molecules and frees the dsDNA from the complex.[71] Freed dsDNA can then be detected using CRISPR–Cas12a and measured through the collateral cleavage of a quenched fluorescent reporter. In another strategy, Yi Lu and colleagues use aptamer or DNAzymes to block the DNA activators that would be released upon detecting metal ion or ATP.(LOD= 400nM)[72]

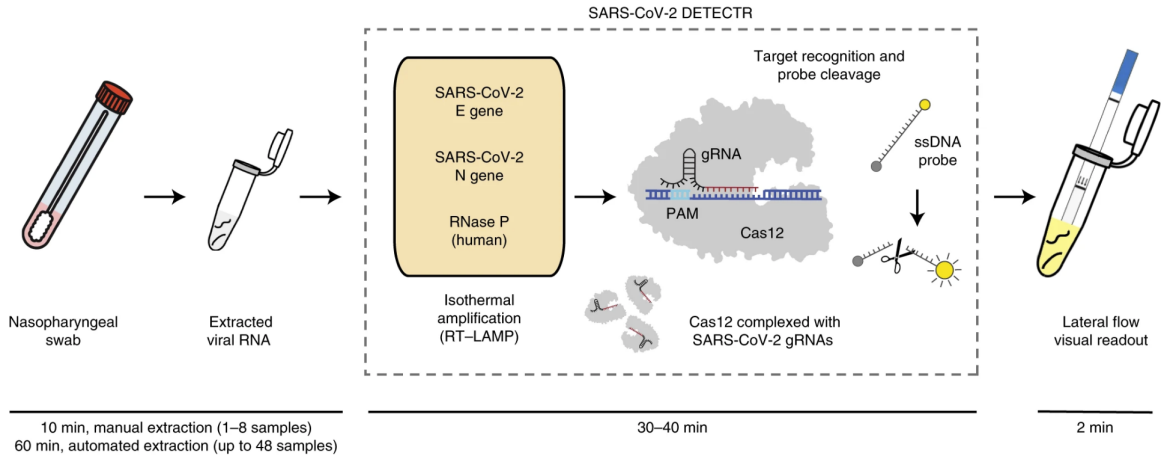

Figure 1.10 Schematic of DETECTR. Reprinted from Ref. 68 with permission of the publisher.

Because of the fast kinetics, robustness, and sensitivity of Cas12a based assay, we developed the Mechano-Cas12a Assisted Tension Sensor (MCATS) which provide a fast, high-throughput method to detect cellular receptor forces which will be introduced in Chapter 3 and Chapter 4.

1.5 Aim and Scope of the Dissertation

The development of DNA based tension probes has greatly broaden our knowledge of how cell mechanics affect essential biological process. However, because molecular forces that are sensed and transduced by cells are fairly weak, at the scale of pN and are highly transient (μs-s) and infrequent (100s-1000s per cell), molecular tension signal requires high resolution fluorescence microscope to quantify, which hinders the widespread adoption and applications of these tension probes in cell and molecular biology study as well as its use in clinical applications. Developing a mechano- "PCR" or "ELISA" that is accurate, sensitive, rapid, and cost-efficient method can democratize mechanobiology and open the door for any lab to access cell mechanics in biological and pathological studies. In this dissertation, we aim to take advantages of catalytic amplification reactions to develop ultrasensitive tension sensors that can facilitate basic studies of cell mechanobiology and explore the potential of using cell forces as a diagnostic marker in the clinic. We aim to answer the following questions: (1) how can we overcome the instrumental limitation of traditional DNA tension probe and develop techniques that can boost the signal of DNA tension probes to achieve rapid, high-throughput tension detection? (2) how can we optimize those techniques to be used with different cell types and receptors? (3) what's the limit of detection for those assays (4) how can we use those techniques for biophysical and mechanobiology studies? (5) can the signal detected by the technology be used for clinical applications such as predicting bleeding for surgery patients or enable personalized medicine?

During my PhD research, I've developed multiple techniques that use mechanically triggered catalytic amplification reactions to address the aims of this dissertation. More specifically,

In **Chapter 2**, I'll describe the development of mechanically triggered hybridization chain reaction (Mechano-HCR) to enable fast readout of receptor forces with conventional plate reader. This is

the first example of using HCR for the quantification of specific pN events mediated by cell surface receptors. **Chapter 3** will introduce the mechano-Cas12a assisted tension sensor (MCATS), which is an ultrasensitive fluorescence-based assay to detect the molecular forces generated by cells. By cooperating CRISPR-Cas12a with DNA tension probes, this assay allows an accurate, rapid, and cost-efficient method to detect molecular forces. We show the clinical potential of MCATS to predict the bleeding risk and the need for platelet transfusion in surgery patients following cardiopulmonary bypass and to assess drug response to a full panel of anti-platelet therapy with only 1ml of blood. In **Chapter 4**, I'll discuss reversible tension probe MCATS that build on the methods from Chapter 3, to enable high throughput readout of T-cell tension. Finally, **Chapter 5** will summarize the development of amplification reactions based ultrasensitive DNA tension sensors and outline promising directions in future development and applications.

1.6 References

1. Ladoux, B. & Mège, R.-M. Mechanobiology of collective cell behaviours. *Nat. Rev. Mol. Cell Biol.* **18**, 743-757 (2017).
2. Orr, A.W., Helmke, B.P., Blackman, B.R. & Schwartz, M.A. Mechanisms of mechanotransduction. *Dev. Cell* **10**, 11-20 (2006).
3. Liu, Y. et al. DNA-based nanoparticle tension sensors reveal that T-cell receptors transmit defined pN forces to their antigens for enhanced fidelity. *Proc. Natl. Acad. Sci. U.S.A.* **113**, 5610-5615 (2016).
4. Vining, K.H. & Mooney, D.J. Mechanical forces direct stem cell behaviour in development and regeneration. *Nat. Rev. Mol. Cell Biol.* **18**, 728-742 (2017).
5. Dunn, S.L. & Olmedo, M.L. Mechanotransduction: Relevance to Physical Therapist Practice—Understanding Our Ability to Affect Genetic Expression Through Mechanical Forces. *Phys. Ther.* **96**, 712-721 (2016).
6. Brockman, J.M. & Salaita, K. Mechanical Proofreading: A General Mechanism to Enhance the Fidelity of Information Transfer Between Cells. *Front. Phys.* **7** (2019).
7. Ting, L.H. et al. Contractile forces in platelet aggregates under microfluidic shear gradients reflect platelet inhibition and bleeding risk. *Nat. Commun.* **10**, 1-10 (2019).
8. Myers, D.R. et al. Single-platelet nanomechanics measured by high-throughput cytometry. *Nat. Mater.* **16**, 230-235 (2017).
9. Carr, M.E. Development of platelet contractile force as a research and clinical measure of platelet function. *Cell Biochem. Biophys.* **38**, 55-78 (2003).
10. Alberts, B. et al. in Molecular biology or the cell (2002).

11. Martino, F., Perestrelo, A.R., Vinarský, V., Pagliari, S. & Forte, G. Cellular mechanotransduction: from tension to function. *Front. Physiol.* **9**, 824 (2018).

12. Kiefer, T.L. & Becker, R.C. Inhibitors of platelet adhesion. *Circulation* **120**, 2488-2495 (2009).

13. Staatz, W.D., Rajpara, S.M., Wayner, E.A., Carter, W.G. & Santoro, S.A. The membrane glycoprotein Ia-IIa (VLA-2) complex mediates the Mg++-dependent adhesion of platelets to collagen. *J. Cell Biol.* **108**, 1917-1924 (1989).

14. Piotrowicz, R.S., Orchekowski, R.P., Nugent, D.J., Yamada, K.Y. & Kunicki, T.J. Glycoprotein Ic-IIa functions as an activation-independent fibronectin receptor on human platelets. *J. Cell Biol.* **106**, 1359-1364 (1988).

15. Ill, C.R., Engvall, E. & Ruoslahti, E. Adhesion of platelets to laminin in the absence of activation. *J. Cell Biol.* **99**, 2140-2145 (1984).

16. Bennett, J.S., Chan, C., Vilaire, G., Mousa, S.A. & DeGrado, W.F. Agonist-activated αvμ3 on Platelets and Lymphocytes Binds to the Matrix Protein Osteopontin. *J. Biol. Chem.* **272**, 8137-8140 (1997).

17. Paul, B.Z.S., Vilaire, G., Kunapuli, S.P. & Bennett, J.S. Concurrent signaling from Gαq- and Gαi-coupled pathways is essential for agonist-induced αvβ3 activation on human platelets. *J. Thromb. Haemost.* **1**, 814-820 (2003).

18. Xu, X.R. et al. Platelets and platelet adhesion molecules: novel mechanisms of thrombosis and anti-thrombotic therapies. *Thromb. J.* **14**, 29 (2016).

19. Chen, Y. et al. An integrin αIIbβ3 intermediate affinity state mediates biomechanical platelet aggregation. *Nat. Mater.* **18**, 760-769 (2019).

20. Zhang, X.F. & Cheng, X. Platelet mechanosensing axis revealed. *Nat. Mater.* **18**, 661-662 (2019).

21. Nurden, A. & Caen, J. An abnormal platelet glycoprotein pattern in three cases of Glanzmann's thrombasthenia. *Br. J. Haematol.* **28**, 253-260 (1974).

22. Mannino, R.G. et al. Smartphone app for non-invasive detection of anemia using only patient-sourced photos. *Nat. Commun.* **9**, 1-10 (2018).

23. MacDonald, E. & Severn, M. in Thromboelastography or Rotational Thromboelastography for Trauma: A Review of the Clinical and Cost-Effectiveness and Guidelines (Canadian Agency for Drugs and Technologies in Health

24. Lodewyks, C. et al. Point-of-care viscoelastic hemostatic testing in cardiac surgery patients: a systematic review and meta-analysis. *Can. J. Anaesth.* **65**, 1333-1347 (2018).

25. Trenk, D. et al. A randomized trial of prasugrel versus clopidogrel in patients with high platelet reactivity on clopidogrel after elective percutaneous coronary intervention with implantation of drug-eluting stents: results of the TRIGGER-PCI (Testing Platelet Reactivity In Patients Undergoing Elective Stent Placement on Clopidogrel to Guide Alternative Therapy With Prasugrel) study. *J. Am. Coll. Cardiol.* **59**, 2159-2164 (2012).

26. Price, M.J. et al. Standard- vs high-dose clopidogrel based on platelet function testing after percutaneous coronary intervention: the GRAVITAS randomized trial. *JAMA* **305**, 1097-1105 (2011).

27. Dhakal, B. et al. Disease burden, complication rates, and health-care costs of heparin-induced thrombocytopenia in the USA: a population-based study. *Lancet Haematol.* **5**, e220-e231 (2018).

28. Style, R.W. et al. Traction force microscopy in physics and biology. *Soft matter* **10**, 4047-4055 (2014).

29. Chaudhuri, O., Parekh, S.H., Lam, W.A. & Fletcher, D.A. Combined atomic force microscopy and side-view optical imaging for mechanical studies of cells. *Nat. Methods* **6**, 383-387 (2009).

30. Liu, Y., Galior, K., Ma, V.P.-Y. & Salaita, K. Molecular tension probes for imaging forces at the cell surface. *Acc. Chem. Res.* **50**, 2915-2924 (2017).

31. Grashoff, C. et al. Measuring mechanical tension across vinculin reveals regulation of focal adhesion dynamics. *Nature* **466**, 263-266 (2010).

32. Zhang, Y., Ge, C., Zhu, C. & Salaita, K. DNA-based digital tension probes reveal integrin forces during early cell adhesion. *Nat. Commun.* **5**, 5167 (2014).

33. Ma, R. et al. DNA probes that store mechanical information reveal transient piconewton forces applied by T cells. *Proc. Natl. Acad. Sci. U.S.A.* **116**, 16949-16954 (2019).

34. Wan, Z. et al. The activation of IgM- or isotype-switched IgG- and IgE-BCR exhibits distinct mechanical force sensitivity and threshold. *Elife* **4** (2015).

35. Zhang, Y. et al. Platelet integrins exhibit anisotropic mechanosensing and harness piconewton forces to mediate platelet aggregation. *Proc. Natl. Acad. Sci. U.S.A.* **115**, 325-330 (2018).

36. Spillane, K.M. & Tolar, P. B cell antigen extraction is regulated by physical properties of antigen-presenting cells. *J. Cell Biol.* **216**, 217-230 (2016).

37. Wang, X. & Ha, T. Defining single molecular forces required to activate integrin and notch signaling. *Science* **340**, 991-994 (2013).

38. Hatch, K., Danilowicz, C., Coljee, V. & Prentiss, M. Demonstration that the shear force required to separate short double-stranded DNA does not increase significantly with sequence length for sequences longer than 25 base pairs. *Phys Rev E Stat Nonlin Soft Matter Phys* **78**, 011920 (2008).

39. Seo, D. et al. A Mechanogenetic Toolkit for Interrogating Cell Signaling in Space and Time. *Cell* **165**, 1507-1518 (2016).

40. Mosayebi, M., Louis, A.A., Doye, J.P. & Ouldridge, T.E. Force-Induced Rupture of a DNA Duplex: From Fundamentals to Force Sensors. *ACS Nano* **9**, 11993-12003 (2015).

41. Rashid, S.A. et al. DNA Tension Probes Show that Cardiomyocyte Maturation Is Sensitive to the Piconewton Traction Forces Transmitted by Integrins. *ACS Nano* **16**, 5335-5348 (2022).

42. Dutta, P.K. et al. Programmable multivalent DNA-origami tension probes for reporting cellular traction forces. *Nano Lett.* **18**, 4803-4811 (2018).

43. Glazier, R. et al. DNA mechanotechnology reveals that integrin receptors apply pN forces in podosomes on fluid substrates. *Nat. Commun.* **10**, 4507 (2019).

44. Zhao, Y., Sarkar, A. & Wang, X. Peptide nucleic acid based tension sensor for cellular force imaging with strong DNase resistance. *Biosens. Bioelectron.* **150**, 111959 (2020).

45. Brockman, J.M. et al. Live-cell super-resolved PAINT imaging of piconewton cellular traction forces. *Nat. Methods* **17**, 1018-1024 (2020).

46. Gaudet, C. et al. Influence of type I collagen surface density on fibroblast spreading, motility, and contractility. *Biophys. J.* **85**, 3329-3335 (2003).

47. Adams, J. Biotin amplification of biotin and horseradish peroxidase signals in histochemical stains. *J. Histochem. Cytochem.* **40**, 1457-1463 (1992).

48. Ding, X. et al. Ultrasensitive and visual detection of SARS-CoV-2 using all-in-one dual CRISPR-Cas12a assay. *Nat. Commun.* **11**, 1-10 (2020).

49. Gootenberg, J.S. et al. Multiplexed and portable nucleic acid detection platform with Cas13, Cas12a, and Csm6. *Science* **360**, 439-444 (2018).

50. Ma, V.P. et al. Mechanically Induced Catalytic Amplification Reaction for Readout of Receptor-Mediated Cellular Forces. *Angew. Chem. Int. Ed.* **55**, 5488-5492 (2016).

51. Dirks, R.M. & Pierce, N.A. Triggered amplification by hybridization chain reaction. *Proc. Natl. Acad. Sci. U.S.A.* **101**, 15275-15278 (2004).

52. Chu, H., Zhao, J., Mi, Y., Zhao, Y. & Li, L. Near-Infrared Light-Initiated Hybridization Chain Reaction for Spatially and Temporally Resolved Signal Amplification. *Angew. Chem. Int. Ed.* **58**, 14877-14881 (2019).

53. Idili, A., Porchetta, A., Amodio, A., Vallée-Bélisle, A. & Ricci, F. Controlling Hybridization Chain Reactions with pH. *Nano Lett.* **15**, 5539-5544 (2015).

54. Koos, B. et al. Proximity-dependent initiation of hybridization chain reaction. *Nat. Commun.* **6**, 7294 (2015).

55. Bi, S., Chen, M., Jia, X., Dong, Y. & Wang, Z. Hyperbranched Hybridization Chain Reaction for Triggered Signal Amplification and Concatenated Logic Circuits. *Angew. Chem. Int. Ed.* **54**, 8144-8148 (2015).

56. Figg, C.A., Winegar, P.H., Hayes, O.G. & Mirkin, C.A. Controlling the DNA Hybridization Chain Reaction. *J. Am. Chem. Soc.* **142**, 8596-8601 (2020).

57. Guo, J., Mingoes, C., Qiu, X. & Hildebrandt, N. Simple, Amplified, and Multiplexed Detection of MicroRNAs Using Time-Gated FRET and Hybridization Chain Reaction. *Anal. Chem.* **91**, 3101-3109 (2019).

58. Bi, S., Zhao, T., Luo, B. & Zhu, J.-J. Hybridization chain reaction-based branched rolling circle amplification for chemiluminescence detection of DNA methylation. *Chem. Commun.* **49**, 6906-6908 (2013).

59. Sun, J., Jiang, W., Zhu, J., Li, W. & Wang, L. Label-free fluorescence dual-amplified detection of adenosine based on exonuclease III-assisted DNA cycling and hybridization chain reaction. *Biosens. Bioelectron.* **70**, 15-20 (2015).

60. Li, X., Wang, Y., Wang, L. & Wei, Q. A surface plasmon resonance assay coupled with a hybridization chain reaction for amplified detection of DNA and small molecules. *ChemComm.* **50**, 5049-5052 (2014).

61. Zheng, J. et al. Universal surface-enhanced Raman scattering amplification detector for ultrasensitive detection of multiple target analytes. *Anal. Chem.* **86**, 2205-2212 (2014).

62. Choi, H.M.T. et al. Third-generation in situ hybridization chain reaction: multiplexed, quantitative, sensitive, versatile, robust. *Development* **145**, dev165753 (2018).

63. Lin, R. et al. A hybridization-chain-reaction-based method for amplifying immunosignals. *Nat. Methods* **15**, 275-278 (2018).

64. Zhou, G. et al. Multivalent capture and detection of cancer cells with DNA nanostructured biosensors and multibranched hybridization chain reaction amplification. *Anal. Chem.* **86**, 7843-7848 (2014).

65. Doudna, J.A. & Charpentier, E. The new frontier of genome engineering with CRISPR-Cas9. *Science* **346**, 1258096 (2014).

66. Kaminski, M.M., Abudayyeh, O.O., Gootenberg, J.S., Zhang, F. & Collins, J.J. CRISPR-based diagnostics. *Nat. Biomed. Eng.* **5**, 643-656 (2021).

67. Chen, J.S. et al. CRISPR-Cas12a target binding unleashes indiscriminate single-stranded DNase activity. *Science* **360**, 436-439 (2018).

68. Broughton, J.P. et al. CRISPR–Cas12-based detection of SARS-CoV-2. *Nat. Biotechnol.* **38**, 870-874 (2020).

69. Li, S.-Y. et al. CRISPR-Cas12a-assisted nucleic acid detection. *Cell Discov.* **4**, 20 (2018).

70. Wang, G., Tian, W., Liu, X., Ren, W. & Liu, C. New CRISPR-derived microRNA sensing mechanism based on Cas12a self-powered and rolling circle transcription-unleashed real-time crRNA recruiting. *Anal. Chem.* **92**, 6702-6708 (2020).

71. Liang, M. et al. A CRISPR-Cas12a-derived biosensing platform for the highly sensitive detection of diverse small molecules. *Nat. Commun.* **10**, 1-9 (2019).

72. Xiong, Y. et al. Functional DNA regulated CRISPR-Cas12a sensors for point-of-care diagnostics of non-nucleic-acid targets. *J. Am. Chem. Soc.* **142**, 207-213 (2019).

Chapter 2. Development of Mechanically-triggered Hybridization Chain Reaction

Adapted from Duan, Y.; Glazier, R.; Bazrafshan, A.; Hu, Y.; Rashid, A; Petrich, B; Ke, Y; Salaita, K Mechanically-triggered Hybridization Chain Reaction. *Angew. Chemie.,* **2021** 60(36):19974-81 DOI:10.1002/anie.202107660 Adapted with permission.

2.1 Abstract

Cells transmit piconewton forces to receptors to mediate processes such as migration and immune recognition. A major challenge in quantifying such forces is the sparsity of cell mechanical events. Accordingly, molecular tension is typically quantified with high resolution fluorescence microscopy, which hinders widespread adoption and application. Here, we report a mechanically-triggered hybridization chain reaction (mechano-HCR) that allows chemical amplification of mechanical events. The amplification is triggered when a cell receptor mechanically denatures a duplex revealing a cryptic initiator to activate the HCR reaction in situ. Importantly, mechano-HCR enables direct readout of pN forces using a plate reader. We leverage this capability and measured mechano-IC50 for aspirin, Y-27632, and eptifibatide. Given that cell mechanical phenotypes are of clinical importance, mechano-HCR may offer a convenient route for drug discovery, personalized medicine, and disease diagnosis.

2.2 Introduction

The ability for cells to sense and respond to mechanical forces is central to a wide range of biological processes and plays an important role in numerous pathologies, including migration, immune recognition, and differentiation.[1-5] Not only is measuring such force of fundamental importance to understanding mechanisms of mechanotransduction, mechanics has also been shown as a diagnostic marker of cell state.[6-8] For example, Sniadecki et al. found that the magnitude of traction forces generated by platelets from patients in emergency room can be used to predict bleeding risk.[6] Diminished platelet contractile forces are also reported by Lam and colleagues in patients presenting with chronic bleeding symptoms and genetic disorder.[7] Thus,

the development of molecular technologies to detect the pN forces transmitted by adhesion receptors can provide robust tools for clinical assays.

A central challenge in this field is that the molecular forces that are sensed and transduced are usually at the scale of piconewtons (pN).[9] For reference, ~ 7 pN applied over a distance of 1 nm is approximately 1 kcal/mol, which is diminishingly small and difficult to detect and investigate. Another challenge with detecting such forces is that mechanical events are highly transient and fairly sparse. [10]

Molecular tension sensors provide a powerful method to detect the pN forces generated by cell receptors.[11] The first molecular tension sensors to detect cell receptor forces were described in 2011 and used an immobilized PEG polymer that was flanked with a fluorophore and quencher to optically detect receptor forces that drive stretching of the polymer.[11-13] Over the past decade, a suite of different classes of tension sensors comprised of nucleic acids[14], proteins[15], and polymers[12] have been reported and applied to the study of a variety of mechanotransduction pathways, ranging from T cell[16] and B cell antigen recognition[17] to cell adhesion[14] and platelet activation (Table 2.3 and 2.4).[18, 19]

Because receptor-mediated forces are highly transient (~msec to 10's of sec), weak (~pN), and fairly rare events (compared to ligand-receptor binding), these signals are difficult to quantify.[3, 16] One solution to this problem is to employ tension probes that irreversibly generate a fluorescence response to the pN input. The tension gauge tether (TGT) was originally developed by Ha and

colleagues to control the forces transmitted by cells,[9] but later it was found that these probes could be modified with a fluorophore and quencher pair to report on the peak forces applied by cell surface receptors.[18] The TGT is simply comprised of a DNA duplex, with one oligo anchored to the surface and the second oligo presenting a ligand specific to the receptor of interest. When the transmitted force exceeds a threshold value, called tension tolerance (T_{tol}), the duplex mechanically denatures, leading to de-quenching of the dye and generating a fluorescence signal proportional to the total number of accumulated mechanical events over time.[14, 20] Nonetheless, the density of mechanical events is typically ~100 events/μm^2.[10, 16] Given the size of a typical mammalian cell of 100's of μm^2, at best each cell can generate a fluorescence signal corresponding to ~10^3-10^4 fluorophores, which is difficult to quantify. Indeed, TGT signal quantification requires microscopes equipped with high NA objectives and single photon counting EMCCDs. Therefore, the instrumentation requirement hinders the widespread adoption of molecular tension probes for many applications including high- and medium-throughput drug and cell screening, as well as integrating such assays into clinics.

Limited signal in bioanalytical chemistry is typically addressed by using enzymes such as horseradish peroxidase[21], DNA polymerases and more recently CRISPR nucleases (Cas12a and Cas13a) in assays such as ELISA and PCR.[22, 23] These types of catalytic amplification assays have transformed modern biochemistry and are the cornerstone of the vast majority of clinical diagnostics. Developing amplification reactions that boost the signal generated by molecular tension probes is therefore highly desirable for mechanobiology and may open the door toward new areas, such as "mechanopharmacology" and "mechanodiagnostics" that can be potentially personalized using primary cells derived from patients.

Herein, we integrate the hybridization chain reaction (HCR) with molecular tension probes to generate a signal-amplification assay for readout of cell forces. HCR is an isothermal and enzyme-free reaction originally developed by Pierce and colleagues.[24] In HCR, two partially self-complementary hairpin oligonucleotides are designed with a large kinetic barrier to hybridization. The assembly of the two hairpins requires opening of one of the hairpins to propagate the formation of the DNA polymers, and this initiation is triggered by a toehold mediated displacement reaction with a short DNA strand called the initiator (*I*) (**Figure 2.2A**). In mechano-HCR, the initiator is concealed and blocked by a complementary strand that is conjugated with a ligand to the receptor of interest. As is shown in **Figure 2.1A**, a DNA duplex is formed between a top strand conjugated to the ligand cyclo-Arg-Gly-Asp-Phe-Lys (cRGDfK) and a bottom strand anchored to the surface. When cells are seeded, membrane receptors such as integrins bind to the cRGDfK ligand on the duplex and apply forces. Forces that exceed the T_{tol} mechanically rupture the DNA duplexes, exposing the bottom strand (initiator) for triggering the HCR (**Figure 2.1B**). Subsequently, hairpin 1 (H1) and hairpin 2 (H2) are added to the well for HCR amplification (Appendix, **table 2.1** for DNA sequences).[25] Because the HCR polymerization reaction is fully compatible with cell culture media, the cells remain active during the amplification process. Importantly, the quantification of the mechano-HCR products can be achieved either by direct imaging with a fluorescence microscope or by using a plate reader. Because measuring cell traction forces can be performed in a multi-well plate, mechano-HCR allows one to screen many different cells that are subjected to different concentrations of drugs that can modulate cell mechanics. We demonstrate the potential significance of mechano-HCR by screening the activity of three drugs with anti-coagulation activity: aspirin, eptifibatide, ROCK-inhibitor. We find a high level of agreement between

published IC_{50} (half maximal inhibitory concentration) of these drugs and their mechano-IC_{50} measured by mechano-HCR. Therefore, this assay represents an important step toward rapid and automated screening of drugs that modulate cell mechanics.

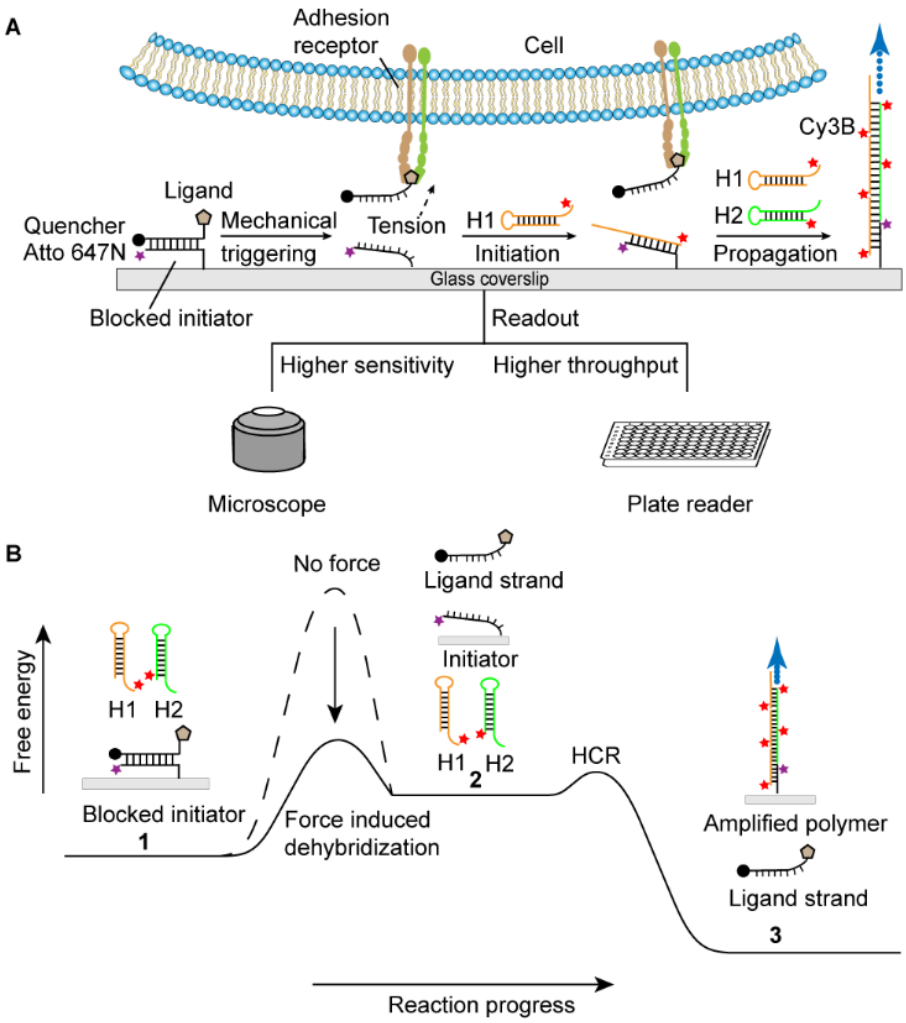

Figure 2.1: Mechanically-triggered hybridization chain reaction (mechano-HCR). A) Schematic showing the triggering mechanism to reveal a cryptic initiator that leads to local growth of a DNA polymer from two hairpin monomers (H1 and H2). In our work, the initiator is tagged with Atto647N while H1 and H2 are tagged with Cy3B. B) Idealized free energy landscape of mechano-HCR showing the transition from state 1 (block initiator, H1 and H2) to state 2 (exposed initiator, H1, and H2), and finally to the thermodynamic minimum state 3 with polymerized monomers. Theoretically, the barrier between 1 and 2 must be large and mechanical forces that denature the top strand are needed to lower this barrier (akin to a catalyst) and accelerate the rate of reaction by orders of magnitude.

2.3 Results and Discussion

2.3.1 Validation and characterization of HCR on surface

To validate the activity of the HCR reaction, we used gel electrophoresis to detect polymerization products. We tuned the initiator concentration (from 0.01 to 10 mM) while maintaining a monomer hairpin concentration of 1 mM. The reactions were allowed to proceed in 150 mM NaCl for 1.5 hr at room temperature (RT). Gel electrophoresis showed that decreasing initiator concentration produces longer HCR products, as anticipated, and the leakage rate of polymerization without initiator was minimal (**Figure 2.2B**). We also found that the HCR polymerization proceeds in cell culture medium with no significant change in reaction rate (**Figure 2.6**). Considering that immobilization of initiator imposes a steric constraint, we therefore studied the kinetics of HCR when the initiator was immobilized on a surface. In this assay, biotinylated single-stranded initiators were incubated on surfaces coated with streptavidin (**Figure 2.2**). We tested different initiator incubation concentrations and found that the surface density of initiator reached maximum coverage when incubated at 100 nM for 1 hr (**Figure 2.7**). We then used a quantitative fluorescence calibration employing supported lipid bilayer standards to determine the initiator surface density.[26] The result showed that the 100 nM incubation concentration led to an initiator density of 1330 ± 60 molecules/μm^2 while the 20 nM concentration produced a density of 260 ± 30 molecules/μm^2 (**Figure 2.8**). To trigger the HCR reaction, we added 62.5 nM of H1 and Cy3B labeled H2 and imaged the surface at different time points (**Figure 2.9**). We next fit the rate of polymerization to a pseudo-first order reaction using these fluorescence-time plots and found that the surface HCR $t_{1/2}$ = 1.6 ± 0.3 hr (R^2=0.9942, $t_{1/2}$ is the time needed to achieve half-maximum signal), when initiator density equals to 1330 molecule/μm^2 (Figure 1D). The $t_{1/2}$ indicated that a reaction time

of 2 hr for the live-cell mechano-HCR assay would be appropriate for sufficient signal amplification while limiting the total time of the assay.

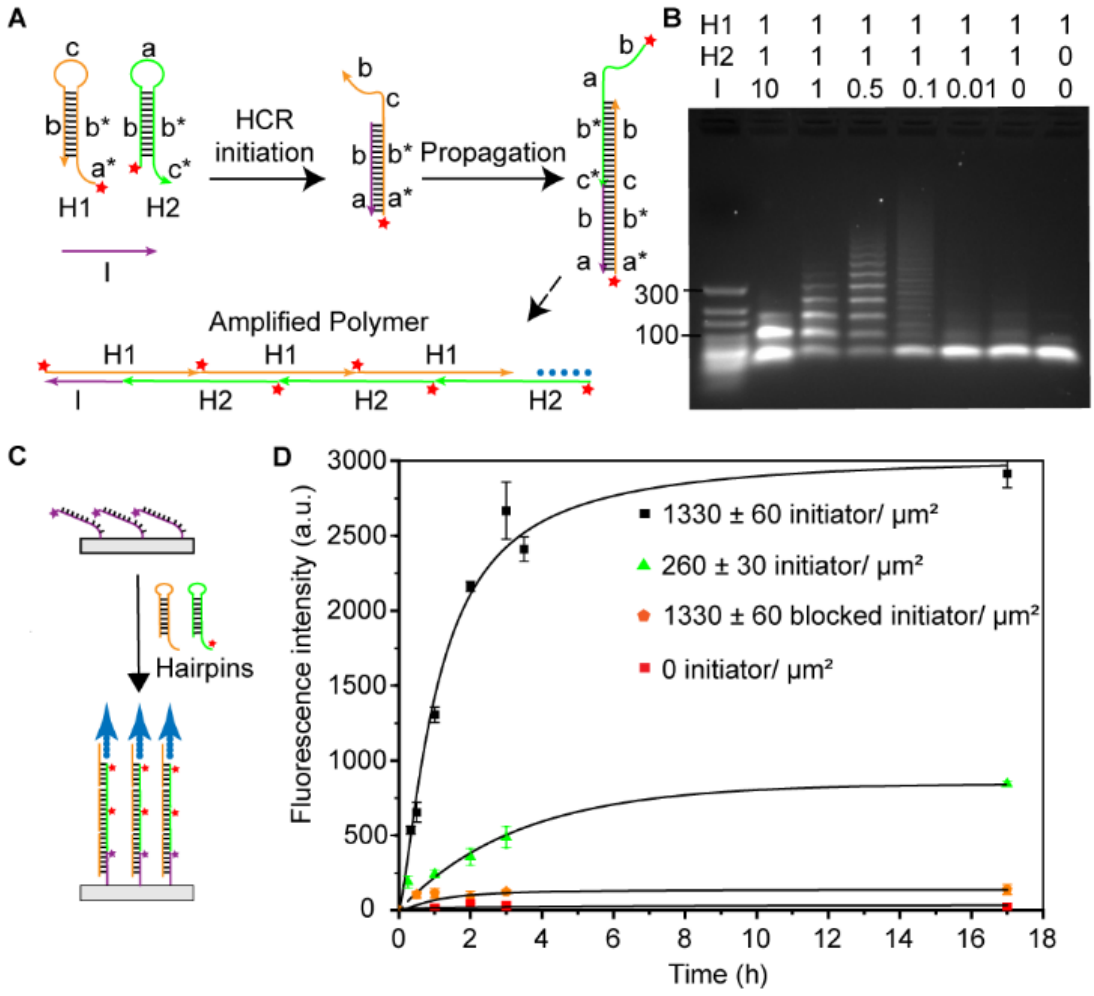

Figure 2.2: Validation of HCR using soluble and surface anchored initiator. A) Schematic showing the different domains of H1, H2, and I that mediate the formation of HCR polymers. Small red star is Cy3B dye. B) Agarose gel image of HCR product with different hairpin to initiator ratio. Lanes left to right: DNA Ladder, 1:10 ratio, 1:1 ratio, 2:1 ratio, 10:1 ratio, 100:1 ratio, no initiator, and H1 only. 90 min reaction time, at RT, in 150 mM NaCl using [H1] = 1 μM. C) Schematic of surface-initiated HCR. D) Plot of time-dependent fluorescence intensity measured using fluorescence microscopy of surface polymerized H1 and H2-Cy3B. Error bar represents S.E.M. obtained from three independent experiments. The intensity of each surface at each time point was determined from 12 images randomly selected from different regions. The black line represents a pseudo-first order fit to $F.I.(t) = A(1\text{-}e^{-xt})$.

2.3.2 Mapping Live-cell tension signal with mechano-HCR

We next applied the mechano-HCR assay to detect integrin mediated forces applied by live-cells. Integrin adhesion receptors are a family of heterodimeric receptors that span the plasma membrane and bridge the cellular cytoskeleton with the extracellular matrix (ECM) to mediate many processes including cell migration, adhesion, and immune recognition. Our past work, as well as the work of others including Ha and Wang, has showed that integrin receptors apply pN forces that are sufficient to mechanically denature DNA duplexes.[18, 27, 28] Hence, measuring integrin forces within cell adhesions is an appropriate model to validate the mechano-HCR assay.

Firstly, we designed two types of DNA duplexes that have identical sequence and thermal melting temperatures, but different geometries and mechanical tolerances (**Figure 2.3A**).[9] In the unzipping geometry, mechanical forces denature the duplex, one base at a time, with a predicted T_{tol}=12 pN, while in shearing geometry the duplex is more mechanically stable and has a predicted T_{tol}=60 pN.[29, 30] The cRGDfK ligand which has a high affinity to the a_vb_3 integrin ($K_D = 1.3 \times 10^{-6}$ M [31]) was conjugated to the DNA duplex via copper(I)-catalyzed azide-alkyne cycloaddition. HPLC, agarose gel electrophoresis and MALDI-TOF characterization of the products confirm successful conjugation (Figure 2.10). cRGDfK-conjugated and fluorophore-quencher tagged DNA duplexes were then immobilized onto the surface. Note that piranha etching of the glass slide is critical as slides activated using other protocols (base etching and plasma etching) showed high background and low reproducibility. NIH/3T3 fibroblast cells were then seeded on these surfaces for 1 hr. As expected, we observed an increase in fluorescence signal for the 12 pN and 60 pN probes due to mechanical denaturation of the duplex (**Figure 2.3B**). We next added the H1 and H2 hairpin monomers to fuel the HCR and allowed the reaction to proceed for 2 hrs. After rinsing away the

excess monomers, we observed strong HCR signals at the 2hr time point (**Figure 2.3B**). We found that the probes in the unzipping geometry were more significantly denatured compared to shearing mode probes (60 pN), in agreement with literature. Importantly, the 12 pN unzipping mode probes also generated a greater HCR signal, reflecting the greater density of exposed initiator (**Figure 2.3E, Figure 2.11**).

To demonstrate real-time tracking of the growth of mechano-HCR signals, we applied total internal reflection fluorescence microscopy (TIRF). As is shown in the **Figure 2.12**, the mechano-HCR signal increased as a function of time and plateaued at ~3-3.5 hrs. The real-time amplification of HCR signal for one representative cell is provided in Movie 2.1. Note that in our live-cell experiments, we did not notice significant steric hinderance of mechano-HCR (**Figure 2.13**).

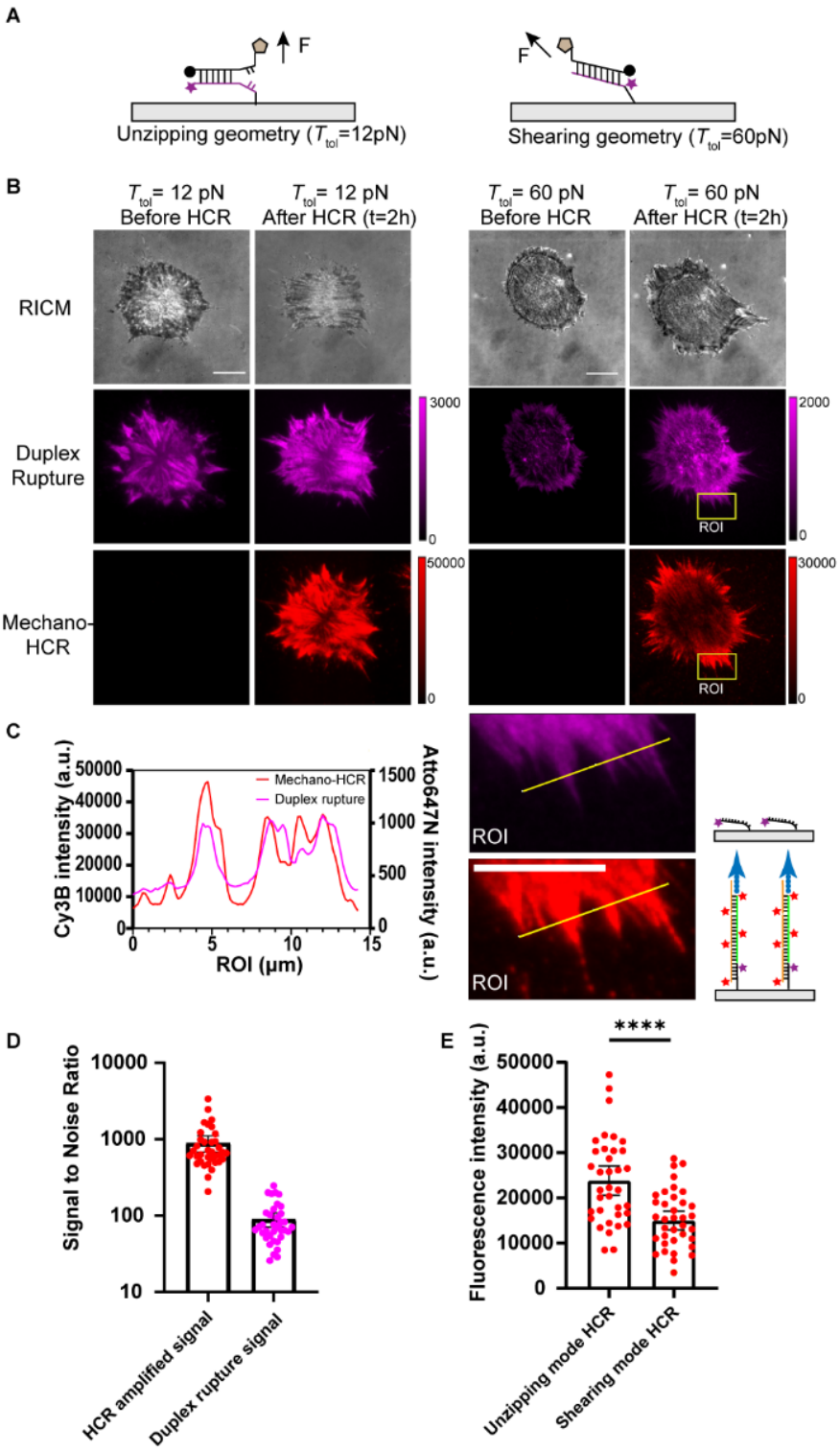

Figure 2.3: Mechano-HCR for live-cell mapping of cell traction forces. A) Schematic of DNA duplex with cryptic initiator used to study integrin-mediated forces. B) Representative RICM and fluorescence images of cells cultured on T_{tol}= 12 pN and T_{tol}= 60 pN surfaces before and after HCR amplification. Scale bar = 12 μm. The magenta color is emission from Atto647N tagging the

initiator while the red channel shows the Cy3B emission from H1 and H2 following HCR. The intensity bar next to each fluorescence image shows the absolute signal intensity for each image. C) Plot of line scan and zoom in of the ROI from (B). Scale bar = 10 μm. D) Bar graph shows S/N of mechano-HCR and initiator rupture signal. Error bars represent S.E.M. from 36 cells in *n*=4 independent experiments. E) Plot of fluorescence intensity of mechano-HCR using probes in the unzipping and shearing geometries. Error bars represent S.E.M. from 36 cells in n=3 independent experiments. (**** $p < 0.0001$, student t-test).

Line scan analysis of representative regions of interest from different cells (**Figure 2.3C**) confirms that the mechano-HCR signal and probe rupture signals are highly colocalized, based on the measured Pearson's correlation coefficient of 0.80 ± 0.08 (*n*=40 cells). However, the mechano-HCR signal is not perfectly colocalized with the initiator exposure signal in the fluorescence images. There are likely three reasons for the discrepancy. First, mechanical events that lead to unblocking of the initiator accumulate continuously over the 2 hr duration and hence mechanical events that occur earlier in time lead to greater amplification. Second, HCR polymerization is inherently heterogeneous and generates polymers with significant polydispersity as recently discussed by Figg and colleagues.[32] Third, regions with limited number of duplex ruptures may only be detectable using mechano-HCR but not with exposed initiators.

2.3.3 Characterization of mechano-HCR with cells and super-resolved HCR

To test whether single z-slice imaging can capture majority of HCR signals, we next acquired z stack images of mechano-HCR and DNA duplex rupture signal with a confocal microscope. As is shown in **Figure 2.14** and movie 2.2, the majority of HCR and duplex rupture signals are located next to the interface, indicating single Z-slice imaging is suitable for mechano-HCR quantification.

One important figure of merit when employing amplification strategies in analytical sensing is the signal to noise ratio (S/N) of amplified signal. To quantify this value, we directly compared the S/N of the mechano-HCR and initiator unblocking signals. By using the standard deviation of the background (regions outside of the cell) as the "noise" and quantifying the fluorescence under the cell as the signal, we estimate that the mechano-HCR S/N = 890 ± 105 (*n*=36 images), which is much greater than the S/N for the probe denaturation signal = 89 ± 9 (*n*=36) (**Figure 2.3D**). Control DNA duplexes with no cRGDfK ligands incubated with cells and hairpins did not show significant initiator exposure or mechano-HCR signal (**Figure 2.15**). To verify the specificity of mechano-HCR to adhesion complexes, GFP-vinculin mouse embryonic fibroblasts were cultured on these surfaces and probed using our mechano-HCR assay. In these experiments we found a high degree of localization between focal adhesions (GFP) and the mechano-HCR signal based on the measured Pearson's correlation coefficient of 0.81 ± 0.05 (*n*=15 cells from 3 independent experiments) (**Figure 2.16**). These results further confirm that the mechano-HCR readout can be used to detect and amplify integrin-mediated tension in live cells and that this signal localizes to active focal adhesions in cells. Another potential merit of mechano-HCR is that mechano-HCR can be combined with superresolution techniques including super-resolution radial fluctuations (SRRF) to improve the resolution of images (**Figure 2.17**).[33] We used SRRF because it offers high speed and live-cell compatibility and is fairly simple to implement without any hardware modification to a conventional wide field microscope.

2.3.4 Rapid detection of cellular tension with mechano-HCR and plate reader

Given that integrin tension plays important roles in cell function, assays that can quantify the molecular traction forces of cells in a rapid fashion are desirable. One can envision applications

for mechano-HCR in screening dose-response curves for drugs that modulate cell mechanics.[34] To achieve these goals, we first validated the mechano-HCR assay by plating an escalating density of NIH/3T3 cells in 96 well plates and measured the associated signal in each well. We expected that the mechano-HCR signal to linearly increase as a function of cell density until the surface is fully covered with cells. In these experiments, we measured the exposed initiator density and compared this to the mechano-HCR signal using a fluorescence microscope. We choose the 12pN duplex probe in the following experiments because the unzipping probe generates greater signals for both NIH/3T3 cells and mouse platelets, and hence facilitates readout in a plate reader (**Figure 2.18**). We found a highly linear relationship between the density of initiator sites (ruptured duplexes) and the final HCR signal (**Figure 2.19**). Because of the strength of the mechano-HCR signal, we next were able to measure the signal using a conventional plate reader. In agreement with the microscopy data, the bulk plate reader data showed a linear relationship between the number of plated cells and the fluorescence signal up to saturating cell densities (cell number ~20,000/32 mm^2) (**Figure 2.4A and 2.4B**). Importantly, amplification was critical, as the probe rupture signal (Atto647N) was not detectable above the background using the plate reader, thus demonstrating that the relatively low S/N ratio of that readout is insufficient for automated plate reader analysis (**Figure 2.20**).

2.3.5 Measuring dose-response function of cell-mechanics modulating molecules with mechano-HCR

We next tested the potential of using mechano-HCR in screening the dose-response function for different small molecules that target cell mechanics. We first investigated the Rho kinase inhibitor, Y-27632, which targets the phosphorylation of myosin light chain [35] and thus is known to dampen

forces transmitted by focal adhesions. We pretreated NIH/3T3 cells with a range of Y-27632 concentrations (0-100 μM) for 30 min.[27] The treated cells were then plated on 96 well plates presenting the 12 pN DNA duplex for 1 hr, which was followed by mechano-HCR amplification and readout. We were satisfied to see that the mechano-HCR signal showed a dose-dependent reduction in intensity as a function of increasing ROCK inhibitor concentration (**Figure 2.4C and 2.4D**), indicating that plate-reader based mechano-HCR readout reported cell traction forces modulated by MLC inhibition. By fitting the data to a standard dose-response inhibition function (signal = 100/(1+[drug]/IC_{50})), we found that the mechano-IC_{50} = 7.7 μM (95% CI = 5.8-10.2 μM), which is in agreement with the reported IC_{50} ~ 5 μM that was obtained with cell morphology and kinase assays.[36] We plotted the fluorescence intensity obtained from microscopy imaging in these experiments in **Figure 2.21**. A two-way ANOVA analysis was performed to compare the plate reader and the microscopy normalized mechano-HCR signal, which showed no significant difference between these two modes for measuring the dose-response curve.

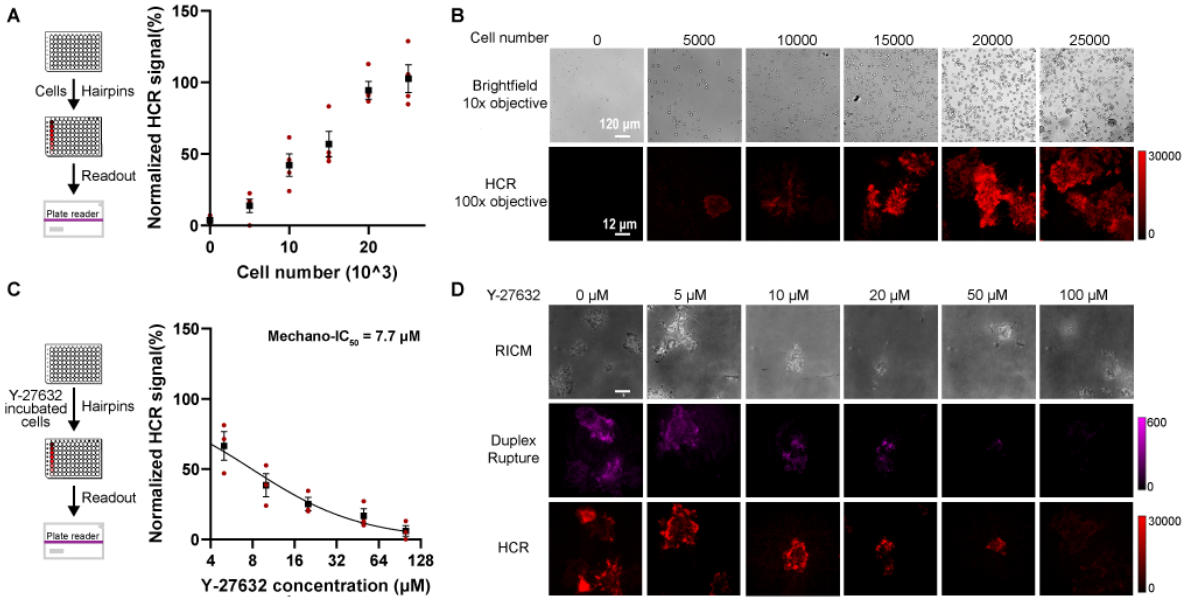

Figure 2.4: **Mechano-HCR to detect cell forces using a plate reader.** A) Schematic and plot showing plate reader mechano-HCR signal as a function of the number of cells seeded. A 96-well plate was used for these measurements. Error bar represents S.E.M. from 4 independent experiments, the individual experiments are shown as small red dots while the mean is indicated by black squares. The values were normalized to the signal obtained from the 25,000 cells/well samples. All measurements were background subtracted using negative control wells lacking cells. There is a strong correlation between the number of cells plated and the mechano-HCR signal. Note that at cell numbers greater than 20000, the signal plateaus. B) Representative bright field (10x objective) and mechano-HCR fluorescence (100x objective) from 96 well plates used to measure signal as a function of cell number. C) Schematic and plot of plate reader measured mechano-HCR signal as a function of Y-27632 concentration. Drug was incubated for 30 min prior to seeding. Error bar represents S.E.M. from 3 independent experiments. Mechano-IC50 was calculated by fitting plot to a standard dose-response function: normalized signal = 100/(1+[drug]/IC50). The values were normalized to the signal obtained from the 20,000 cells/well samples without drug treatment. All measurements were background subtracted using negative control wells lacking cells. D) Representative RICM and initiator rupture (magenta) and mechano-HCR (red) fluorescence images from wells used in dose-response measurement. Scale bar = 12 μm. 2.3.6 Dose-response screening drugs in mouse platelets

2.3.6 Drug screening of inhibitors for mouse platelet mechanics with mechano-HCR

Finally, to demonstrate mechano-HCR dose-response screening of drugs in primary cells, we investigated the mechanical signal of platelets under the influence of different antiplatelet drugs. Platelets are well suited for this type of screen because contractile forces are central in the function of platelets in resisting blood shear flow and in mechanically sealing of wound sites. Several platelet receptors such as glycoprotein Ib and integrin adhesion receptors have been identified as mechanosensors that mediate these functions.[37, 38] Moreover, abnormal force generation in human platelets is related to clotting disorders which can be mediated by genetic mutations as shown by Lam and colleagues[7] as well as trauma induced coagulopathy as demonstrated recently by Sniadecki et al.[6]. Therefore, rapid detection of platelet tension may offer new tools for diagnostic screening. We tested three drugs that target platelet coagulation function: ROCK inhibitor Y-27632 which inhibits MLC phosphorylation (as described above), integrin $\alpha_{IIb}\beta_3$ antagonist

eptifibatide - an FDA approved anti-clotting drug[39], and aspirin which inhibits the activity of cyclooxygenase (COX) and prevents formation of thromboxane A2 and thus functions as an anti-coagulation agent.[40, 41] In these experiments, we incubated purified mouse platelets with each drug at room temperature for 30 minutes. Then we plated 2×10^6 mouse platelets in each well for 1h and then performed the mechano-HCR assay. At the completion of the assay, and for each drug concentration tested, we measured the 12 pN duplex rupture signal (Atto647N) as well as the mechano-HCR signal (Cy3B) using both plate reader and high-resolution fluorescence microscopy. For all the compounds tested, we observed a dose-dependent decrease in the 12 pN duplex rupture in microscopy images (magenta color in **Figure 2.5A, 2.5C and 2.5 E**). Imaging of the same regions of interest in the mechano-HCR channel showed nearly identical patterns of signal (red color in **Figure 2.5A, 2.5C and 2.5 E**) based on the measured Pearson's correlation coefficient of 0.76 ± 0.07 (n=30 cells from 3 independent experiments). The agreement between these two fluorescence channels confirmed that mechano-HCR robustly amplified the density of initiator that was mechanically exposed by platelets.

We next took these same 96 well plates and measured the signal in the Cy3B channel using a conventional plate reader and this intensity was plotted alongside the average intensities obtained from optical microscopy (**Figure 2.5B, 2.5D, and 2.5F**). The plots for each dose-response curve represent the signal averaged from n=3 animals. The unamplified 12 pN DNA duplex rupture signal in the Atto647N channel was not detectable. As expected, the plate reader signal reflected the microscopy data and showed a dose-dependent decrease in the intensity for each well. A two-way ANOVA analysis comparing the plate reader and the microscopy mechano-HCR signal showed no significant difference between these two modes for measuring the dose-response curve.

Furthermore, the difference in signal intensity between different doses tested were statistically significant regardless of the readout mode ($P<0.0001$). By fitting the dose-response plots from the plate reader, we determined that the mechanical IC_{50} for Y-27632, eptifibatide, and aspirin were 1.6 μM (95% CI = 0.98-2.5 μM), 3.2 μM (95% CI = 2.6-3.8 μM), and 0.07 mM (95% CI = 0.06-0.09 mM), respectively. These values were found to be similar to reported IC_{50}'s in the literature (1 μM for Y-27632[42, 43], 5.7 μM for epitifibate[44], and 0.04 mM for aspirin[45]). This agreement is impressive given that the literature assays are fundamentally different and were inferred from platelet shape change or aggregation measurements. Table 2.5 summarizes the different methods used to determine literature IC_{50} values for these inhibitors. It is important to note that the plate reader readout is orders of magnitudes more rapid compared to the microscopy-based measurement, as the later requires the acquisition of hundreds of images that then further require masking and image analysis to determine the signal intensity from each cell. Second, microscopy data is markedly more heterogenous both when comparing between cells in the same well and when comparing cells in different wells (**Figure 2.5 and Figure 2.21**). Of course, the plate reader instrument is significantly less sensitive as a detector, but it has the inherent advantage of averaging the intensity from millions of cells in each well thus average the heterogeneity in signal caused by fluctuation in probe surface density and cell state. Although the sample preparation and cell incubation required ~3 hrs to complete, the mechano-HCR plate reader readout for 6 different drug concentrations required less than 1 minute. Therefore, this type of amplification and readout strategy represents an important milestone in enhancing the speed of data acquisition for characterizing cell traction forces.

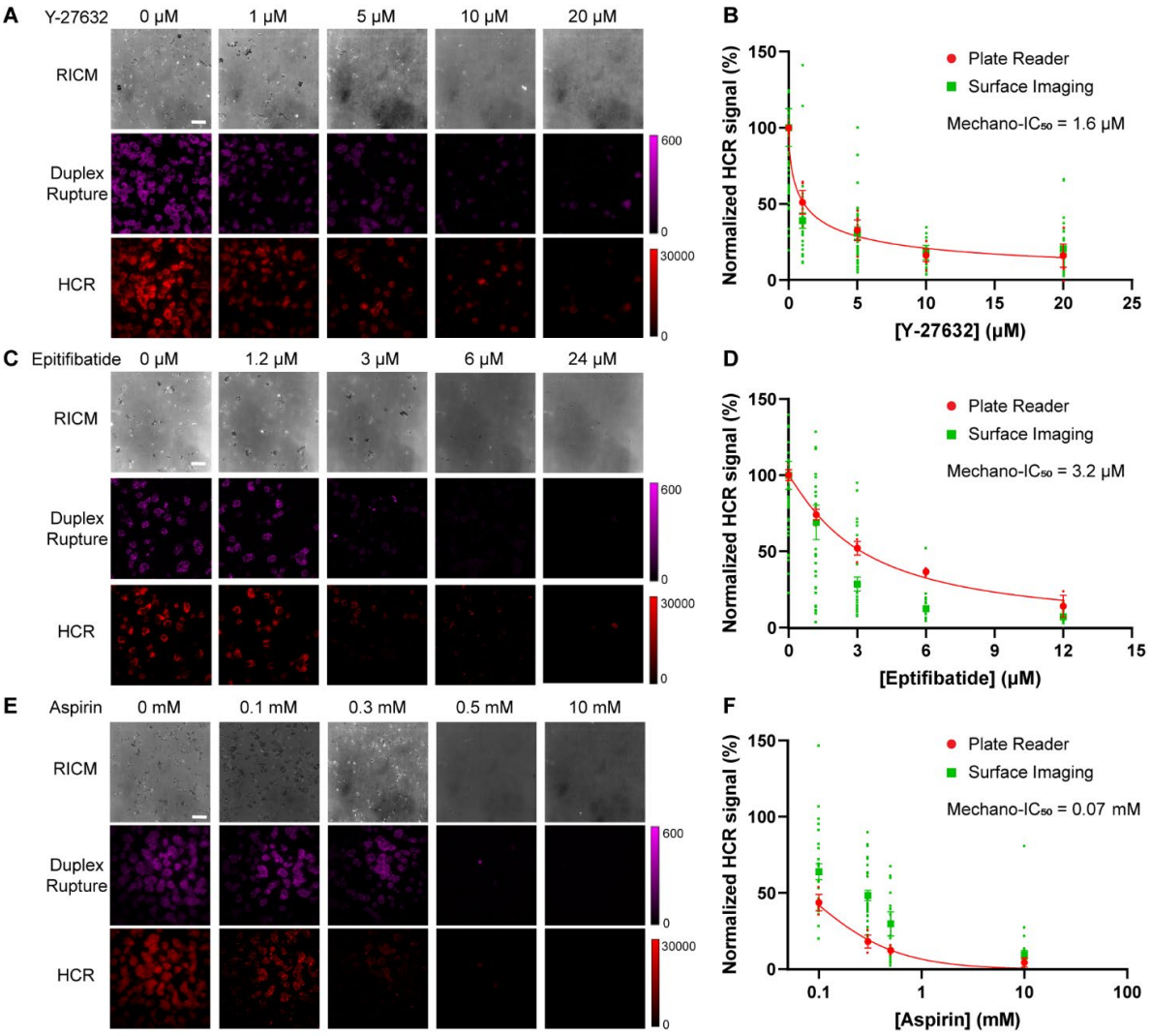

Figure 2.5: Using mechano-HCR to determine mechano-IC_{50} of platelet inhibitors. (A), (C) and (E) show representative RICM and initiator duplex rupture (magenta) and mechano-HCR (red) fluorescence images of mouse platelets that were treated with the ROCK inhibitor Y-27632, eptifibatide, and aspirin, respectively. Cells were treated with each drug for 30 min prior to mechano-HCR. Scale bar = 12 μm. $2x10^6$ cells were seeded in each well. (B), (D), and (F) show plots of normalized mechano-HCR signal as a function of Y-27632, eptifibatide, and aspirin concentration, respectively. Error bar represents S.E.M. from n=3 independent animal samples for plate reader readout, and n=30 cells from three independent animal samples for imaging-based readout. The values were normalized to the signal obtained from the $2x10^6$ cells/well samples without drug treatment. All measurements were background subtracted using negative control wells lacking cells. Mechano-IC_{50} was calculated by fitting plate reader tension readout to normalized signal = $100/(1+[drug]/IC_{50})$. The red data points are the mechano-HCR signals measured using a plate reader while the green data points were obtained using a fluorescence microscope from individual platelets.

2.4 Conclusion

In summary, we demonstrated that HCR can be triggered using a molecular biophysical event that exposes a cryptic initiator. While the HCR assay is widely used in mRNA detection in cells and tissue,[46] our work here represents the first example of using this amplification strategy for the quantification of specific pN events mediated by cell surface receptors. We applied the mechano-HCR assay to investigate the integrin receptor forces in fibroblasts and platelets and showed that this readout offers ~ one order of magnitude enhancement in S/N when compared to directly quantification of duplex rupture. As a result of this enhanced signal, we showed the ability for direct readout of integrin tension using a conventional plate reader without having to employ high magnification EMCCD-equipped fluorescence microscopy. Importantly, this capability enabled screening of the traction forces generated by different cells and their response to drug treatment on a plate reader instrument in a rapid manner. Mechano-HCR signal is linear proportional to the density of cells as lower cell densities and this signal plateaus as cells reach confluency. We also determined the mechano-IC_{50}, defined here as the concentration of drug that diminishes integrin traction forces by 50%, for two representative cell models: NIH/3T3 fibroblasts, mouse platelets, and tested responses of different classes of drugs such as ROCK inhibitor, eptifibatide and aspirin. The measured IC_{50} of each inhibitor closely agreed with reported values obtained using indirect methods that measure secondary signals and cell morphology. Currently, the gold-standard for measuring platelet function employs aggregation assays which are highly sensitive and are used in the clinic.[47] The mechano-HCR assay offers a complementary and potentially more direct method of screening cell function by measuring receptor forces. This assay could also be useful in evaluating therapeutics for other diseases of altered cellular contractility, such as asthma and cardiomyopathies.[48, 49] Moreover, the ability to conduct readout using a fluorescence plate reader

may offer more convenient and accessible readout. Also note that because of the isothermal and enzyme-free conditions used for HCR, the mechano-HCR assay carries advantages in sample preparation and reagent storage when compared to enzyme catalyzed amplification such as mechanically induced catalytic amplification reaction.[50] This feature allows potential integration of mechano-HCR with automated plate washers and plate imagers for higher throughput and automation. Note that mechano-HCR reflects the traction forces present at earlier time points because of the kinetics of HCR. Assays such as "exchange-mechano-HCR assay" where the hairpin monomers are barcoded with different dyes and washed into the sample periodically may offer the ability to time-stamp the mechano-HCR signals. Furthermore, advances in HCR such as controlled HCR[32], branched HCR[51] and FRET HCR [52] suggest future directions to improve mechano-HCR S/N, convenience by reducing wash steps, and other advantages in simplifying quantification to address the challenge. Finally, Mechano-HCR offers important potential in adoption for applications such as medium-throughput drug and cell screening in both biological research and clinics.

2.5 Materials and Methods

2.5.1 Chemicals and oligonucleotides

Cy3B-NHS ester (PA63101) was purchased from GE Healthcare Life Sciences (Pittsburgh, PA). Atto647N-NHS ester (18373) was purchased from Sigma Aldrich (St. Louis, MO). Cyclo[Arg-Gly-Asp-d-Phe-Lys(PEG-PEG)] (PCI-3696-PI) (cRGD) was acquired from Peptides International (Louisville, KY). Streptavidin (S000-01) was purchased from Rockland-Inc (Pottstown, PA). µ-Slide VI0.4 6-channel slides (80606) and 25 mm x 75 mm glass coverslips (10812) were purchased from Ibidi (Verona, WI). ProPlate® Microtiter (204969) are purchased from Thermo-Fisher Scientific. N-hydroxyl succinimide-5 kDa PEG-biotin (NHS-PEG-biotin, HE041024-5K) was purchased from Biochempeg (Watertown, MA). Sulfo-N-hydroxyl succinimide-acetate (sulfo-NHS-acetate26777) was purchased from Thermo-Fisher (Waltham, MA). (3-Aminopropyl) triethoxysilane (APTES, 440140, 99% purity) was purchased from Sigma-Aldrich, Adenosine 5‘-diphosphate (ADP, A2754, 95% purity) was purchased from sigma -Aldrich. All oligonucleotides are listed in Table 2.1 and purchased from Integrated DNA Technologies (Coralville, IA). All other reagents and materials (unless otherwise stated) were purchased from Sigma-Aldrich and used without purification. All buffers were prepared with 18.2 MΩ nanopure water.

Table 2.1. List of used oligonucleotides used in this Chapter

Name	Sequence (5' to 3')
Unzipping mode Initiator	/5AmMC6/GAG GAG GGC AGC AAA CGG GAA GAG TCT TCC TTT ACG TTT T /3Bio/
Shearing mode Initiator	/5Biosg/ TT/iAmMC6T/ GAG GAG GGC AGC AAA CGG GAA GAG TCT TCC TTT ACG T
BHQ2 Ligand Strand	/5 hexynyl/ ACG TAA AGG AAG ACT CTT CCC GTT TGC TGC CCT CCT C/3BHQ2/
H1	/5AmMC6/CGT AAA GGA AGA CTC TTC CCG TTT GCT GCC CTC CTC GCA TTC TTT CTT GAG GAG GGC AGC AAA CGG GAA GAG
H2	/5AmMC6/GAG GAG GGC AGC AAA CGG GAA GAG TCT TCC TTT ACG CTC TTC CCG TTT GCT GCC CTC CTC AAG AAA GAA TGC
Scramble ssDNA control	/5Hexynyl/CGC ATC TGT GCG GTA TTT CAC /iAmMC6T/TT T/3Bio/

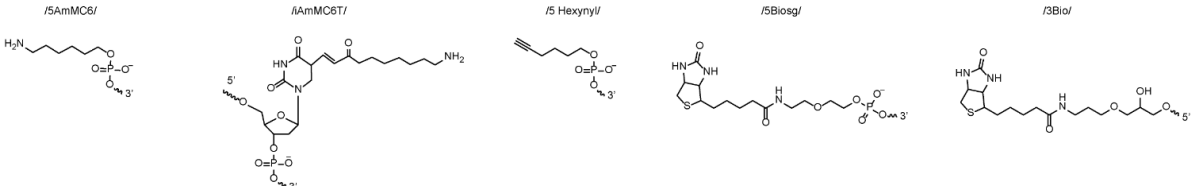

2.5.2 Instruments

We used two main microscopes for the work. The first was a Nikon Eclipse Ti microscope, operated by Nikon Elements software, using a 1.49 numerical aperture (NA) CFI Apo ×100 objective, perfect focus system, a TIRF laser launch, a Chroma quad cube (ET-405/488/561/640 nm Laser Quad Band) and an RICM (Nikon: 97270) cube for mechano-HCR experiments. The second was an N-STORM Nikon microscope (Ti E motorized inverted microscope body), operated by Nikon Elements software, equipped with an Intensilight epifluorescence source (Nikon), a CFI Apo 100X NA 1.49 objective was used in surface density characterization experiments and a Plan Fluor 10X objective was used to capture brightfield images of NIH/3T3 cells on 96 well plates. Bulk fluorescence measurements were conducted using a Synergy H1 plate reader (Bio-Tek) using fluorescence filter sets. All ultrapure water was obtained from a Barnstead Nanopure water purifying system (Thermo Fisher) that indicated a resistivity of 18.2 MΩ. Nucleic acid purification was performed using a high-performance liquid chromatography (HPLC, Agilent 1100) equipped with a diode array detector. Microvolume absorbance measurements were obtained using a Nanodrop 2000 UV-Vis Spectrophotometer (Thermo Scientific). Mass identification of product was performed with a Matrix-assisted laser desorption/ionization time-of-flight mass spectrometer (MALDI-TOF-MS, Voyager STR). Agarose gels were run with a Mini-Sub Cell GT Horizontal electrophoresis system and imaged with Gel Doc EZ imager (Bio-Rad)

2.5.3 Surface preparation method

Mechano-HCR surface preparation method was modified from previously published protocols.[3] Briefly, rectangular glass coverslips (25 x 75 mm, Ibidi) were rinsed with water and sonicated for

20 minutes in water and 20 minutes in 50% ethanol. The glass converslips were then cleaned with piranha solution. The piranha solution was prepared using a 1:3 mixture of H_2O_2 and H_2SO_4. WARNING: Piranha solution becomes very hot upon mixing, and is highly oxidizing and may explode upon contact with organic solvents. Then, slides were washed 6 times in beakers with ultrapure water, followed by 4 successive washes using ethanol. In a separate beaker of ethanol, slides were reacted with 3% v/v APTES at room temperature for 1 h. Coverslips were then washed 6 times with ethanol, baked in oven for 20 minutes at 80 °C. Slides were then reacted with NHS-PEG-biotin (1% w/v) for 1 hr in ultrapure water. Next, slides were washed 3 times with ultrapure water, dried under N_2 gas, and then stored at -30°C for up to 2 weeks before use. At the day of imaging, the 5kDa PEG-biotin surface was adhered onto µ-Slide VI0.4 6-channel ibidi slide or proplate microtiter with adhesive bottom. Wells were then reacted for 1hr with sulfo-NHS-acetate (1% w/v) in 0.5 M K_2SO_4 and 0.1M $NaHCO_3$ (pH 9) to consume any unreacted amines on the surface. To further reduce non-specific DNA binding during the imaging, the wells were then washed with 1XPBS and passivated with 5% v/v Tween 20 in T50 buffer for 30 min. The wells were then washed with 1XPBS and incubated with 50µg/ml streptavidin for one hour. The wells were then washed with 1XPBS and incubated with 100nM DNA probe solutions for 1 hr. Finally, the wells were washed with cell imaging buffer before imaging.

2.5.4 DNA hybridization

DNA oligonucleotides and DNA hairpins were hybridized at 100 nM in a 0.2 µL PCR tube. DNA was firstly heated to 90°C and then cooled at a rate of 1.3°C per min to 35°C. Hairpin strands were also annealed on the experimental day before use using this same protocol to ensure that the oligos adopt the folded state and hence reduce leakage of HCR polymerization. [53]

2.5.5 Oligo dye/ligand coupling and purification

All sequences of DNA strands used in this work are provided in **Supplementary 2.1**. Firstly, 100 nmoles of c(RGDfK(PEG-PEG)) was reacted with ~ 200 nmoles of NHS-azide in DMSO overnight (**Fig. 2.10**). Product 1 was then purified via reverse phase HPLC using a Grace Alltech C18 column (Solvent A: water + 0.05% TFA, Solvent B: acetonitrile + 0.05% TFA; starting condition: 90% A + 10 % B, 1%/min; Flow rate: 1 mL/min)

Purified product 1 was ligated to the BHQ_2 ligand strand via 1,3-dipolar cycloaddition click reaction. Briefly, 5 nmoles of alkyne ligand strand was reacted with ~70 nanomoles of product 1. The total reaction volume is 50 µL, composed of 0.1 M sodium ascorbate and 0.1 mM Cu-THPTA for 2h at room temperature. The product was then purified with a P2 size exclusion column, and then purified with reverse phase HPLC using Agilent Advanced oligo column (Solvent A: 0.1M TEAA, Solvent B: acetonitrile; starting condition: 90% A + 10 % B, 0.5%/min gradient B, Flow rate: 0.5 mL/min) (**Fig. 2.10**).

10 nmole Amine labelled hairpin strands were reacted overnight with a 20x excess of Cy3B-NHS dissolved in 10 µL DMSO. The total volume of the reaction was 100 µL, composed of 1x PBS supplemented with 0.1M $NaHCO_3$. Then P2 size exclusion gel was used to remove unreacted dye. The product was then purified by reverse phase HPLC using Agilent Advanced oligo column (Solvent A: 0.1M TEAA, Solvent B: acetonitrile; starting condition: 90% A + 10 % B, 1%/min gradient B, Flow rate: 0.5 mL/min) to purify products 4 and 5 (**Fig. 2.10**).

The retention times of all products and starting reagents are shown in **Fig. 10**. Concentrations of purified oligonucleotide conjugates were determined by measuring their A260 absorption value on a Nanodrop 2000 UV-Vis Spectrophotometer (Thermo Scientific). MALDI-TOF mass spectrometry was performed on high performance MALDI time-of-flight mass spectrometer (Voyager STR). The matrix for all experiments was freshly prepared by dissolving excess 3-hydroxypicolinic acid (3-HPA) in the matrix solvent (50% MeCN/H_2O, 1% TFA, 10% of 50 mg/mL ammonium citrate).

Table 2.2 MALDI-TOF analysis of modified oligonucleotides for this study

Sample	Calculated mass	m/z found	Error
Atto 647N Unzipping mode Initiator	14467	14882	2%
Atto 647N Shearing mode Initiator	13788	13372	3%
cRGDfk-BHQ2 strand	12783	12840	0.4%
Cy3B-H1	23376	23411	0.1%
Cy3B-H2	22986	23357	1%

2.5.6 Solution based hybridization chain reaction (HCR) and agarose gel electrophoresis

HCR reactions shown in **Figure 2.3** and **Figure 2.6** were performed at room temperature for 1.5 h with each hairpin at 1 μM concentration. DNA initiator was diluted to different concentrations (30, 3, 1.5, 0.3, and 0.03 μM) in ultrapure water. The initiator was added to H1 and H2 mixture solution to bring the final initiator concentration to 10, 1, 0.5, 0.1, and 0.01 μM. When initiator was absent (lane 7, **Figure 2.3b**), ultrapure water was added to bring the reaction volume to 30 μL.

After incubation, HCR samples were mixed with 6 μL of 6× gel loading buffer (15% (w/v) Ficoll (Type 400; Pharmacia) in H_2O) and loaded into a native 2% agarose gel, prepared with 1× TBE buffer and stained with ethidium bromide. The gel was run at 60 V for 90 min at 4ºC and imaged using a gel imager (Bio-Rad).

2.5.7 Mouse platelet handling

Blood from C57Bl/6J mice was collected by cardiac puncture, anticoagulated with acid citrate dextrose, added to equal volumes modified Tyrode's buffer (140mM NaCl, 2.7mM KCl, 0.4mM NaH_2PO_4, 10mM $NaHCO_3$, 5mM Dextrose, 10mM HEPES) containing 3U apyrase and centrifuged at 200xg for 5min. The platelet fraction was removed and to it added 1U apyrase and 1uM prostaglandin E1. Platelets were centrifuged at 700xg for 5min and resuspended in Walsh buffer (137mM NaCl, 2.7mM KCl, 1mM $MgCl_2$, 3.3mM NaH_2PO_4, 20mM HEPES, pH 7.4, 0.1% glucose, 0.1% bovine serum albumin) at a concentration of $1x10^9$ platelets/ml.[54] Experimental procedures were approved by the Emory University Institutional Animal Care and Use Committee.

2.5.8 Cell culture

Mouse embryonic fibroblasts (MEF) and NIH/3T3 fibroblasts were cultured according to ATCC guidelines. Briefly, cells were cultured in DMEM supplemented with 10% fetal bovine serum (v/v) and penicillin/streptomycin. Cells were passaged every 2-3 days as required.

2.5.9 Mechanically-triggered hybridization chain reaction

Mechanically-triggered Hybridization chain reaction was performed on the prepared biotin surface as described in the surface preparation section. First, hybridized TGT probes (prehybridized initiator and ligand strands) were incubated on biotin surface in 1x PBS buffer for 1h. The wells were washed with cell imaging buffer (DMEM with 1% FBS for 3T3 cells and Tyrodes buffer for platelets). Then, cells were added onto the cRGDfK-labelled duplex surfaces for 1h to promote cell adhesion. Subsequently, H1 and H2 solution were mixed in imaging buffer and added to the wells (96 well plates) or channels(ibidi slides) to initiate the HCR reaction with mechanically exposed initiator. After 2h of incubation, wells and channels were gently washed with 1ml cell imaging medium to remove non-reacted hairpins to decrease background. Afterwards, surfaces with exposed initiators and HCR polymers were imaged directly with fluorescence microscopy for high resolution characterization and quantification. Bulk fluorescence intensities on 96 well plates were measured with a Bio-Tek® Synergy H1 plate reader (Ex/Em = 540/590 nm for HCR channel and Ex/Em = 620/680 nm duplex rupture channel).

2.5.10 Dose-dependent inhibition of integrin mediated tension

For dose-dependent inhibition of integrin experiments, the cell density of 3T3 fibroblasts was first characterized with a hemocytometer. Same number of 3T3 cells (20000) in cell culture medium were then incubated with different concentrations of inhibitor in the cell culture incubator for 30 minutes before plating onto 96 well plates. Afterwards, cells were incubated for 1h to promote cell adhesion. Then the mechano-HCR protocol was followed to achieve amplification and quantification.

For platelet mechano-HCR measurements, mouse platelets were purified and incubated at room temperature for at least 30 min before beginning experiments. Platelets were then treated with drugs for 30 min before seeding onto 96 well-plates. 2 mM ADP was added to promote cell adhesion. Then platelets were incubated at room temperature for 1h. The same mechano-HCR protocols were followed to achieve amplification and quantification for platelets as is the case for 3T3 cells.

2.5.11 Microscopy imaging

For mechano-HCR experiments, Images were acquired on a Nikon Eclipse Ti microscope, operated by Nikon Elements software, a 1.49 NA CFI Apo 100x objective, perfect focus system, and a total internal reflection fluorescence (TIRF) laser launch with 488 nm (10 mW), 561 nm (50 mW), and 638 nm (20 mW). A reflection interference contrast microscopy (RICM) (Nikon: 97270) cube and a Chroma quad cube (ET-405/488/561/640 nm Laser Quad Band) were used for imaging. Imaging was performed on 96 well plates and glass coverslips using DMEM as cell imaging media for 3T3 cells and Tyrode's buffer for platelets. All imaging data was acquired at room temperature.

For surface characterization experiments, a Nikon Eclipse Ti microscope equipped with Evolve electron multiplying charge coupled device (Photometrics), an Intensilight epifluorescence source (Nikon), a CFI Apo 100X NA 1.49 objective was used. All of the imaging was performed using reflection interference contrast microscopy (RICM) and the Chroma filter cubes: TRITC, Cy5. Note that a Nikon Plan Fluor 10X objective was used to capture brightfield images of NIH/3T3 cells on 96 well plates shown in **Figure 2.4B**.

2.5.12 Determination of DNA surface density

We adapted a reported surface density quantification assay,[55] which converts the raw fluorescence intensity of a surface to the density of fluorescent molecules. In this assay, lipid membranes are used as fluorescence standards, because of their known density of fluorescent species. In this calibration, the intensity of labeled oligonucleotides and small unilamellar vesicles (SUVs) in solution are compared to determine the F factor, which relates molecular brightness of two fluorophores. The concentration of oligonucleotide probes on mechano-HCR surfaces is calculated using the F factor, along with a fluorescence calibration curve generated by imaging supported lipid bilayers (SLBs) of known dye density.

Small unilamellar vesicles (SUV) were made from 1,2-dioleoyl-sn-glycero-3-phosphocholine (DOPC) (850375C, Avanti Polar Lipids) and 1,2-dioleoyl-sn-glycero-3-phosphoethanolamine-N-(Cyanine 5) (Cy5-PE, 810335, Avanti Polar Lipids). First, lipids were added to a round-bottom flask containing chloroform. The mixture contained either 100 mol % DOPC or 99.9 mol% DOPC and 0.1 mol % Cy5 PE. Lipids were placed under rotary evaporation followed by an ultra-high-purity nitrogen stream to remove chloroform. SUVs were formed by sonicating the lipids in Nanopure water, with a lipid concentration of 2 mg/mL. To generate monodisperse unilamellar vesicles SUVs were freeze-thawed 3x and were extruded 10x. Extrusion was performed with a 10 mL LIPEX Extruder (Transferra Nanosciences, Inc.) containing a 0.08 μm polycarbonate filter (WHA110604, Whatman) and a drain disc (WHA230600, Whatman). The working concentration of Cy5-PE in the sample was experimentally calculated using a Thermo Scientific Nanodrop 2000c spectrophotometer.

To relate dye brightness, the brightness of known concentrations of labeled oligonucleotides and SUVs were measured in solution. Glass was passivated with 1% BSA in PBS for 35 min. Good quality measurements was assessed by looking at the ratio of concentration to intensity, as deviations can indicate nonspecific adsorption. The F factor labeled oligonucleotide and SUV brightness was defined as, $F = I_{\text{Atto647N}-DNA} / I_{\text{Cy5}-DHPE}$.

SUVs were also used to make supported lipid bilayers (SLBs) in glass-bottom 96-well plates (265300, Nunc). The glass was treated with a 2.6 M NaOH etch and was thoroughly washed with water followed by 1x PBS. To create a fluorescence calibration curve, SLBs with varying fluorophore concentration were prepared by adding mixtures of labeled and unlabeled SUVs in known stoichiometries. Excess SUVs were rinsed using water and PBS. The intensity of the SLBs was measured using epifluorescence microscopy. Using the known lipid footprint[55] (DOPC lipid footprint in supported bilayers of 0.72 nm^2), the resulting curve was used to relate absolute density of fluorophores to arbitrary fluorescence units. These data were then used to convert the intensity of initiator surfaces incubated with varying concentrations of initiators to initiators per micron squared. The equation of this conversion is shown in the **Figure 2.8**, $DNA\ density = 2 \times intensity \div (F \times slope)$.

2.6 Acknowledgement

I thank the help from Dr. Brian Petrich for providing insights and purifying mouse platelets in mouse platelets study. I thank Dr. Roxanne Glazier's help in preparing SLB and characterizing DNA density on surface. I thank Dr. Alisina Bazrafsan for his help with super-resolution images.

2.7 Appendix

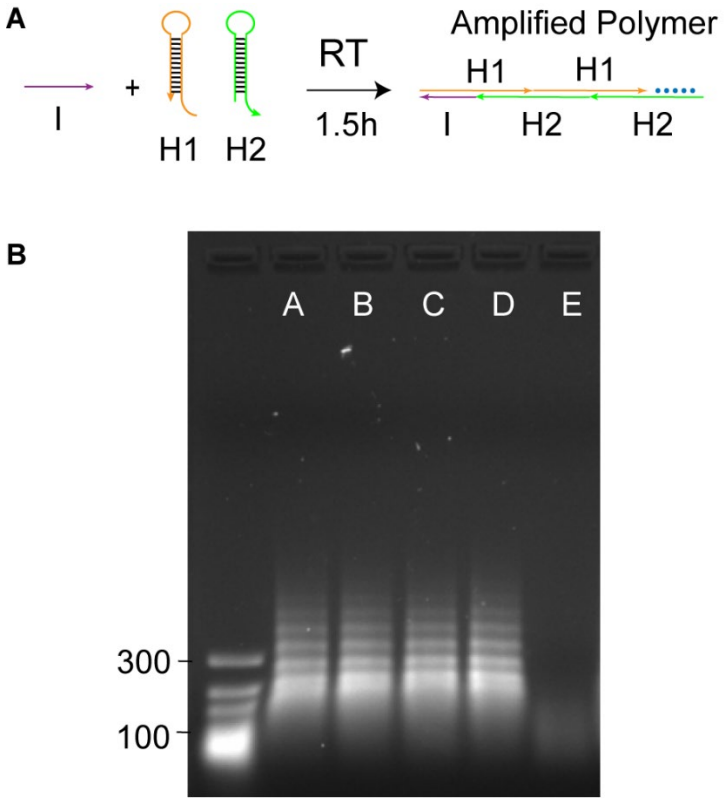

Figure 2.6. Agarose gels used to validate HCR polymers in different buffers. (A) Schematic shows the protocol used to initiate HCR. (B) Agarose gel electrophoresis of HCR products in different buffers. H1, H2 and initiator are at 1 μM concentration. Left lane: ultra-low range DNA ladders. A: HCR in 1xPBS, B: HCR in DMEM buffer, C: HCR in Hanks' buffer, D: HCR in Tyrode's buffer. E: H1 in 1xPBS buffer without I and H2.

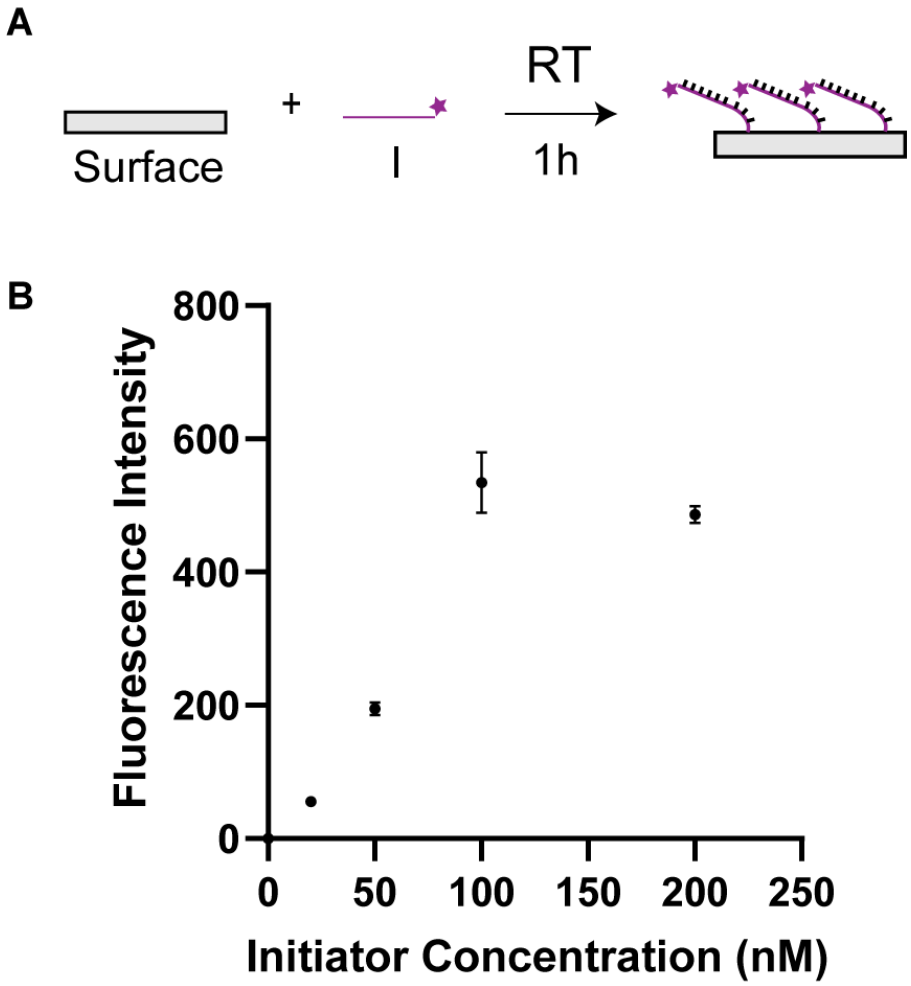

Figure 2.7: Characterization of surface coverage with different initiator concentration when incubated on prepared surface. (A) Schematic of immobilization of biotin labeled initiator on streptavidin surface (B) plots of fluorescence intensity of initiator on surface with initiator concentration when incubated on streptavidin surface (6 measurements per concentration per experiment, n = 3 independent experiments). Error bars represent the standard deviation from three independent experiments.

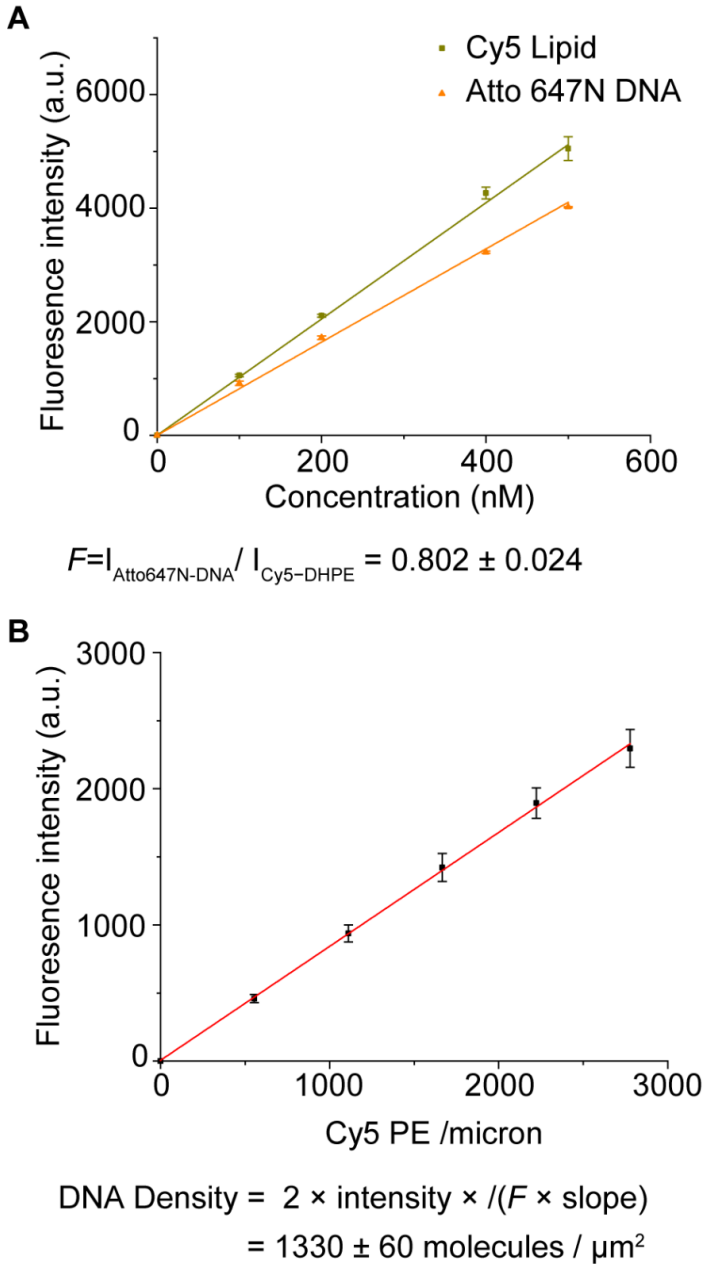

Figure 2.8. Quantifying DNA probe density on surface. (A) Plot of fluorescence intensity versus concentration for Cy5-tagged phospholipid vesicles and Atto647N-DNA. These measurements were performed in solution. Error bars represent the standard deviation from n = 3 independent preparations where each preparation was measured 5 times. F factor was calculated as the ratio of Atto647N to Cy5 fluorescence. Error calculated from the propagated standard deviation of Atto647N-DNA/Cy5-DHPE measurements. (B) Plot of fluorescence intensity versus Cy5 phospholipid per micron within the SLB (6 measurements from $n = 3$ independent experiments. This plot was used to convert the fluorescence measurements of Atto 647N-DNA initiator surface into molecular density. Probe density was 1330 ± 60 probes per square micron (Error calculated from propagated SEM).

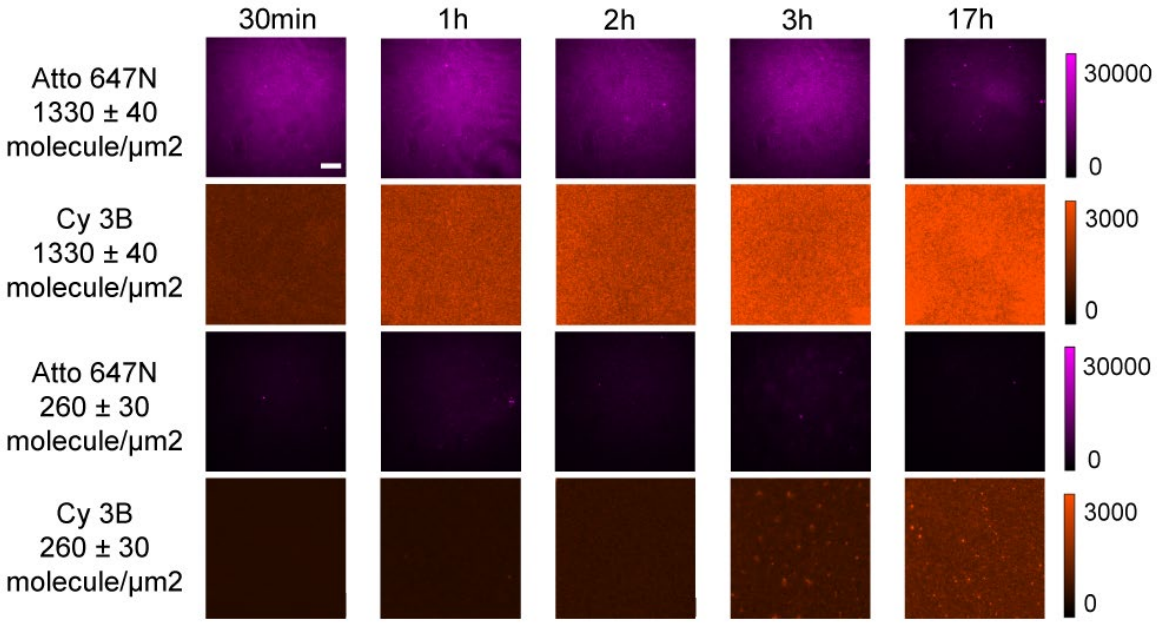

Figure 2.9. Representative fluorescence images showing surface density and surface HCR activity at different time point. The high-density initiator surfaces (top two rows) were generated by incubating the surface with 100 nM bulk concentration of DNA for 1 hr. The lower density surfaces (lower two rows) were created by incubating the substrates with 20 nM biotinylated DNA for 1 hr. Note that the magenta (Atto647N) signal is constant or is reduced as a function of time, since this signal only reports the density of initiator. In contrast, the Cy3B signal grows as a function of time due to the progress of the HCR. This data was used to generate the plot in figure 2D. Scale bar = 10 µm

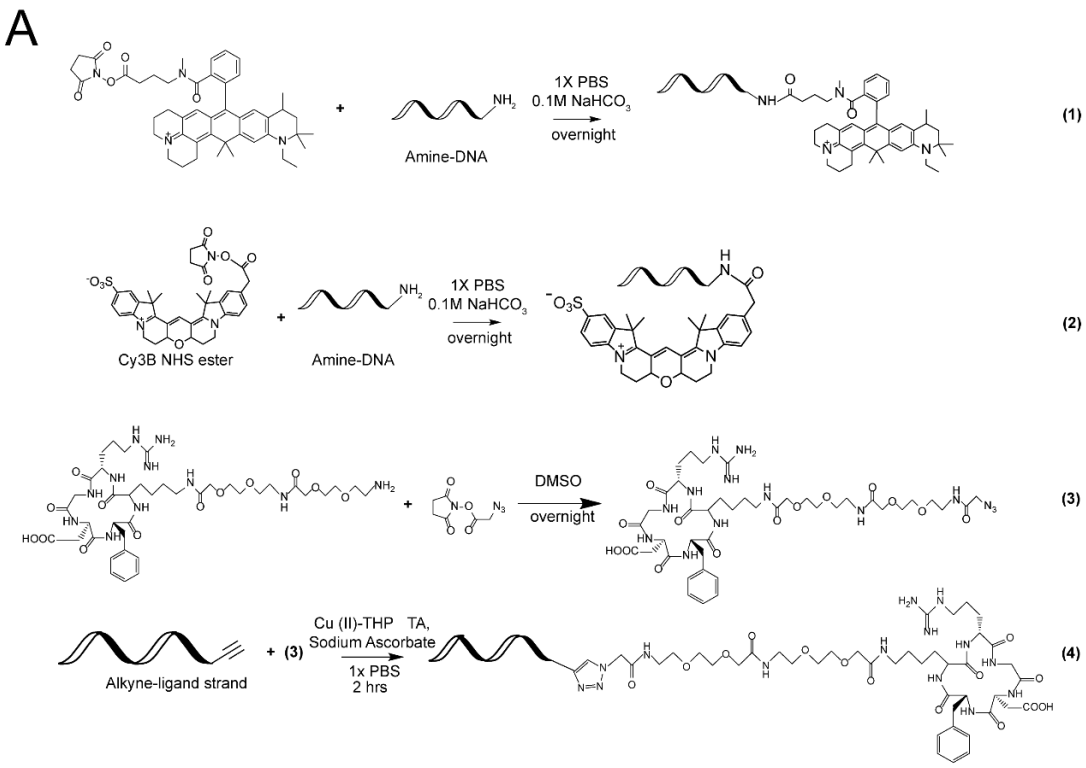
A
1X PBS
0.1M NaHCO3
overnight
Amine-DNA
(1)
Cy3B NHS ester
Amine-DNA
1X PBS
0.1M NaHCO3
overnight
(2)
DMSO
overnight
(3)
Alkyne-ligand strand
+ (3)
Cu (II)-THP TA,
Sodium Ascorbate
1x PBS
2 hrs
(4)

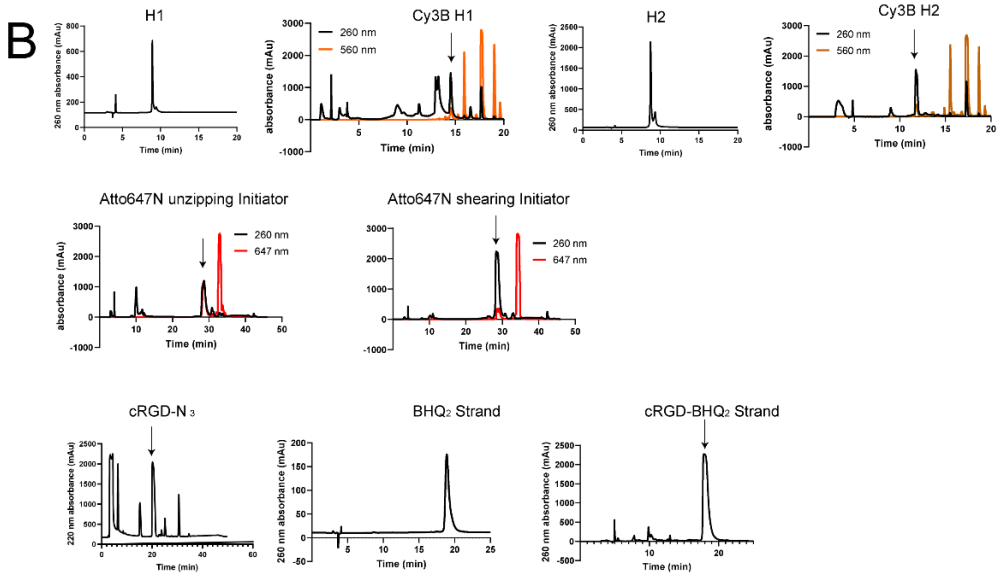
B
H1
Cy3B H1
H2
Cy3B H2
260 nm
560 nm
Time (min)
Atto647N unzipping Initiator
Atto647N shearing Initiator
260 nm
647 nm
cRGD-N3
BHQ2 Strand
cRGD-BHQ2 Strand

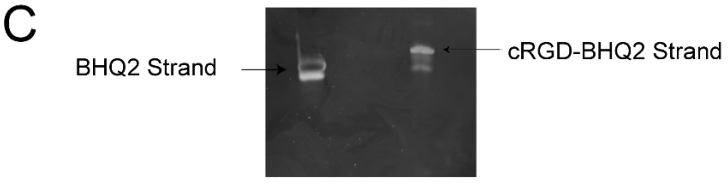
C
BHQ2 Strand
cRGD-BHQ2 Strand

Figure 2.10: Characterization of modified oligonucleotides. A) Chemical structures and reactions of oligonucleotides, dye NHS esters and cRGDfk peptides. (B) HPLC traces of reaction products. Reactions were monitored using 260 nm absorbance unless otherwise noted. Arrows indicate the peaks associated with the products and that were isolated for mass spectrometry analysis. (C) PAGE gel electrophoresis of BHQ2 strand starting material and the cRGDfk modified BHQ_2 strand product.

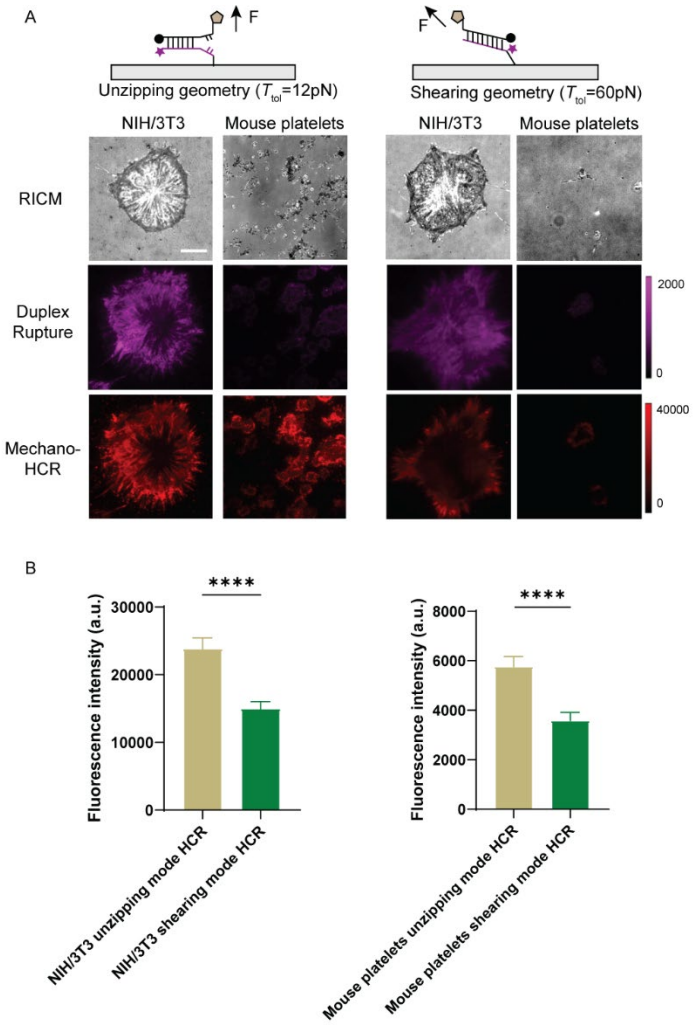

Figure 2.11. Comparison of mechano-HCR triggered by unzipping and shearing duplex rupture. (A) Schematic of DNA duplexes in the shearing and unzipping geometries with cryptic initiator used to study integrin-mediated forces (top). Representative RICM and fluorescence images of cells cultured on unzipping (T_{tol}=12 pN) and shearing (T_{tol}= 60 pN) surfaces after HCR amplification. Scale bar = 10 μm. The magenta color is emission from Atto647N that was used to tag the initiator (bottom strand), while the red channel shows the Cy3B emission that is due to H1 and H2 accumulation following HCR. The intensity bar next to each fluorescence image shows the absolute signal intensity for each image. (B) Bar graph quantifying the HCR fluorescence intensity for NIH/3T3 cells and mouse platelets on unzipping (T_{tol}= 12 pN) and shearing (T_{tol}= 60 pN) surfaces. The error bar represents S.E.M. from 36 cells in n=3 independent experiments (**** $p < 0.0001$, student t-test).

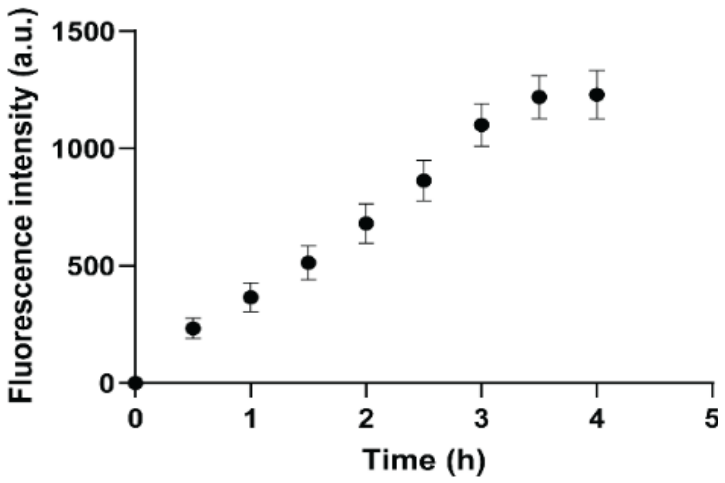

Figure 2.12. Time-resolved mechano-HCR using TIRF microscopy. Plot of time-dependent fluorescence intensity of mechano-HCR under cells measured with total internal reflection fluorescence (TIRF). Error bars represent S.E.M. obtained from three independent experiments. The intensity at each time point was determined by averaging the fluorescence signal from 12 cells in each experiment. The background intensity was quantified from regions outside of the cell at t = 0 hr, and this signal was subtracted from the measurements. The mechano-HCR experiment was performed as described in the methods section. NIH/3T3 cells were incubated on the surface for 1h before hairpin monomers were added. Representative real-time change of fluorescence for one cell is shown in movie 2.1

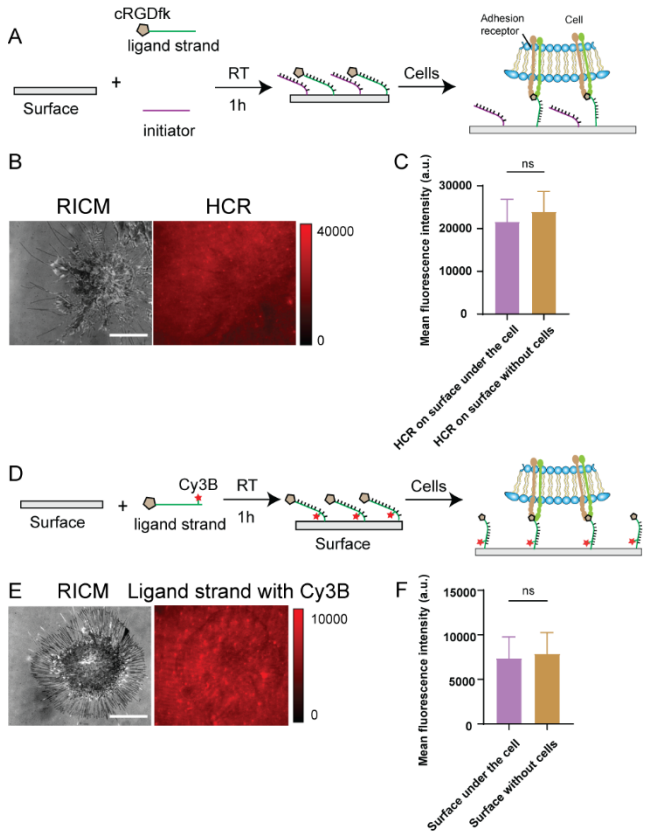

Figure 2.13. Controls showing that cell-surface junction does not significantly hinder mechano-HCR. (A) Schematic showing control surfaces that present a binary mixture of two oligonucleotides. The first was modified with the cRGD peptide and the second oligo functioned as the initiator for HCR. The surface was prepared by mixing a 1:1 ratio of these two oligonucleotides with total concentration = 100 nM. To test the mechano-HCR assay, we seeded 20,000 cells on the surface for 1h before hairpins were added to drive HCR amplification. (B) Representative RICM and fluorescence (Cy3B) images showing the signal due to HCR reaction. The HCR was allowed to proceed for 2 hr. Scale bar = 10 µm. (C) Plot of HCR fluorescence intensity in areas under the cell and outside cells. Error bar represents the standard deviation from n = 20 cells. The HCR signal is slightly reduced under the cell, but the decrease is not statistically significant (based on student's *t* test). (D) To test if nucleases contribute to the loss of fluorescence under the cells, we designed control surface that presented a monolayer of ssDNA that is Cy3B and cRGD modified. Surfaces were prepared by incubating with a 100 nM solution of the nucleic acid. Following our standard procedures, 20,000 cells were seeded on the surface for 1h prior to imaging. (B) Representative RICM and fluorescence (Cy3B) images of this control experiment. Scale bar = 10 µm. Note that the brightness of this surface is lower here because there was no HCR amplification performed in this control. (F) Plot of fluorescence intensity of Cy3B in areas under the cell and outside the cell attachment regions. Error bar represents SD from n = 20 cells. Consistent with the plots in (C), the fluorescence signal under the cells is slightly reduced but is not significantly different from that of the regions outside of the cell.

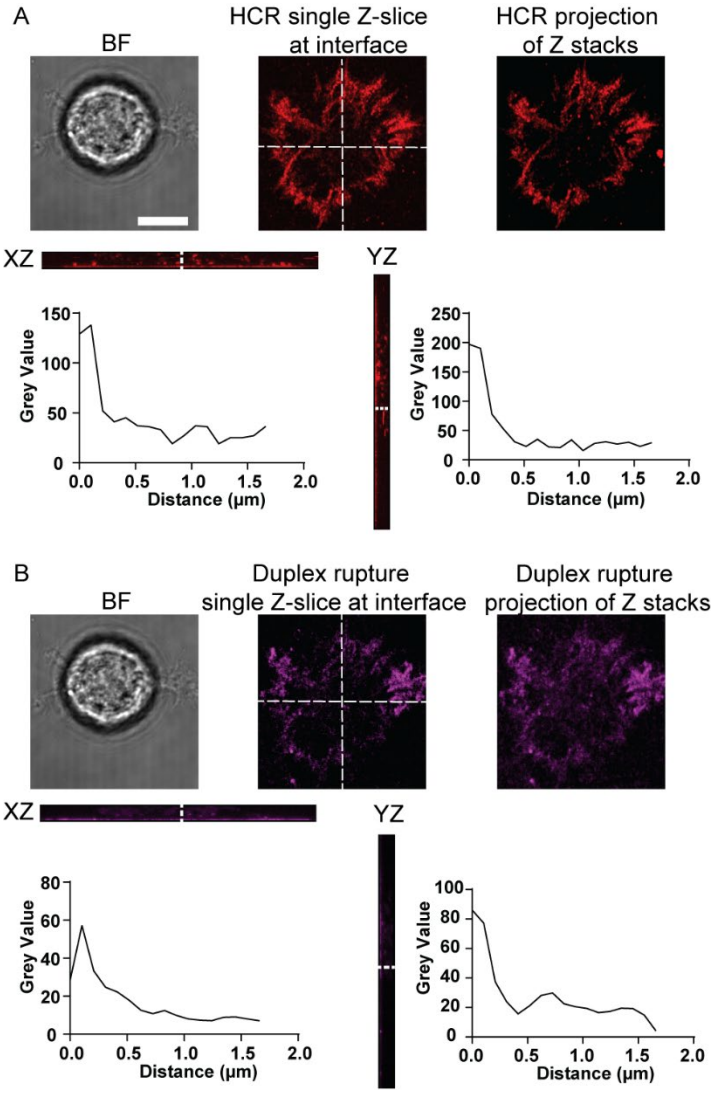

Figure 2.14. Confocal Z-stack images showing mechano-HCR signal is primarily localized to the cell-surface junction. (A) Representative brightfield, fluorescence image showing a single z slice of the HCR signal, and projection of *z* stack of images on the *x*-*y* plane. The single z-slice was collected at the cell-surface junction. Dashed white lines indicate the location of line scans in the *x*-*z* and the *y*-*z* projection. Scale bar = 10 μm. Plots show the fluorescence intensity as a function of distance for the line scans indicated on the image. The data indicates that the HCR product is confined to a diffraction limited plane along the substrate surface. (B) Representative brightfield, fluorescence image showing a single z slice of the duplex rupture signal, and projection of *z* stack of images on the *x*-*y* plane. The single z-slice was collected at the cell-surface junction. Dashed white lines indicate the location of line scans in the *x*-*z* and the *y*-*z* projection. Scale bar = 10 μm. Plots show the fluorescence intensity as a function of distance for the line scans indicated on the image. The data indicates that the duplex rupture signal is localized to the substrate surface as expected.

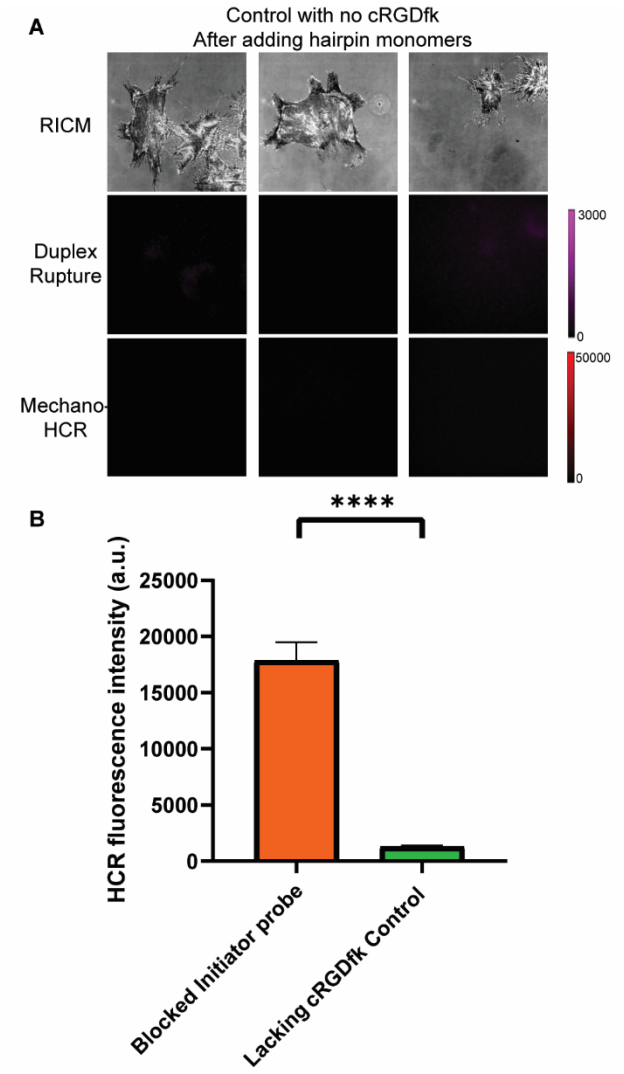

Figure 2.15. Characterization of nonspecific HCR signal using cRGDfk lacking oligonucleotide controls. (A) Representative RICM, Atto647N and Cy3B images for cells incubated on DNA duplex surface lacking cRGDfk ligand after the H1 and H2 monomers were added for 2h. Scale bar = 10 μm. (B) Bar graph showing the fluorescence intensity of mechano-HCR chips measured using fluorescence microscopy. The orange bar shows the +cRGDfK (positive control group) while the green bar shows identical substrates that were modified with -cRGDfK (negative control group). Error bar representative S.E.M. of 8 measurements from $n = 3$ independent experiments (****$p < 0.0001$, student t-test).

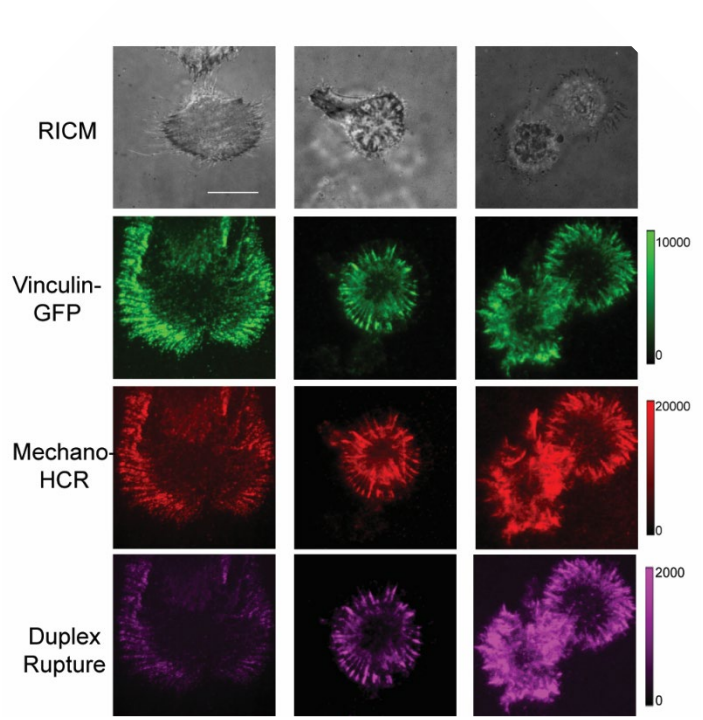

Figure 2.16. Colocalization between focal adhesion and mechano-HCR with vinculin-GFP MEF cells. (A) Representative RICM, FITC, Cy3B and Atto647N channel microscope images of mechano-HCR performed using vinculin-GFP expressing mouse embryonic fibroblasts. Fluorescence images show colocalization between focal adhesions and the mechano-HCR amplified signal with a measured Pearson's correlation coefficient of 0.81 ± 0.05 (n = 15 cells from 3 independent experiments). Scale bar = 12 μm.

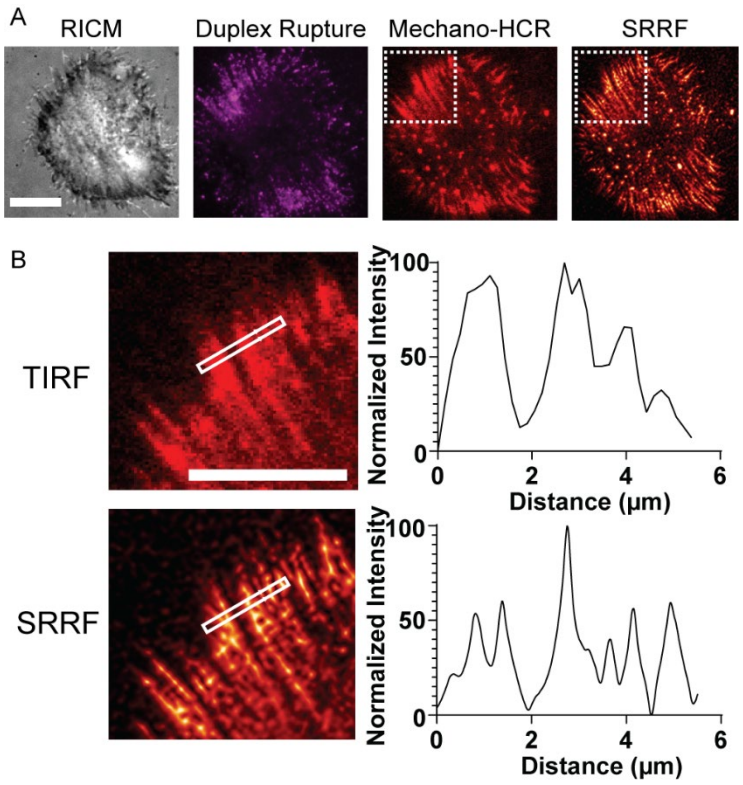

Figure 2.17. SRRF super resolution imaging showing improved resolution of mechano-HCR. (A) Representative RICM and fluorescence images of NIH/3T3 cells imaged using super-resolution radial fluctuations (SRRF) experiments. The image shown in magenta represents the Atto647N channel used to tag the initiator (bottom strand) while the red channel shows the Cy3B emission from H1 and H2 accumulation following HCR. Scale bars = 10 um. White dashed box indicates the region of interest that is highlighted in B. Super resolved imaging via SRRF was performed on a 20 second time lapse series of 1000 frames with 20 ms exposure time in the mechano-HCR channel. In SRRF analysis, ring radius was set as 0.5; ring magnification was 10 and the axes in ring were set to 8. (B) Zoom in of the ROI from (A) and plot of line scan showing improved resolution using SRRF compared to conventional TIRF image. Scale bar = 10 μm. This data shows that the mechano-HCR signal is amenable to super resolution imaging methods. SRRF HCR images are representative of 3 independent experiments.

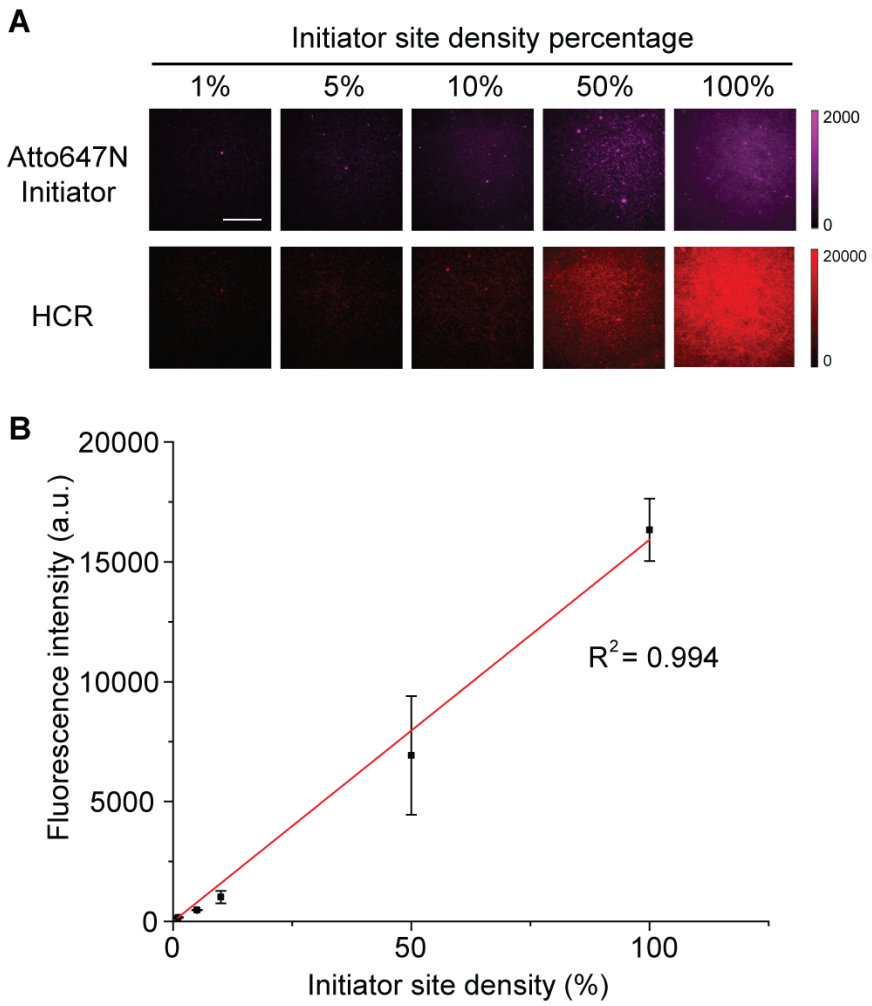

Figure 2.18. Quantification of HCR intensity as a function of initiator site density. (A) Representative fluorescence images showing Atto647N intensity and Cy3B intensity as a function of initiator site density following 2 hr HCR. Scale bar = 10 μm. To tune the initiator surface density, we mixed the initiator with a scrambled initiator that was also biotinylated. The total oligonucleotide concentration was maintained at 100 nM for all measurements. (B) Plot of HCR fluorescence intensity versus initiator site density. Linear regression showed an $R^2 = 0.994$ which indicates a linear relationship at the conditions tested. Error bar represents SD from 8 measurements from $n = 3$ experiments.

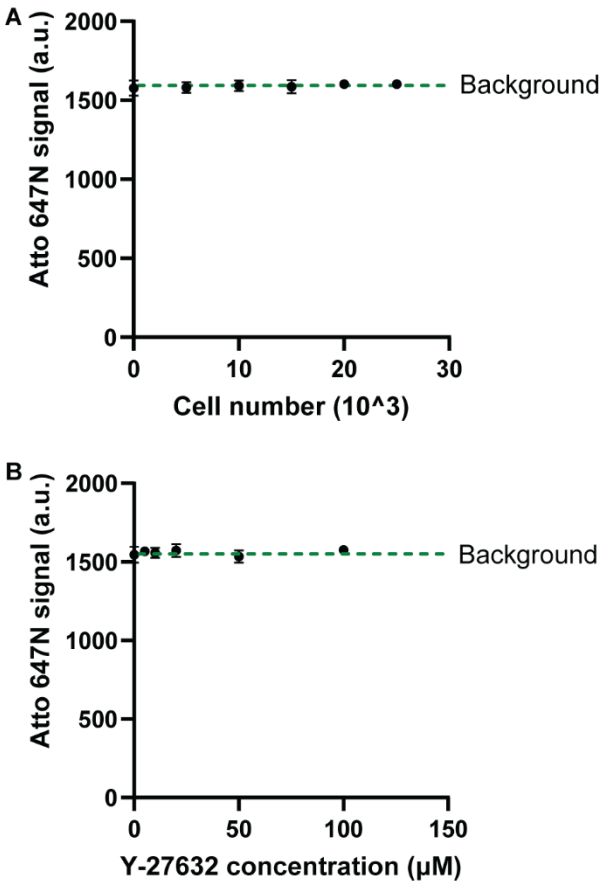

Figure 2.19. Controls showing that plate reader fails to detect duplex rupture signal. (A) Plot of DNA duplex unzipping fluorescence as a function of cell plating number (NIH/3T3 cells). (B) Plot of DNA unzipping fluorescence intensity as a function of Y-27632 dose for 20,000 cells plated per well. For both plots, the data was collected using a plate reader measuring the emission of the Atto647N reporter >2 hrs after cell seeding. Note that the same plate reader and settings were used to detect the mechano-HCR signal shown in Figure 3 & 4 in the main text. Error bar represents S.E.M. from n = 3 independent experiments. Dashed green line represents the background intensity generated from a surface that lacked the DNA probes. The background was calculated by averaging the signal from three control surfaces lacking DNA.

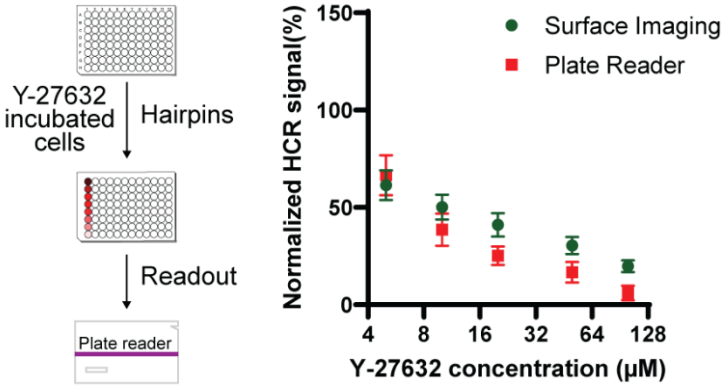

Figure 2.20. Comparison between microscopy and plate reader HCR signal for NIH/3T3 cells. Schematic and plot of plate reader measured mechano-HCR signal as a function of Y-27632 concentration. Drug was incubated for 30 min prior to seeding. Error bar represents S.E.M. from 3 independent experiments. The values were normalized to the signal obtained from the 20,000 cells/well samples without drug treatment. All measurements were background subtracted using negative control wells lacking cells. The red points are the mechano-HCR signals measured using a plate reader while the green points were obtained using a fluorescence microscope from individual platelets.

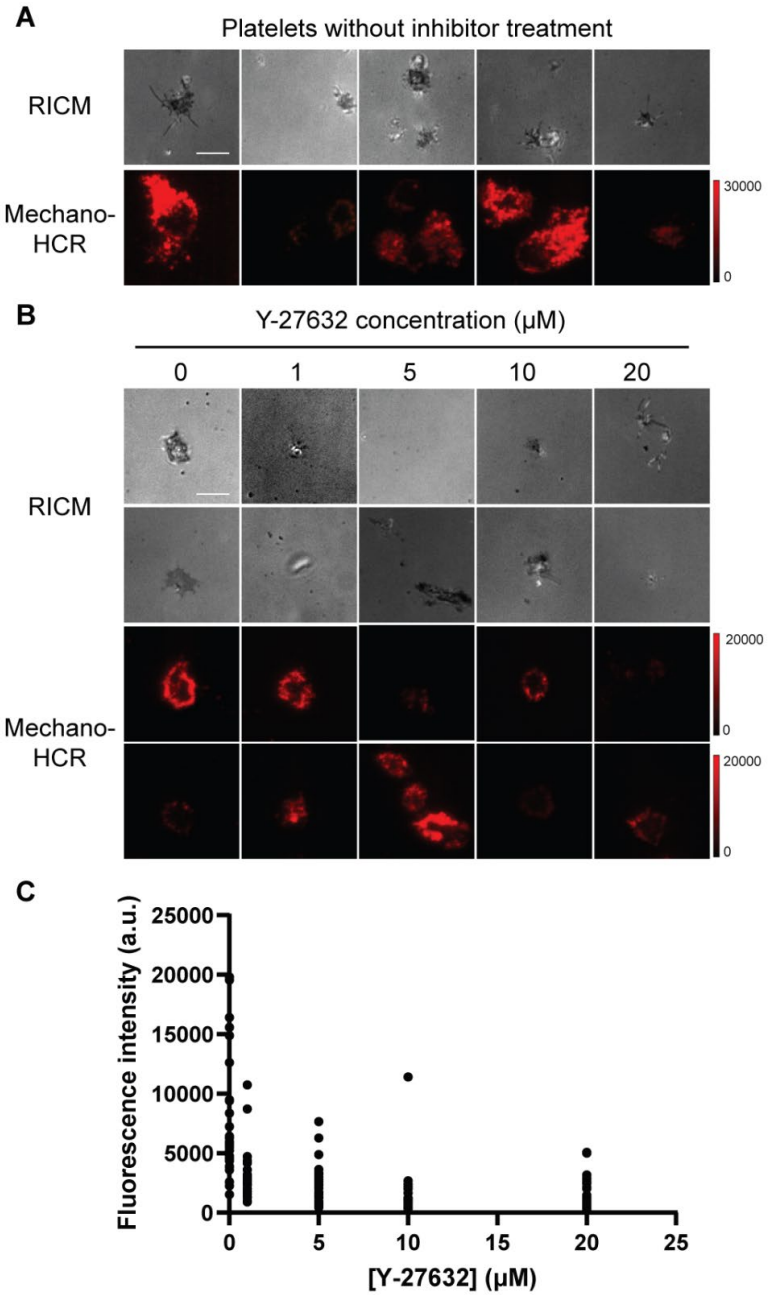

Figure 2.21. Examples showing cell to cell heterogeneity for mouse platelets mechano-HCR signal. (A) Representative RICM and fluorescence images showing the variability between individual platelets that were isolated from the same animals and cultured in the same well under identical conditions. Scale bar = 5 μm. (B) Representative RICM and fluorescence images showing cell to cell variability of individual platelet mechano-HCR signal when compared between different wells. Scale bar = 5 μm. Mouse platelets were incubated with different doses of the ROCK inhibitor for 30 min and then added to 96 well plates for 1 hr and then imaged. (C) Plot of mechano-HCR fluorescence intensity of individual platelets obtained from fluorescence images as a function of Y-27632 concentration, n=30 cells from three independent animal samples.

Table 2.3. Representative literature investigating force spectroscopy of DNA

Title	Year	Journal	Notes
Dynamic force spectroscopy of single DNA molecules[56]	1999	Proc. Natl. Acad. Sci. USA	AFM force-spectroscopy to study separation of DNA duplex
Force-induced melting of a short DNA double helix[57]	2001	Eur. Biophys. J.	AFM measurements of force-induced melting of short DNA duplexes
Measurement of the phase diagram of DNA unzipping in the temperature-force plane[58]	2004	Phys. Rev. Lett.	Magnetic tweezer study of DNA unzipping at different temperatures
Single-molecule cut-and-paste surface assembly[59]	2008	Science	AFM based transfer of DNA strands across a surface
Unraveling the structure of DNA during overstretching by using multicolor, single-molecule fluorescence imaging[60]	2009	Proc. Natl. Acad. Sci. USA	Combined optical tweezers/fluorescence microscopy of DNA meltings under force
Single-molecule derivation of salt dependent base-pair free energies in DNA[61]	2010	Proc. Natl. Acad. Sci. USA	Optical tweezer and modeling of mechanical unzipping of single DNA molecules
Maximum pull out force on DNA hybrids[62]	2001	C. R. Acad. Sci., Ser. IV: Phys.	Modeling of forces on DNA hybrids
Shear unzipping of DNA[63]	2009	J. Phys. Chem. B	Modeling of unzipping of DNA duplexes
Force-induced rupture of a DNA duplex: from fundamentals to force sensors[64]	2015	ACS Nano	Modeling of force-induced rupture of DNA duplexes with course-grained oxDNA

Table 2.4 Representative literature describing the use of DNA-based tension sensors to characterize cell forces.

Title	Year	Journal	Notes
DNA-based digital tension probes reveal integrin forces during early cell adhesion[65]	2014	Nat. Commun.	First report of a DNA hairpin tension sensor
DNA-based nanoparticle tension sensors reveal that T-cell receptors transmit defined pN forces to their antigens for enhanced fidelity[65]	2016	Proc. Natl. Acad. Sci. USA	T cells transmit pN forces to their TCRs to regulate immune response
Notch-Jagged complex structure implicates a catch bond in tuning ligand sensitivity[66]	2017	Science	DNA probes to study Notch mechanosensor model
B cell antigen extraction is regulated by physical properties of antigen-presenting cells[19]	2017	J. Cell Biol.	DNA probes to study B cell receptors mechanobiology
Platelet integrins exhibit anisotropic mechanosensing and harness piconewton forces to mediate platelet aggregation[18]	2018	Proc. Natl. Acad. Sci. USA	DNA probes used to study platelet activation and shows that 12-56 pN integrin tension is associated with the earliest steps of platelet activation.
Real-time measurement of molecular tension during cell adhesion and migration using multiplexed differential analysis of tension gauge tethers[67]	2019	ACS Biomater. Sci. Eng.	DNA duplex rupture probes to study fibroblast cell forces
EGFR activation attenuates the mechanical threshold for integrin tension and focal adhesion formation[68]	2020	J. Cell Sci.	DNA duplex probes used to study how EGFR regulates integrin tension and organization of focal adhesions
Live-cell super-resolved PAINT imaging of piconewton cellular traction force[69]	2020	Nat. Methods	DNA tension probes imaged using DNA-PAINT technique

Table 2.5 Literature reported IC_{50} for drugs used in this Chapter

Inhibitors	Target	Measuring approach	IC_{50}	Reference
Y-27632	*Fibroblast*	*Kinase Essay in vitro*	*~5 μM*	*Mitchison et al.*[70]
Y-27632	Fibroblast	Morphology assays (Focus formation)	10 μM (Full inhibation concentration)	Treisman et al. [36]
Y-27632	*Platelets*	*Shape change*	*~1.1 μM*	*Kunapuli et al.*[71]
Epitifibatide	*Platelets*	*Shear induced Adhesion*	*5781 nM*	*Feuerstein et al.*[44]
Epitifibatide	Platelets	ADP induced aggregation	0.66 μM	*Kleiman et al*[72]
Aspirin	*Platelets*	*AA induced aggregation*	*41.2 μM*	*Osawa et al.*[73]
Aspirin	Platelets	AA induced aggregation	24.3 μM	*Sorensen et al.*[74]
Aspirin	COX-1	Enzyme immunoassay	3.57 μM	*Galdo e al.* [75]

*Note that the entries denoted in italic text indicates the literature IC_{50} values that we compare against the mechano-IC_{50} values we measured in this work. These were selected from amongst the various reported values because the cell type and protocols best matched our approaches.

Movie 2.1: Real time mechano-HCR amplification in cell experiments. Raw timelapse of fibroblasts showing the mechano-HCR with hairpins in 240 minutes time window. Tension signal in TIRF quickly increased during the first 2h. Scale bar (in white) = 12 μm

Movie 2.2: Z stack images of mechano-HCR signal with a confocal microscope. Confocal images of Z stack show that mechano-HCR signal mainly locate at the cell-surface interaction. Scale bar (in white) = 8 μm.

2.8 References

1. Ladoux, B. & Mège, R.-M. Mechanobiology of collective cell behaviours. *Nat. Rev. Mol. Cell Biol.* **18**, 743-757 (2017).
2. Orr, A.W., Helmke, B.P., Blackman, B.R. & Schwartz, M.A. Mechanisms of mechanotransduction. *Dev. Cell* **10**, 11-20 (2006).
3. Liu, Y. et al. DNA-based nanoparticle tension sensors reveal that T-cell receptors transmit defined pN forces to their antigens for enhanced fidelity. *Proc. Natl. Acad. Sci. U.S.A.* **113**, 5610-5615 (2016).
4. Vining, K.H. & Mooney, D.J. Mechanical forces direct stem cell behaviour in development and regeneration. *Nat. Rev. Mol. Cell Biol.* **18**, 728-742 (2017).
5. Orr, A.W., Helmke, B.P., Blackman, B.R. & Schwartz, M.A. Mechanisms of mechanotransduction. *Dev. Cell* **10**, 11-20 (2006).
6. Ting, L.H. et al. Contractile forces in platelet aggregates under microfluidic shear gradients reflect platelet inhibition and bleeding risk. *Nat. Commun.* **10**, 1-10 (2019).
7. Myers, D.R. et al. Single-platelet nanomechanics measured by high-throughput cytometry. *Nat. Mater.* **16**, 230-235 (2017).
8. Carr, M.E. Development of platelet contractile force as a research and clinical measure of platelet function. *Cell Biochem. Biophys.* **38**, 55-78 (2003).
9. Wang, X. & Ha, T. Defining single molecular forces required to activate integrin and notch signaling. *Science* **340**, 991-994 (2013).
10. Gaudet, C. et al. Influence of type I collagen surface density on fibroblast spreading, motility, and contractility. *Biophys. J.* **85**, 3329-3335 (2003).

11. Liu, Y., Galior, K., Ma, V.P.-Y. & Salaita, K. Molecular tension probes for imaging forces at the cell surface. *Acc. Chem. Res.* **50**, 2915-2924 (2017).

12. Stabley, D.R., Jurchenko, C., Marshall, S.S. & Salaita, K.S. Visualizing mechanical tension across membrane receptors with a fluorescent sensor. *Nat. Methods* **9**, 64-67 (2012).

13. Ma, V.P.Y. & Salaita, K. DNA nanotechnology as an emerging tool to study mechanotransduction in living systems. *Small* **15**, 1900961 (2019).

14. Zhang, Y., Ge, C., Zhu, C. & Salaita, K. DNA-based digital tension probes reveal integrin forces during early cell adhesion. *Nat. Commun.* **5**, 1-10 (2014).

15. Kim, S.B., Nishihara, R., Citterio, D. & Suzuki, K. Genetically encoded molecular tension probe for tracing protein–protein interactions in mammalian cells. *Bioconjug. Chem.* **27**, 354-362 (2016).

16. Ma, R. et al. DNA probes that store mechanical information reveal transient piconewton forces applied by T cells. *Proc. Natl. Acad. Sci. U. S. A.* **116**, 16949-16954 (2019).

17. Wan, Z. et al. The activation of IgM-or isotype-switched IgG-and IgE-BCR exhibits distinct mechanical force sensitivity and threshold. *Elife* **4**, e06925 (2015).

18. Zhang, Y. et al. Platelet integrins exhibit anisotropic mechanosensing and harness piconewton forces to mediate platelet aggregation. *Proc. Natl. Acad. Sci. U. S. A.* **115**, 325-330 (2018).

19. Spillane, K.M. & Tolar, P. B cell antigen extraction is regulated by physical properties of antigen-presenting cells. *J. Cell Biol.* **216**, 217-230 (2017).

20. Jo, M.H., Cottle, W.T. & Ha, T. Real-time measurement of molecular tension during cell adhesion and migration using multiplexed differential analysis of tension gauge tethers. *ACS Biomater. Sci. Eng.* **5**, 3856-3863 (2018).

21. Adams, J. Biotin amplification of biotin and horseradish peroxidase signals in histochemical stains. *J. Histochem. Cytochem.* **40**, 1457-1463 (1992).

22. Gootenberg, J.S. et al. Multiplexed and portable nucleic acid detection platform with Cas13, Cas12a, and Csm6. *Science* **360**, 439-444 (2018).

23. Ding, X. et al. Ultrasensitive and visual detection of SARS-CoV-2 using all-in-one dual CRISPR-Cas12a assay. *Nat. Commun.* **11**, 4711 (2020).

24. Dirks, R.M. & Pierce, N.A. Triggered amplification by hybridization chain reaction. *Proc. Natl. Acad. Sci. U. S. A.* **101**, 15275-15278 (2004).

25. Choi, H.M., Beck, V.A. & Pierce, N.A. Next-generation in situ hybridization chain reaction: higher gain, lower cost, greater durability. *ACS Nano* **8**, 4284-4294 (2014).

26. Galush, W.J., Nye, J.A. & Groves, J.T. Quantitative fluorescence microscopy using supported lipid bilayer standards. *Biophys. J.* **95**, 2512-2519 (2008).

27. Glazier, R. et al. DNA mechanotechnology reveals that integrin receptors apply pN forces in podosomes on fluid substrates. *Nat. Commun.* **10**, 1-13 (2019).

28. Brockman, J.M. et al. Live-cell super-resolved PAINT imaging of piconewton cellular traction forces. *Nat. Methods* **17**, 1018-1024 (2020).

29. Mosayebi, M., Louis, A.A., Doye, J.P. & Ouldridge, T.E. Force-induced rupture of a DNA duplex: from fundamentals to force sensors. *ACS Nano* **9**, 11993-12003 (2015).

30. Hatch, K., Danilowicz, C., Coljee, V. & Prentiss, M. Demonstration that the shear force required to separate short double-stranded DNA does not increase significantly with sequence length for sequences longer than 25 base pairs. *Phys. Rev. E* **78**, 011920 (2008).

31. Pfaff, M. et al. Selective recognition of cyclic RGD peptides of NMR defined conformation by alpha IIb beta 3, alpha V beta 3, and alpha 5 beta 1 integrins. *J. Biol. Chem.* **269**, 20233-20238 (1994).

32. Figg, C.A., Winegar, P.H., Hayes, O.G. & Mirkin, C.A. Controlling the DNA hybridization chain reaction. *J. Am. Chem. Soc.* **142**, 8596-8601 (2020).

33. Gustafsson, N. et al. Fast live-cell conventional fluorophore nanoscopy with ImageJ through super-resolution radial fluctuations. *Nat. Commun.* **7**, 1-9 (2016).

34. Krishnan, R., Park, J.-A., Seow, C.Y., Lee, P.V. & Stewart, A.G. Cellular biomechanics in drug screening and evaluation: mechanopharmacology. *Trends Pharmacol. Sci.* **37**, 87-100 (2016).

35. Ishizaki, T. et al. Pharmacological properties of Y-27632, a specific inhibitor of rho-associated kinases. *Curr. Mol. Pharmacol.* **57**, 976-983 (2000).

36. Sahai, E., Ishizaki, T., Narumiya, S. & Treisman, R. Transformation mediated by RhoA requires activity of ROCK kinases. *Curr. Biol.* **9**, 136-145 (1999).

37. Gibbins, J.M. Platelet adhesion signalling and the regulation of thrombus formation. *J. Cell Sci.* **117**, 3415-3425 (2004).

38. Estevez, B. & Du, X. New concepts and mechanisms of platelet activation signaling. *Physiol.* **32**, 162-177 (2017).

39. Investigators, P.T. Inhibition of platelet glycoprotein IIb/IIIa with eptifibatide in patients with acute coronary syndromes. *N. Engl. J. Med.* **339**, 436-443 (1998).

40. Vane, J. & Botting, R. The mechanism of action of aspirin. *Thromb. Res.* **110**, 255-258 (2003).

41. Roth, G. & Majerus, P.W. The mechanism of the effect of aspirin on human platelets. I. Acetylation of a particulate fraction protein. *J. Clin.* **56**, 624-632 (1975).

42. Paul, B.Z., Daniel, J.L. & Kunapuli, S.P. Platelet shape change is mediated by both calcium-dependent and-independent signaling pathways: role of p160 Rho-associated coiled-coil-containing protein kinase in platelet shape change. *J. Biol. Chem.* **274**, 28293-28300 (1999).

43. Uehata, M. et al. Calcium sensitization of smooth muscle mediated by a Rho-associated protein kinase in hypertension. *Nature* **389**, 990-994 (1997).

44. Wang, X. et al. Comparative analysis of various platelet glycoprotein IIb/IIIa antagonists on shear-induced platelet activation and adhesion. *J. Pharmacol. Exp. Ther.* **303**, 1114-1120 (2002).

45. Abe, M. & Ozawa, Y. Y. Uda, Y. Morimitsu, Y. Nakamura, T. Osawa,"A novel labdane-type trialdehyde from myoga (zingiber mioga roscoe) that potently inhibits human platelet aggregation and human 5-lipoxygenase". *Biosci. Biotechnol. and Biochem* **70**, 2494-2500 (2006).

46. Choi, H.M. et al. Third-generation in situ hybridization chain reaction: multiplexed, quantitative, sensitive, versatile, robust. *Development* **145**, dev165753 (2018).

47. Paniccia, R., Priora, R., Liotta, A.A. & Abbate, R. Platelet function tests: a comparative review. *Vasc. Health Risk Manage.* **11**, 133 (2015).

48. Galior, K. et al. Molecular tension probes to investigate the mechanopharmacology of single cells: a step toward personalized mechanomedicine. *Adv. Healthcare Mater.* **7**, 1800069 (2018).

49. Vikhorev, P.G. & Vikhoreva, N.N. Cardiomyopathies and related changes in contractility of human heart muscle. *Int. J. Mol. Sci.* **19**, 2234 (2018).

50. Ma, V.P.Y. et al. Mechanically Induced Catalytic Amplification Reaction for Readout of Receptor‐Mediated Cellular Forces. *Angew. Chem. Int. Ed.* **128**, 5578-5582 (2016).

51. Bi, S., Chen, M., Jia, X., Dong, Y. & Wang, Z. Hyperbranched Hybridization Chain Reaction for Triggered Signal Amplification and Concatenated Logic Circuits. *Angew. Chem. Int. Ed.* **54**, 8144-8148 (2015).

52. Guo, J., Mingoes, C., Qiu, X. & Hildebrandt, N. Simple, Amplified, and Multiplexed Detection of MicroRNAs Using Time-Gated FRET and Hybridization Chain Reaction. *Anal. Chem.* **91**, 3101-3109 (2019).

53. Dirks, R.M. & Pierce, N.A. Triggered amplification by hybridization chain reaction. *Proc. Natl. Acad. Sci. U.S.A.* **101**, 15275-15278 (2004).

54. Prévost, N., Kato, H., Bodin, L. & Shattil, S.J. Platelet integrin adhesive functions and signaling. *Meth. Enzymol.* **426**, 103-115 (2007).

55. Galush, W.J., Nye, J.A. & Groves, J.T. Quantitative fluorescence microscopy using supported lipid bilayer standards. *Biophys. J.* **95**, 2512-2519 (2008).

56. Strunz, T., Oroszlan, K., Schäfer, R. & Güntherodt, H.-J. Dynamic force spectroscopy of single DNA molecules. *Proc. Natl. Acad. Sci. U.S.A.* **96**, 11277-11282 (1999).

57. Pope, L.H. et al. Force-induced melting of a short DNA double helix. *Eur. Biophys. J.* **30**, 53-62 (2001).

58. Danilowicz, C. et al. Measurement of the Phase Diagram of DNA Unzipping in the Temperature-Force Plane. *Physical Review Letters* **93**, 078101 (2004).

59. Kufer, S.K., Puchner, E.M., Gumpp, H., Liedl, T. & Gaub, H.E. Single-Molecule Cut-and-Paste Surface Assembly. *Science* **319**, 594-596 (2008).

60. van Mameren, J. et al. Unraveling the structure of DNA during overstretching by using multicolor, single-molecule fluorescence imaging. *Proc. Natl. Acad. Sci. U.S.A.* **106**, 18231-18236 (2009).

61. Huguet, J.M. et al. Single-molecule derivation of salt dependent base-pair free energies in DNA. *Proc. Natl. Acad. Sci. U.S.A.* **107**, 15431-15436 (2010).

62. de Gennes, P.-G. Maximum pull out force on DNA hybrids. *Comptes Rendus de l'Académie des Sciences - Series IV - Physics* **2**, 1505-1508 (2001).

63. Chakrabarti, B. & Nelson, D.R. Shear Unzipping of DNA. *J. Phys. Chem. B* **113**, 3831-3836 (2009).

64. Mosayebi, M., Louis, A.A., Doye, J.P.K. & Ouldridge, T.E. Force-Induced Rupture of a DNA Duplex: From Fundamentals to Force Sensors. *ACS Nano* **9**, 11993-12003 (2015).

65. Liu, Z. et al. Nanoscale optomechanical actuators for controlling mechanotransduction in living cells. *Nature methods* **13**, 143-146 (2016).

66. Luca, V.C. et al. Notch-Jagged complex structure implicates a catch bond in tuning ligand sensitivity. *Science* **355**, 1320-1324 (2017).

67. Jo, M.H., Cottle, W.T. & Ha, T. Real-Time Measurement of Molecular Tension during Cell Adhesion and Migration Using Multiplexed Differential Analysis of Tension Gauge Tethers. *ACS Biomat. Sci. Eng.* **5**, 3856-3863 (2019).

68. Rao, T.C. et al. EGFR activation attenuates the mechanical threshold for integrin tension and focal adhesion formation. *Journal of Cell Science* **133** (2020).

69. Brockman, J.M. et al. Live-cell super-resolved PAINT imaging of piconewton cellular traction forces. *Nat. Methods* **17**, 1018-1024 (2020).

70. Yarrow, J.C., Totsukawa, G., Charras, G.T. & Mitchison, T.J. Screening for cell migration inhibitors via automated microscopy reveals a Rho-kinase inhibitor. *Chem. Biol.* **12**, 385-395 (2005).

71. Paul, B.Z., Daniel, J.L. & Kunapuli, S.P. Platelet shape change is mediated by both calcium-dependent and -independent signaling pathways. Role of p160 Rho-associated coiled-coil-containing protein kinase in platelet shape change. *J. Biol. Chem.* **274**, 28293-28300 (1999).

72. Tardiff, B.E. et al. Pharmacodynamics and Pharmacokinetics of Eptifibatide in Patients With Acute Coronary Syndromes. *Circulation* **104**, 399-405 (2001).

73. ABE, M. et al. A Novel Labdane-Type Trialdehyde from Myoga (Zingiber mioga Roscoe) That Potently Inhibits Human Platelet Aggregation and Human 5-Lipoxygenase. *Biosci. Biotechnol. Biochem.* **70**, 2494-2500 (2006).

74. Fontana, P. et al. The dual thromboxane receptor antagonist and thromboxane synthase inhibitor EV-077 is a more potent inhibitor of platelet function than aspirin. *J. Thromb. Haemost.* **9**, 2109-2111 (2011).

75. Blanco, F.J., Guitian, R., Moreno, J., de Toro, F.J. & Galdo, F. Effect of antiinflammatory drugs on COX-1 and COX-2 activity in human articular chondrocytes. *J. Rheumatol.* **26**, 1366-1373 (1999).

Chapter 3. Development of Mechano-Cas12a Assisted Tension Sensor

Adapted from Duan, Y.; Szlam, F.; Hu, Y.; Chen, W; Li, R; Ke, Y; Sniecinski, R; Salaita, K Democratizing Mechanobiology with Massively Amplified High-Throughput Traction Force Measurements using a Force-Triggered CRISPR-Cas12a Assay. To be submitted. We acknowledge that F.S., Y.H., W.C. helped to perform the experiment and validate MCATS. R.L., R.S. provided key resources. and helped to design the study.

3.1 Abstract

Cells transmit piconewton forces to mediate essential biological process such as coagulation and cell migration. One challenge is that cell-generated forces are infrequent, transient, and difficult to detect. Here, we report the development of Mechano-Cas12a Assisted Tension Sensor (MCATS) that utilizes the CRISPR-Cas12a nuclease to transduce and amplify the molecular forces generated by cells. We demonstrate the power of MCATS by detecting the forces generated by as few as ~10^2 human platelets in a high-throughput manner. Platelet forces are significantly inhibited when blood samples are treated with FDA-approved drugs such as aspirin, eptifibatide(integrilin®), 7E3(Reopro®), and the inhibitors Plavix® and Brelinta®. Because MCATS requires <5uL of blood/measurement, a single blood draw (~mL's) can be used to generate a personalized dose-response curve and IC_{50} for this panel of drugs. Platelet activity and force-generation are tightly associated, and hence MCATS was used to quantify platelet dysfunction following cardiopulmonary bypass (CPB) surgery in a pilot study of 5 patients. We found that MCATS detects platelet dysfunction in this group which correlated with the need for platelet transfusion to limit bleeding. These results indicate MCATS may be a useful assay for clinical applications.

3.2 Introduction

The ability for cells to generate mechanical forces is central to a wide range of biological processes ranging from immunology to coagulation and plays an important role in numerous pathologies such as cancer.[1-4] Therefore, developing methods to quantify cell-generated force has important biomedical applications. A central challenge in this field is that molecular forces that are sensed and transduced by cells are fairly weak, at the scale of piconewtons (pN)[5] and are highly transient

and infrequent [6]. Our lab and others recently developed DNA-based tension sensors that respond to cell generated pN forces and can be imaged using high-power microscopes with single molecule sensitivity.[7] Despite the advances in mechanobiology enabled by DNA tension sensors,[3, 5, 7] the use of these probes remains limited because of the weak signal and need for dedicated microscopy instrumentation. To facilitate the study of mechanobiology, it is important to develop facile, robust, and sensitive assays that can be broadly adopted by the community.

In biochemistry and molecular biology, weak or difficult to detect signal is typically enhanced by using catalytic amplification reactions such as PCR and ELISA. We considered leveraging such as assays, but we decided to avoid PCR and ELISA-like assays because of their poor compatibility with live cell measurements. For example, thermal cycling in PCR would destroy most cells. An emerging class of enzymatically amplified reactions that are used in molecular diagnostics are based on clustered regularly interspaced short palindromic repeats (CRISPR) and CRISPR-associated proteins (Cas).[8, 9] One notable Cas enzyme used in diagnostics is CRISPR-Cas12a (Cpf1) which is a class 2 type V-A enzyme that is loaded with single-stranded guide RNA (gRNA) and is activated upon binding to a complementary single stranded activator DNA. Upon activation of Cas12a, the enzyme undergoes a conformation change that unleashes its indiscriminate cleavage activity (trans activity) which hydrolyzes any ssDNA in proximity.[10] The nuclease activity of Cas12a is robust, highly efficient with $k_{cat}/K_m \sim 10^6$-10^7 $M^{-1}s^{-1}$, and thus has been used for a number of diagnostic assays for nucleic acid sensing such as DETECTR[11]and for metal ion detection as demonstrated by Yi Lu and colleagues.[11, 12] Given the sensitivity and specificity of Cas12a based assays, we were inspired to adopt Cas12a enzyme to address the limited signal in cellular tension sensing assays.

Specifically, we developed a Mechano-Cas12a Assisted Tension Sensor (MCATS), which is an ultrasensitive fluorescence-based assay to detect the molecular forces generated by cells. In MCATS, the activator is a ssDNA anchored to a surface, such as a glass slide. The activator is concealed by hybridization to a complementary strand that is in turn conjugated to a peptide such as, cyclo-Arg-Gly-Asp-Phe-Lys (cRGDfK), or any protein ligand specific to the cell receptor of interest (Fig. 1A-B). When cells are seeded on this surface, surface receptors such as integrins bind to the cRGDfK ligand on the duplex and apply forces. Forces that exceed the mechanical tolerance of the duplex lead to its rupture, exposing the activator (bottom strand) and thus triggering Cas12a nuclease activity. Upon activation, Cas12a will indiscriminately and catalytically cleave fluorogenic single stranded DNA reporter for amplification. Because Cas12a is highly efficient, its activation generates a massive fluorescence signal output that can be measured using a conventional fluorometer or plate reader for facile and high throughput readout.

MCATS is a platform technology and can be applied to study many different types of cells and different biological processes. As a proof-of-concept demonstration, we used MCATS to investigate the forces generated by human platelets because of their small size, and the importance of mechanical forces in platelet function. Indeed, recent studies using micropatterned polymer structures showed that platelets forces can be used to detect underlying genetic clotting disorders[13], and also for predicting trauma-induced coagulopathy. [13, 14] Because MCATS only requires ~5 uL of blood or less to conduct each measurement, a typical blood draw (~5 mL) allows one to run ~1000 assays in a rapid manner. We leverage this capability to screen the activity of a panel of clinically approved anti-platelet drugs such as aspirin, integrilin, and abciximab, Plavix and

Brelinta. These experiments demonstrate the potential of MCATS to be used for personalized tailoring of anti-coagulant drugs and may help guide therapeutic intervention in the clinic.[15] We also applied MCATS to detect platelet dysfunction following cardiopulmonary bypass (CPB) surgery. In a pilot study of five CPB patients, we found that the change in MCATS signal correlated with the need for platelet transfusion. More broadly, MCATS offers an accurate, rapid, and cost-efficient method to detect molecular forces generated by cells and will hence open the door to integrating mechanical measurements in the clinic.

3.3 Results

3.3.1 Design and optimization of MCATS

We first designed a double stranded DNA tension probe that can be mechanically ruptured by cell generated forces to expose the immobilized activator. Because the DNA tension probe is specifically designed without PAM sequence, the concealed double strand tension probe fails to activate the Cas12a nuclease without mechanical activation. Upon mechanical denaturation of the duplex, the exposed activator can then activate gRNA/Cas12a complex to cleave single strand reporter DNA. We intentionally designed the reporter DNA with a short poly T sequence to minimize secondary structure and then tagged its two termini with a quencher-fluorophore labelled pair that dequenched upon DNA hydrolysis.

Given that surface-tethered Cas12a had not been reported in the literature, and the potential for hindered activity due to immobilization[16], we first measured the kinetics of Cas12a when the activator is immobilized on a surface and compared it to reactions where the activator was in

solution. In this assay, biotinylated activator (100 nM) was anchored to streptavidin-coated surfaces by incubating for 1 hr at RT. Based on our previous surface calibration, this procedure generates a DNA density of 1330 ± 60 molecules/μm^2.[17] Next, the gRNA-Cas12a complex (20 nM) and reporter DNA (100 nM) were added to the surface and a fluorescence plate reader was used to monitor the fluorescence signal in each well of the 96 well plate. The measurement showed that ss-activator triggered the Cas12a nuclease and generated a strong fluorescent response. In contrast, the ds-activator (concealed activator) only showed minimal signal (**Figure 3.1C**).

Next, we tested whether adding a spacer to the activator may boost Cas12a cleavage rates. We tested four activators with different length polyT spacers of 0, 6, 60, and 160 nt. The surface density calibration showed that 6 and 60 polyT spacers only reduced surface density slightly (~18%) while the long 160nt spacer caused the surface density to decrease to 60% of the 0-nt spacer probe (**Figure 3.5**). The initial rate constant for these immobilized activators is plotted in Fig.1D and showed that the initial rate constant was enhanced with longer spacers with the exception for the 160 nt activator. The enhanced activity with longer spacers is likely due to reduced steric hinderance, but this effect is offset by the reduced effective activator density at extreme spacer lengths. Notably, we expect that the Cas12a will release the activator from the surface with suitable length spacers. This is supported by the observation that activator surface density is diminished by 70% for the 60 polyT spacer after 1 hr of adding the Cas12a (**Figure 3.6**). All subsequent work with MCATS employed activator with 60T spacer due to its superior signal amplification.

To further optimize MCATS, we measured Cas12a activity as a function of assay temperature, buffer and reaction time (**Figure 3.7**). The results indicate the Cas12a work best at 37 ℃, in cell culture medium with 10mM of Mg^{2+}. We also compared the S/N of the assay using two reporter oligonucleotides (**Figure 3.8**). The reporter strand tagged with Atto565N-BHQ2 shows a ~three times higher S/N compared with FAM-Lowa black reporter strand because of its better quenching efficiency. Using the optimized conditions, we investigated the limit of detection (LOD) of our assay both for surface tethered activator as well as soluble activator as a reference (**Figure 3.1E-F**). To tune the activator surface density, we created surfaces comprised of a binary mixture of ssDNA activator with the blocked (double stranded) and exposed activator. Here we maintained a total activator solution concentration of 100 nM but tuned the ratio between the blocked and single stranded activator. We then added Cas12a-gRNA and fluorogenic reporter to the well and measured the final fluorescence intensity after 1hr of enzyme activity. The LOD was then inferred from the ratio of 3.3 x standard deviation of the background normalized by the slope of the fluorescence versus concentration plot. The results showed that the LOD for nucleic acid sensing in solution was 20 fM and 525 molecule/mm^2 on a surface. This analysis provides the basis for using MCATS to sensitively detect molecular forces generated by cells.

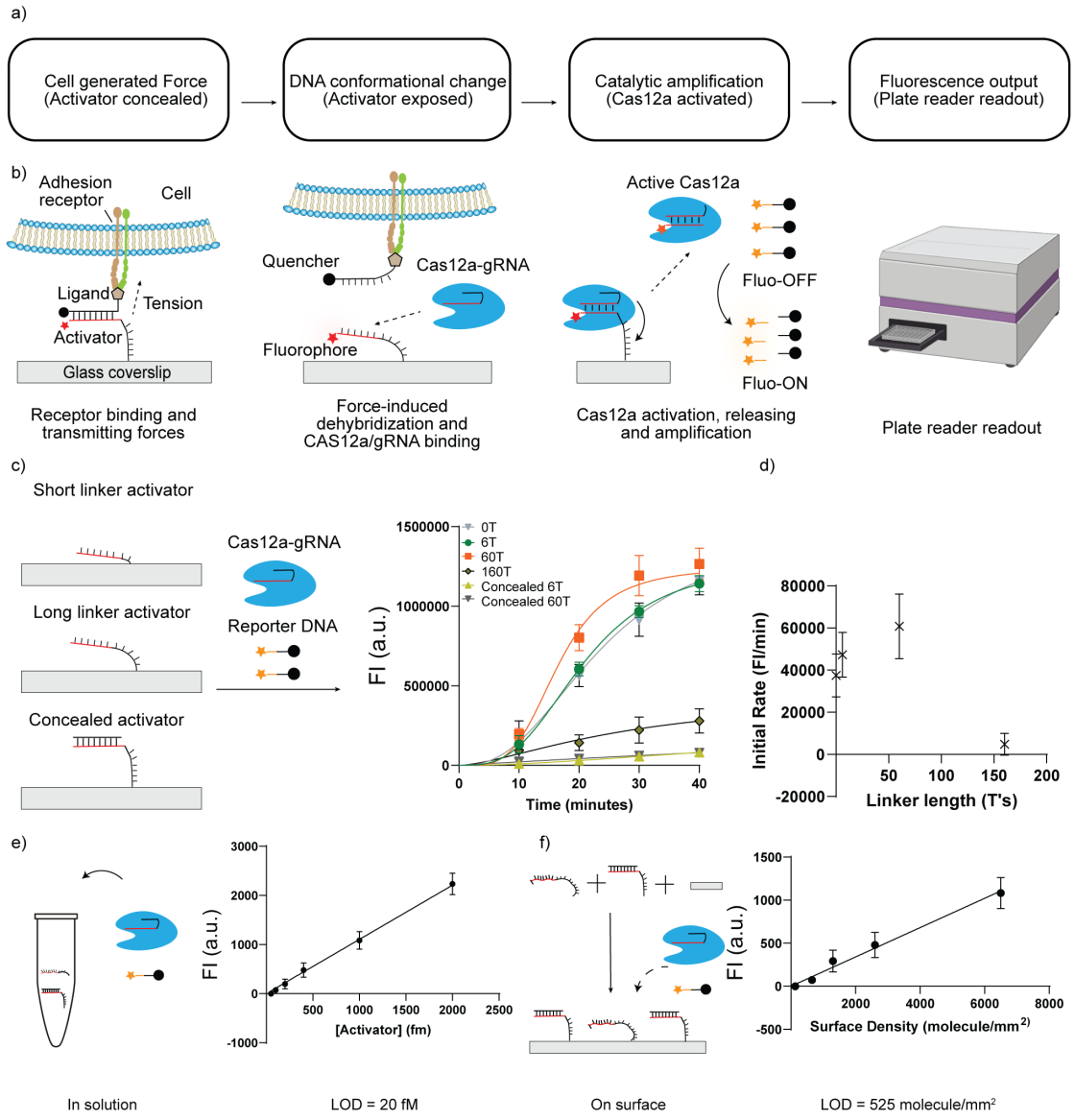

Figure 3.1. Scheme and characterization of MCATS. a-b) Schematic showing MCATS detection assay. Cellular molecular force would reveal an activator that activate Cas12a to cleave reporter strands in solution. In our work, the activator is tagged with Atto647N while the reporter DNA are tagged with Atto565 and BHQ2. c) characterization of Cas12a cleavage kinetics with immobilized activator and optimization of linker length of activator. Plot of time-dependent fluorescence intensity measured using plate reader. Error bar represents S.E.M. obtained from three independent experiments. d) Plot of initial cleavage rate of Cas12a over linker length of immobilized activator. e) 20nM Cas12a-gRNA complex and 100nM reporter DNA was added to 100nM ssDNA and concealed activator in solution, plot of fluorescence intensity-ssActivator concentration. LOD = 3.3(Sy/S) = 20fM. f) 20nM Cas12a-gRNA complex and 100nM reporter DNA was added to surface incubated with 100nM ssDNA and concealed activator, plot of fluorescence intensity-ssActivator density on surface. LOD = 3.3(Sy/S) = 525 molecule/mm^2.

3.3.2 Rapid, robust, ultrasensitive detection of cellular tension with MCATS

We next applied the MCATS assay to detect integrin-mediated cell traction forces in immortalized cell lines. Integrins are a family of heterodimeric cell surface adhesion receptors that bridge the cellular cytoskeleton with the extracellular matrix (ECM) to mediate a variety of processes including cell adhesion, and migration.[2] Previous research has shown that integrin receptors can apply pN forces which are sufficient to mechanically denature DNA duplexes.[18] Hence, measuring integrin receptor forces with NIH/3T3 cells is an appropriate model to validate the MCATS assay.

As is shown in **Figure 3.2A**, DNA duplexes that present cRGDfk ligand and concealed Cas12a activator were immobilized on the surface. The conjugation of ligand to duplex was achieved via copper(I)-catalyzed azide-alkyne cycloaddition and was verified with ESI-MS (**Figure 3.9**). NIH/3T3 fibroblast cells were then seeded on these surfaces for 1 hr.

We designed two types of DNA duplexes that have identical sequence and thermal melting temperatures, but different geometries and mechanical tolerances (**Figure 3.2B**). When the activator is anchored through its 5' terminus, the cRGDfK ligand is presented on the 3' terminus of the top strand. Hence this probe denatures through an unzipping process which has a lower activation barrier and displays a mechanical rupture threshold of 12 pN. In contrast, when the activator is anchored through its 3'terminus, the probe denatures by shearing which has a larger mechanical threshold of 56 pN.

The same number of cells (25,000 cells) were incubated on the two types of surfaces for 1 hr before running the Cas12a amplification assay. As expected, we observed an increase in fluorescence

signal for both the 12 pN and 56 pN probes (tagged with fluorophore quencher pairs) due to mechanical denaturation of the duplex (**Figure 3.2C**). As expected, the probes in the unzipping geometry (12 pN) were more significantly denatured compared to shearing mode probes (56 pN), in agreement with past literature (**Figure 3.2B-C**). We next added the Cas12a and reporter DNA to trigger the MCATS assay for 1 hr and then measured bulk fluorescence (λ_{ex} = 540 nm and λ_{em}=590 nm) using the plate reader (**Figure 3.2D**). Importantly, the 12 pN unzipping mode probes also generated a greater MCATS signal, reflecting the greater density of exposed activator. MCATS produced over 100-fold greater signal compared to mechano-HCR which confirms that this assay is more sensitive and offers a simplified experimental process as no washing steps are required (**Figure 3.10**).[17]

We further validated the MCATS assay by seeding increasing numbers of NIH/3T3 cells in 96 well plates and measuring associated MCATS signal in each well. We observed that increasing cell densities led to greater MCATS signal (**Figure 3.2E-G**). Impressively, we found that MCATS can detect the tension generated from as few as 50 fibroblasts in a 96 well plate using a conventional plate reader (**Figure 3.2F inset**). We further tested whether MCATS can be used to produce a dose response curve for NIH-3T3 cell incubated with Rho kinase inhibitor, Y-27632, which targets the phosphorylation of myosin light chain and therefore dampens forces transmitted by focal adhesions. We pretreated NIH/3T3 cells with a range of Y-27632 concentrations (0-50 μM) for 30 min and then ran MCATS with the drug treated cell. MCATS signal showed a dose-dependent reduction as a function of increasing Y-27632 concentration (**Figure 3.2H-J**), indicating that plate-reader based MCATS readout can report cell forces modulated by MLC inhibition. By fitting the data to a standard dose-response inhibition function (signal

=100/(1+[drug]/IC50)), we found that the mechano-IC_{50} = 7.9 μM (95% CI = 5.5 -11.6 μM), which matches previous literature reporting IC_{50} of 5-10 μM .[19]

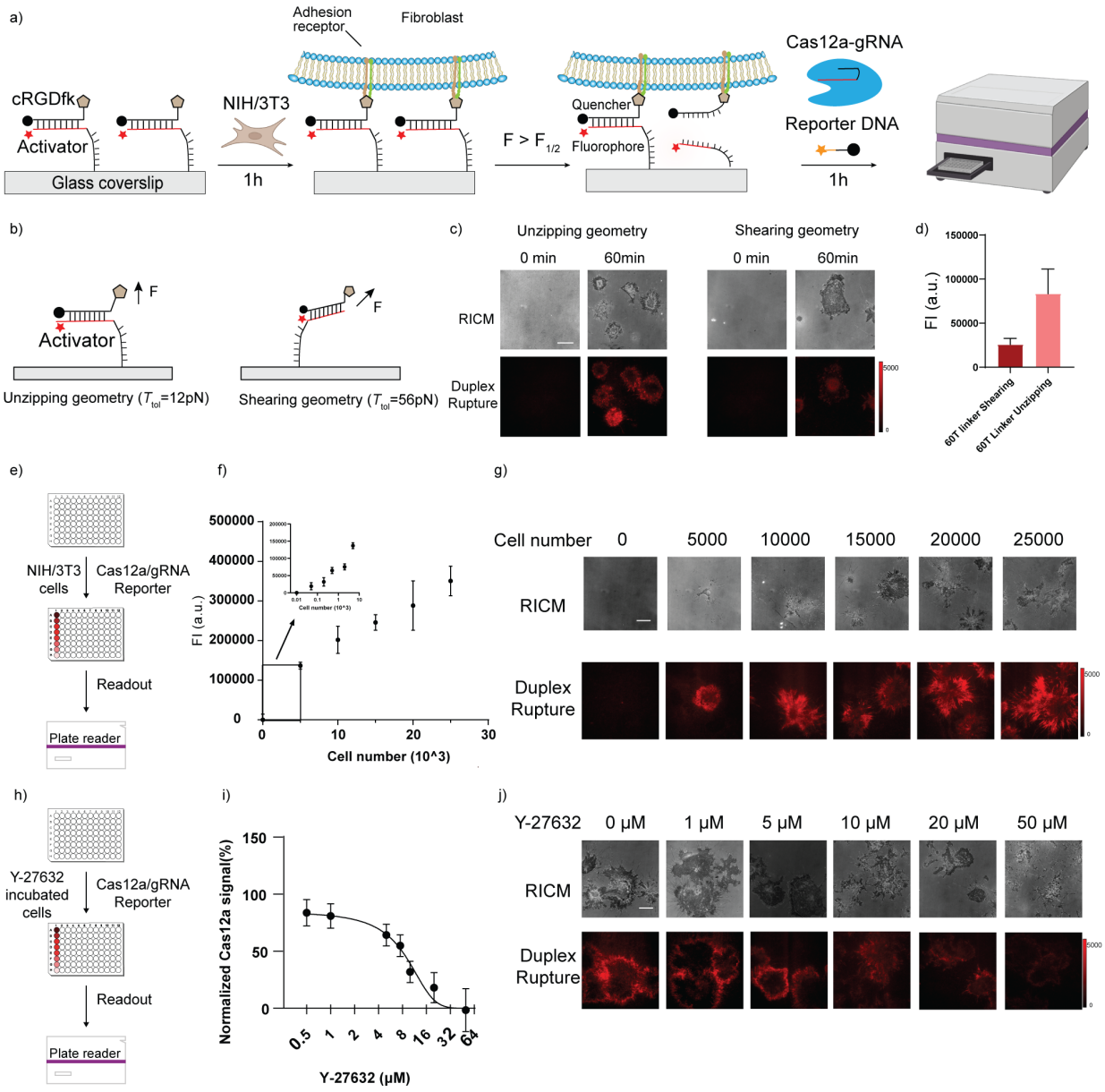

Figure 3.2. MCATS to detect cell forces using a plate reader. a) Schematic of MCATS assay to study NIH/3T3 integrin-mediated forces. b-c) Schematic of DNA duplex with concealed activator, Representative RICM and fluorescence images of cells cultured on T_{tol}= 12 pN and T_{tol}= 56 pN surfaces for 1hr. Scale bar = 12 μm. The red color is emission from Atto647N tagging the activator. The intensity bar next to each fluorescence image shows the absolute signal intensity for each image. d) Bar graph shows MCATS signal of same number of cells incubated on T_{tol}= 12 pN and T_{tol}= 56 pN surfaces. Error bars represent S.E.M. from n=3 independent experiments. e-f) Schematic and plot showing plate reader measured MCATS signal as a function of the number of cells seeded when different number of cells are seeded on the surface. Error bar represents S.E.M. from three independent experiments. Insets showing when measuring tension signal from low number of cells (10-5000) using MCATS. g) Representative RICM and duplex rupture (red)

fluorescence images. Scale bar = 12 μm. h-i) Schematic and plot of plate reader measured MCATS signal as a function of Y-27632 concentration. Drug was incubated for 30 min prior to seeding. Error bar represents S.E.M. from 3 independent experiments. Mechano-IC50 was calculated by fitting plot to a standard dose-response function: normalized signal = 100/(1+[drug]/IC50). The values were normalized to the signal obtained from the 25,000 cells/well samples without drug treatment. All measurements were background subtracted using negative control wells lacking cells. k) Representative RICM and duplex rupture (red) fluorescence images. Scale bar = 12 μm.

3.3.3 High-throughput determination of platelet inhibitors' influence on platelet tension

We next investigated the MCATS signal of human platelets under the influence of different antiplatelet drugs. Platelets are primary cells and are well suited for analysis by because contractile forces are critical in platelet function in forming clots that mechanically resist blood shear flow and seal a wound. Anti-platelet agents are some of the most commonly prescribed drugs in the world. Currently, 30 million Americans take anti-platelet medications such as daily aspirin to reduce the risk of cardiovascular events, but ~16.6 of 100 patients experience bleeding as a side effect and 5% are resistant to aspirin.[20] The commonly prescribed blood thinner, Plavix is also well-known for showing a diverse response among populations as ~20% of the general population is insensitive to Plavix.[21]

We tested multiple types of FDA-approved antiplatelet drugs: aspirin which inhibits the activity of cyclooxygenase (COX), the integrin αIIbβ3 antagonists eptifibatide, 7e3 (monoclonal antibody) as well as the P2Y12 inhibitors Plavix and Ticagrelor. [22-24]As is shown in **Figure 3.3A**, we first purified human platelets from blood samples collected in collection tubes containing sodium citrate or EDTA from donors (Emory Hospital). The sample was then centrifuged for 12 min at 140 *g* (with 0.02U Apyrase). Then platelet rich plasma was separated and centrifuged for 5 min at

700 *g* with 3 μM PGE-1 and 0.02 U Apyrase. The platelets were then resuspended in Tyrodes buffer with 3μM PGE-1 and centrifuged for 5 min at 700 *g*. Finally, platelets were resuspended in Tyrodes buffer. It is worth noting that Apyrase is important in the platelet purification process to prevent hemolysis mediated platelet aggregation (**Figure 3.11C**). In additional controls, we found that tubes containing either EDTA or citrate will not influence platelet tension after purification. (**Figure 3.11D**)

We first tested MCATS as a function of the number of platelets seeded on the unzipping duplex surfaces. We found that MCATS detected tension signal from as few as 2000 platelets (**Figure 3.12**). We choose $n = 2 \times 10^6$ human platelets in the following experiments because this concentration of platelets in a 96-well plate offered the strongest signal for the assay. Comparing MCATS signal on the unzipping and shearing duplex probes with 2×10^6 human platelets showed that platelets produced more signal on the unzipping mode probes which is consistent with literature reports (**Figure 3.13**).[2, 17] In a second set of experiments, we incubated platelets with different drugs at room temperature for 30 minutes and plated 2×10^6 treated human platelets in each well for 1hr and then performed MCATS.

For all the compounds tested, we observed a dose-dependent decrease in the 12 pN duplex rupture in both microscopy imaging of duplex ruptures as well as MCATS signal that was detected using a plate reader (**Figure 3.3C-3.3G**, **Figure 3.14**). All drugs with the exception of Plavix showed a significant drop in signal upon treating platelets. (p=0.007, 0.009, <0.0001, 0.04 for aspirin, Eptifibatide, 7E3 and Ticagrelor respectively) The data for Plavix showed two patients are resistant

to the Plavix, which is consisted with the report of high number of non-responders to Plavix. By fitting the plot of MCATS signal with a standard dose-response inhibition function (Signal=Bottom + (Top-Bottom)/(1+([drug]/IC_{50})), we determined the mechano-IC_{50} for aspirin, eptifibatide, 7E3, Plavix and Ticagrelor for each individual donor and plotted the data in **Figure 3.3C-3.3G**. MCATS was found to be robust as the signal generated from the same blood draw of the same donor was highly consistent (sigma ~ 10%). However, we found donor-to-donor variability in mechano-IC50 which likely reflects the biological heterogeneity of the drug response especially in Aspirin and Plavix treated group. Importantly, the values we measured were consistent with literature precedent.[25-27] Due to limited time, triplicates for Ticagrelor will be tested in the future. Another parameter that could influence platelet forces is ADP agonist which is well known to trigger platelet activation and adhesion. We therefore tested the dose-response of platelets to agonist using MCATS and found increasing tension signal as a function of ADP. These results were further validated with light transmission aggregometry which is commonly used to assess platelet function (**Figure 3.3h, Figure 3.15**). Aggregometry however requires higher sample volume and dedicated instruments which shows the advantage of MCATS in assessing platelet function with cellular forces. Other agonists such as TRAP and collagen were also tested and showed increasing tension signal as a function of dose of agonist. (**Figure 3.16**). Because each measurement only requires 2×10^6 platelets while 1ml of blood usually contains ~10^9 platelets, therefore, a typical 5ml blood draw can be used to run hundreds of assays and screen different type of drugs in a single run.

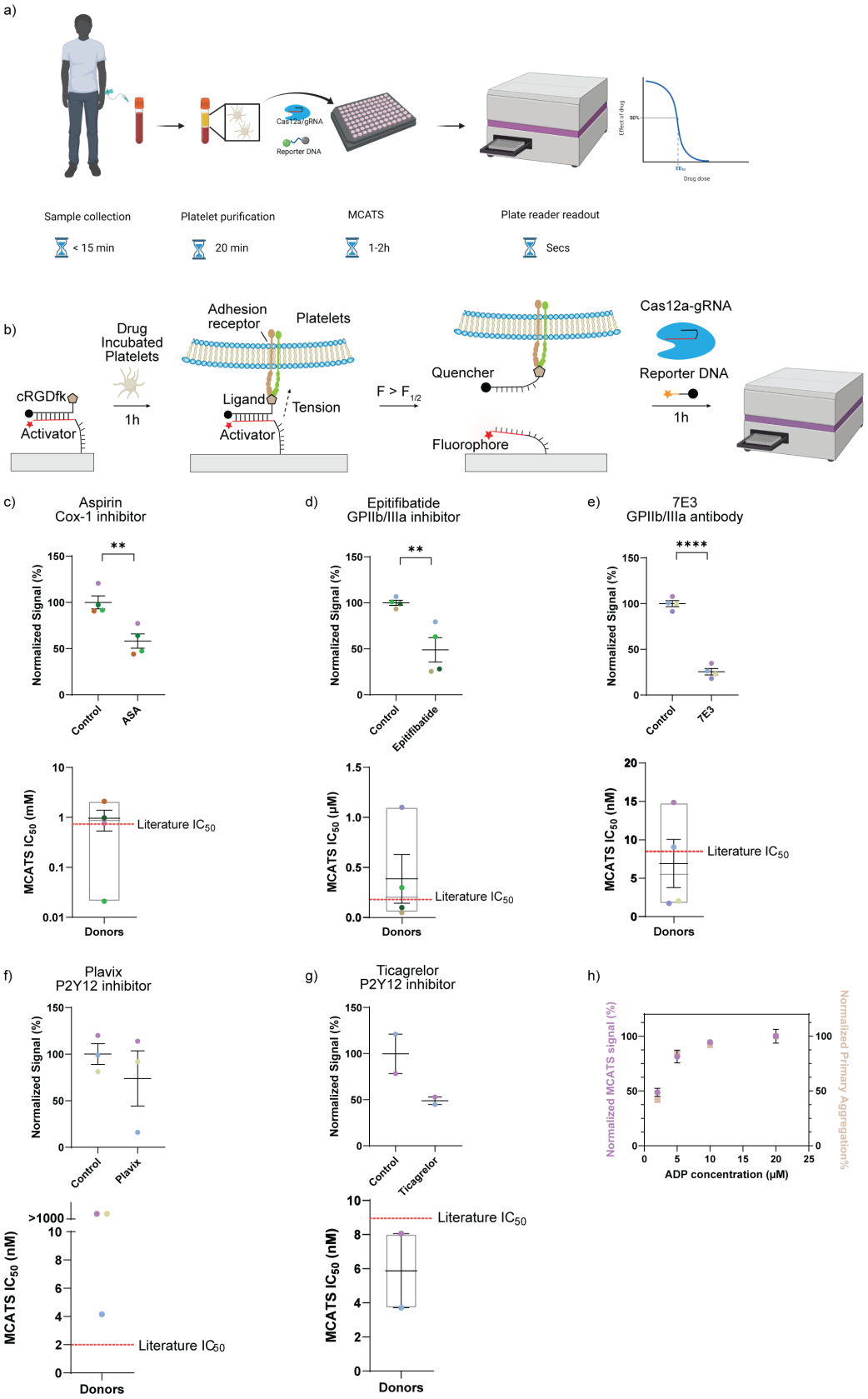
a)
Cas12a/gRNA
Reporter DNA
Effect of drug
50%
Drug dose
Sample collection
< 15 min
Platelet purification
20 min
MCATS
1-2h
Plate reader readout
Secs
b)
Drug Incubated Platelets
1h
cRGDfk
Activator
Adhesion receptor
Platelets
Ligand
Tension
Activator
F > F1/2
Quencher
Fluorophore
Cas12a-gRNA
Reporter DNA
1h
c)
Aspirin
Cox-1 inhibitor
Normalized Signal (%)
Control
ASA
MCATS IC50 (mM)
Literature IC50
Donors
d)
Epitifibatide
GPIIb/IIIa inhibitor
Normalized Signal (%)
Control
Epitifibatide
MCATS IC50 (μM)
Literature IC50
Donors
e)
7E3
GPIIb/IIIa antibody
Normalized Signal (%)
Control
7E3
MCATS IC50 (nM)
Literature IC50
Donors
f)
Plavix
P2Y12 inhibitor
Normalized Signal (%)
Control
Plavix
MCATS IC50 (nM)
Literature IC50
Donors
g)
Ticagrelor
P2Y12 inhibitor
Normalized Signal (%)
Control
Ticagrelor
MCATS IC50 (nM)
Literature IC50
Donors
h)
Normalized MCATS signal (%)
Normalized Primary Aggregation%
ADP concentration (μM)

Figure 3.3. Using MCATS to determine Mechano-IC50 for antiplatelets drugs. a) Schematic showing workflow to run MCATS assay with human platelets. Platelet's purification protocol. b) Schematic of MCATS assay to study platelets mediated forces c-g) Plot of MCATS signal for donors before and after inhibition of thromboxane formation using 0.1 mM aspirin, inhibition of GPIIb/IIIA with eptifibatide (1μM) and 7E3 (10μg/ml), inhibition of ADP activation of P2Y12 with Plavix (1 μM) and Ticagrelor (1 μM) show a significant decrease in platelets tension signal. Plot of mechano-IC_{50} calculated from individual donors with MCATS, Body of the box plots represent first and third quartiles. Red line represents literature report value. Data was normalized to average of control group and background signal. Error bar represents S.E.M. obtained from n=4 donors. Drug was incubated for 30 min prior to seeding. Mechano-IC50 was calculated by fitting plot to a standard dose-response function: Signal=Bottom + (Top-Bottom)/(1+([drug]/IC50) h) Plots of MCATS signal when same number of platelets was activated by different concentration of ADP. Error bar represents S.E.M. obtained from n=2 measurements. h) plots of MCATS tension signal (purple) and primary aggregation (orange) when cells are activated with different concentration of ADP. The values were normalized to the signal obtained from the wells with 20 μM ADP.

3.3.4 Platelet tension predicts transfusion need in CPB patients

Finally, we investigated whether MCATS can be used to assess platelet dysfunction and predict bleeding risk in patients undergoing CPB surgery. In a subset of patients (10-23%), CPB leads to severe postoperative bleeding requiring blood transfusion. The bleeding is difficult to predict as platelet function assays such as aggregometry and thromboelastography show only 40% predictive value in identifying post operation bleeding.[28-33] Accordingly, the ability to anticipate the risk for uncontrolled bleeding is highly desirable as it would aid in offering blood transfusions more rapidly and to the patients that need it the most. Past literature has demonstrated that CPB surgery and specifically extracorporeal circulation led to change in membrane glycoprotein on platelets and results in platelets dysfunction.[34] Therefore, a rapid and sensitive detection assay that detects platelet receptor mediated tension may provide a better tool for predicting severe bleeding after CPB.

We performed MCATS measurement on n=3 healthy donors as well as n=5 CPB patients pre- and post-operation. (**Figure 3.4A**) The demographic information and related health information can be found in **Table 3.2**. All samples were tested with TEG as a standard benchmark to compare against MCATS. We considered patients before surgery and healthy donor's samples as a baseline. In general, healthy donors (n=3) showed similar MCATS tension signal and this was similar to the tension signal for CPB donors prior to surgery. However, after CPB surgery, donors showed a significant decrease in their platelet MCATS signal (**Figure 3.4B, 3.4D**). This decrease was consistent with the clinical need to administer blood transfusions to patients as 4 of the 5 patients required blood transfusions due to bleeding.. More importantly, the platelet transfer units in the OR were strongly positively correlated with the drop in platelet MCATS signal following CPB surgery (**Figure 3.4E, Pearson's R= 0.8**). The TEG results, however, showed inconclusive results in linking the pre- and post-operation results to platelets function and transfusion need (**Figure 4C, Pearson's R= 0.2**). Taken together, platelet tension, TEG, and aggregometry data support CPB's negative effect on platelet function. Though, only MCATS measured platelet forces Though, only MCATS measured platelet forces offered a strong correlation with post-op bleeding risk following CBP.

In CPB operations, patients were treated with heparin prior to the surgery to minimize blood clotting and this was neutralized with protamine post operation. To confirm that the decrease in MCATS signal is not due to inhibition of heparin, we performed MCATS on controlled platelets that were treated with heparin and then neutralized with protamine. The results showed that heparin would decrease the platelets tension slightly, but this inhibition effect was fully reversed after

protamine treatment (**Figure 3.17**). We also tested the mechano-IC50 of aspirin, Plavix and Ticagrelor for the CPB donors before and after surgery. The results showed that the surgery did not influence the mechano-IC_{50} significantly (**Figure 3.18**), which confirms that MCAT is insensitive to platelet counts and that CPB surgery did not influence the AA or ADP induced platelets activation pathways.

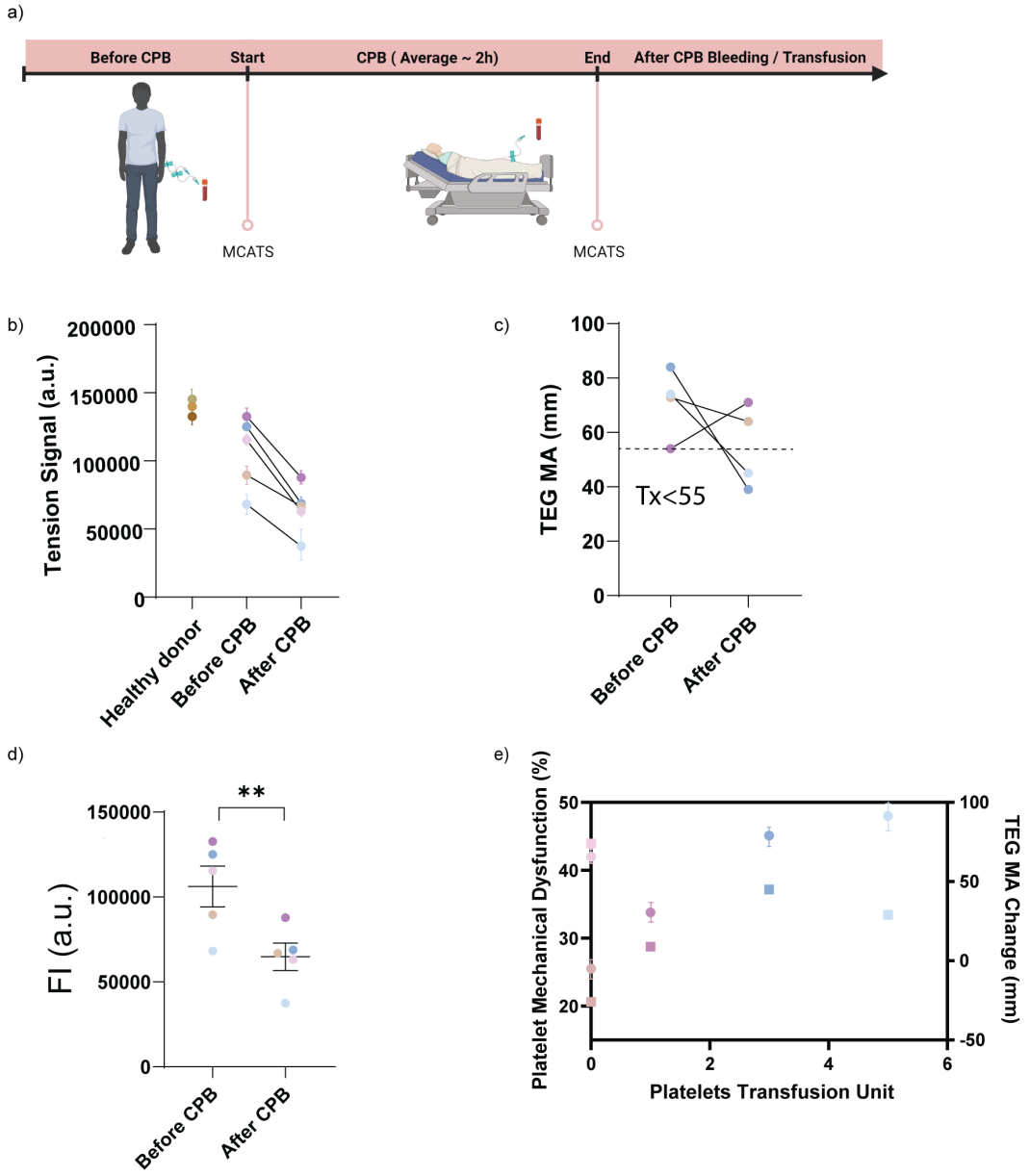

Figure 3.4. Using MCATS to predict bleeding risk for CPB patient. a) Schematic showing workflow to run MCATS assay to assess platelets dysfunction for CPB patients. b) Plots of MCATS signal for healthy donor, pre-surgery and post-surgery sample. Error bar represents S.D. obtained from n=3 wells for the same condition. c) Plot of TEG MA for healthy donor, pre-surgery and post-surgery sample. d) plots of before and after CPB patient tension signal. Error bar represents S.E.M. obtained from n=4 patients. Significance is calculated from student t test. 3e) Plots of decreased MCATS signal vs platelets transfusion needs. Dots indicate MCATS results while squares indicate TEG results. Data point is color coded by donors. Error bar represents S.D. from measurements using MCATS for the same donor.

3.4 Discussion

The current state of the art tools for measuring platelet function are based on aggregometry and thromboelastography assays.[35] For example, the Emory University Hospital Coagulation Core routinely measures patient clotting function by using a Platelet Function Analyzer (PFA) instrument that measures platelet aggregation under shear conditions or thromboelastography (TEG) which measure the viscoelastic properties of clots. The limitations of these assays are multifold. First, conventional assays require dedicated instrumentation which may be prohibitive for wide dissemination in certain settings. Secondly, PFA and TEG require ~mL quantities of blood for each measurement which may not seem significant, but this prohibits running triplicates and performing drug screens. Even more importantly, TEG and PFA assays have limited sensitivity given that these assays can assess only platelet aggregation which ignores other aspects of platelet function and aggregation is highly dependent on platelet count.[31, 32] Patients with higher platelet counts will tend to form aggregates more readily regardless of the functional activity of each individual platelet. According to the PLATFORM study, TEG shows 40% predictive value in identifying post operation bleeding for cardiopulmonary bypass patients.[36]

A unique merit of MCATS is that it measures molecular forces directly using conventional plate reader and it uses Cas12a amplification to boost the signal for fast and sensitive readout. As a result, MCATS only requires ~5 μL of blood or less, and hence a typical blood draw (~5 mL) is enough to run 1000 assays. Antiplatelet therapies are commonly prescribed to prevent acute arterial thrombosis. However, antiplatelet therapy assessment based on aggregometry has not shown improved outcomes and better benefit/risk for cardiovascular patient.[37] MCATS can generate personalized dose-response curves for specific drugs rapidly to optimize treatment in a

dynamic manner, which may increase the sensitivity and specificity required to guide personalized platelet therapy. So far, we measured the forces applied by GPIIb/IIIa which mediates platelet adhesion and aggregation to assess platelet functions. Other platelet forces mediated by GPIb-IX-V and GPVI can potentially be investigated by attaching different ligands/proteins on DNA tension probe to understand the platelet forces with different receptors under shear flow or in different hemostasis states. It is also worth noting that live and active cells are required to perform MACTS assay, and we confirmed that lyophilized platelets (fixed platelets with intact protein structure) failed to generate MCATS signal (Figure **3.19**).

In MCATS experiments, different platelet handling may lead to significantly different platelet response. Therefore, we tested different platelet purification procedures and the results indicated that MCATS can detect tension signal from purified platelets, platelet rich plasma and whole blood sample. However, whole blood showed decreased tension signal in MCATS experiments because red blood cells block platelets' access to the surface. Platelet rich plasma shows slightly decreased signal compared to purified platelets and platelet rich plasma may be further explored to decrease the reaction time and simplify the procedure (**Figure 3.11**). Also, the number of platelets incubated on the surface in MCATS can be controlled and therefore reducing the impact of different patient platelet counts. This is in contrast to PFA and TEG that are highly dependent on patient platelet counts. Another important parameter to consider in the assay is the amplification time. We monitored MCATS signal in the platelets and fibroblasts experiments with different amplification times. The results showed that 30min amplification provides sufficient signal while 60 min reaction time provides enhanced signal for better sensitivity. Further increasing amplification time dose not lead to significantly improved signal (**Figure 3.20**). These results indicate that MCATS

applications can potentially utilize 30min amplification in a more rapid assay or use 60 min amplification for higher sensitivity.

Finally, MCATS may be potentially used in diagnosing heparin induced thrombocytopenia (HIT). Although HIT is relatively rare, there are consistently about 20,000 cases annually in the United States with about a 10% overall mortality rate. [38] Because of the severity of the disease, testing for HIT is frequent among hospitalized patients. However, HIT testing requires a screening test to detect HIT antibodies which is often followed by a serotonin release assay (SRA) for confirmation. The SRA test involves radioactive agents and typically requires several days to perform. Hence platelet SRA assays are only performed at a limited number of centers in the US, forcing clinicians to place patients on alternate anticoagulants with increased bleeding risk while waiting for results. MCATS can potentially be used to test for HIT by measuring the heparin/platelet factor 4 and antibody induced platelet activation in these patients. We found that MCATS detects platelet tension in serum, though the serum significantly inhibits platelet tension (**Figure 3.21A**). We further titrated different doses of heparin in serum that contained HIT mimicking antibody KKO,[39] purified platelets. We noticed that heparin concentration at 0.1 U/ml would activate platelets with increased tension signal compared with no heparin group with MCATS (**Figure 3.21B**). These results indicate a potentially more cost-effective, sensitive HIT diagnostic assay with MCATS.

3.5 Conclusion

In summary, we developed an ultrasensitive fluorescence-based assay MCATS to rapidly measure cell receptor mediated tension. When cell receptors apply sufficient force, the DNA duplex tension sensor denatures exposing single stranded DNA. We amplify the peeled DNA using Cas12a to produce ~10^4 fluorophores in response to each 12 pN event, which allows rapid (~1-2 hrs) high-throughput detection of cellular tension without requiring any dedicated hardware. Instead, the assay uses modified 96 well plates that are read out in a conventional plate reader found in all clinical chemistry laboratories. We take advantage of these features and use the MCATS platform to detect platelet dysfunction which may predict bleeding risk and the need for platelet transfusion in CPB patients. High throughput detection of platelet forces may provide a more integrative, inexpensive, and accurate measurement of platelet function.

3.6 Materials and Methods

3.6.1 Chemicals and oligonucleotides

Cy3B-NHS ester (PA63101) was purchased from GE Healthcare Life Sciences (Pittsburgh, PA). Atto647N-NHS ester (18373) was purchased from Sigma Aldrich (St. Louis, MO). Cyclo[Arg-Gly-Asp-d-Phe-Lys(PEG-PEG)] (PCI-3696-PI) (cRGD) was acquired from Peptides International (Louisville, KY). Streptavidin (S000-01) was purchased from Rockland-Inc (Pottstown, PA). µ-Slide VI0.4 6-channel slides (80606) and 25 mm x 75 mm glass coverslips (10812) were purchased from Ibidi (Verona, WI). ProPlate® Microtiter (204969) are purchased from Thermo-Fisher Scientific. N-hydroxyl succinimide-5 kDa PEG-biotin (NHS-PEG-biotin, HE041024-5K) was purchased from Biochempeg (Watertown, MA). (3-Aminopropyl) triethoxysilane (APTES, 440140, 99% purity) was purchased from Sigma-Aldrich, Adenosine 5‘-diphosphate (ADP, A2754, 95% purity), KKO, PF4 was purchased from sigma -Aldrich. Plavix and Ticagrelor were purchased from Salk Chemistry. 7E3 (Abciximab) was purchased from Abcam. Apyrase and LbCas12 was purchased from New England Biolabs. (Ipswich, MA) All DNA oligonucleotides are listed in Table 3.1 and purchased from Integrated DNA Technologies (Coralville, IA), crRNA was purchased from Dharmacon Inc. (Lafayette, CO). All other reagents and materials (unless otherwise stated) were purchased from Sigma-Aldrich and used without purification. All buffers were prepared with 18.2 MΩ nanopure water.

Table 3.1: List of Oligonucleotides

Name	Sequence (5' to 3')
No Spacer Cas12a TGT Btm Strand	/5AmMC6/CC TCC TCA AGG AAC AAC ATT GC/3Bio/
Cas12a TGT Top Strand	/5Hexynyl/GC AAT GTT GTT CCT TGA GGA GG/3BHQ_2/
6T Spacer Cas12a TGT Btm Strand	/5AmMC6/CC TCC TCA AGG AAC AAC ATT GCT TTT TT/3Bio/
60T Spacer Cas12a TGT Btm Strand	/5AmMC6/GT GTC GTG CCT CCG TGC TGT GTT TTT TTT TTT TTT TTT TTT TTT TTT TTT TTT TTT TTT TTT TTT TTT TTT TTT TTT TTT T/3Bio/
ATTO 565N Reporter DNA	/5ATTO565N/TT ATT /3BHQ_2/
FAM reporter DNA	/56-FAM/TT ATT /3IABkFQ/
TGT crRNA	UAA UUU CUA CUA AGU GUA GAU GCA AUG UUG UUC CUU GAG GA

3.6.2 Instruments

We used a Nikon Eclipse Ti microscope, operated by Nikon Elements software, using a 1.49 numerical aperture (NA) CFI Apo ×100 objective, perfect focus system, a TIRF laser launch, a Chroma quad cube (ET-405/488/561/640 nm Laser Quad Band) and an RICM (Nikon: 97270) cube for this work. Bulk fluorescence measurements were conducted using a Synergy H1 plate reader (Bio-Tek) using fluorescence filter sets. All ultrapure water was obtained from a Barnstead Nanopure water purifying system (Thermo Fisher) that indicated a resistivity of 18.2 MΩ. Nucleic acid purification was performed using a high-performance liquid chromatography (HPLC, Agilent 1100) equipped with a diode array detector. Microvolume absorbance measurements were obtained using a Nanodrop 2000 UV-Vis Spectrophotometer (Thermo Scientific). Mass identification of product was performed with an Exactive™ Plus Orbitrap Mass Spectrometer. Platelets counts were determined on a Sysmex XP- 300 automated hematology analyzer

3.6.3 Surface preparation method

MCATS surface preparation method was modified from previously published protocols.[17, 40] Briefly, rectangular glass coverslips (25 x 75 mm, Ibidi) were rinsed with water and sonicated for 20 minutes in water and 20 minutes in ethanol. The glass coverslips were then cleaned with piranha solution. The piranha solution was prepared using a 1:3 mixture of H_2O_2 and H_2SO_4. WARNING: Piranha solution becomes very hot upon mixing, and is highly oxidizing and may explode upon contact with organic solvents. Then, slides were washed 6 times in beakers with ultrapure water, followed by 4 successive washes using ethanol. In a separate beaker of ethanol, slides were reacted with 3% v/v APTES at room temperature for 1 h. Coverslips were then washed 6 times with ethanol, baked in oven for 20 minutes at 80 °C. Slides were then reacted with NHS-

PEG-biotin (3% w/v) for 1 hr in ultrapure water. Next, slides were washed 3 times with ultrapure water, dried under N_2 gas, and then stored at -30°C for up to 2 weeks before use. At the day of imaging, the 5kDa PEG-biotin surface was adhered onto ProPlate microtiter with adhesive bottom. Wells were then reacted with 50µg/ml streptavidin for one hour. The wells were then washed with 1XPBS and incubated with 100nM DNA probe solutions for 1 hr. Finally, the wells were washed with 1x PBS.

3.6.4 DNA hybridization and gRNA/Cas12a binding

DNA oligonucleotides were hybridized at 100 nM in a 0.2 µL PCR tube. DNA was firstly heated to 90°C and then cooled at a rate of 1.3°C per min to 35°C. gRNA and Cas12a were incubated for 10min at 37 °C at 500nM in a 0.2 µL PCR tube just before adding on surface and stored on ice for maximum preservation of activity.

3.6.5 Oligo dye/ligand coupling and purification

All sequences of DNA strands used in this work are provided in **Table 3.1**. Firstly, 100 nmoles of c(RGDfK(PEG-PEG)) was reacted with ~ 200 nmoles of NHS-azide in DMSO overnight (**Fig. 3.9**). Product 3 was then purified via reverse phase HPLC using a Grace Alltech C18 column (Solvent A: water + 0.05% TFA, Solvent B: acetonitrile + 0.05% TFA; starting condition: 90% A + 10 % B, 1%/min; Flow rate: 1 mL/min)

Purified product 3 was ligated to the BHQ_2 top strand via 1,3-dipolar cycloaddition click reaction. Briefly, 5 nmoles of alkyne ligand strand was reacted with ~70 nanomoles of product 4. The total

reaction volume is 50 µL, composed of 0.1 M sodium ascorbate and 0.1 mM Cu-THPTA for 2h at room temperature. The product was then purified with a P2 size exclusion column, and then purified with reverse phase HPLC using Agilent Advanced oligo column (Solvent A: 0.1M TEAA, Solvent B: acetonitrile; starting condition: 90% A + 10 % B, 0.5%/min gradient B, Flow rate: 0.5 mL/min) (**Fig. 3.9**).

10 nmole Amine labelled TGT strands were reacted overnight with a 20x excess of Cy3B-NHS or ATTO 647N-NHS dissolved in 10 µL DMSO. The total volume of the reaction was 100 µL, composed of 1x PBS supplemented with 0.1M $NaHCO_3$. Then P2 size exclusion gel was used to remove unreacted dye. The product was then purified by reverse phase HPLC using Agilent Advanced oligo column (Solvent A: 0.1M TEAA, Solvent B: acetonitrile; starting condition: 90% A + 10 % B, 1%/min gradient B, Flow rate: 0.5 mL/min) to purify products 1 and 2 (**Fig. 3.9**).

The retention times of all products and starting reagents are shown in **Fig. 3.9**. Concentrations of purified oligonucleotide conjugates were determined by measuring their A260 absorption value on a Nanodrop 2000 UV-Vis Spectrophotometer (Thermo Scientific). ESI- mass spectrometry was performed to confirm the successful ligation. **(Fig. 3.9)**

3.6.6 Solution based Cas12a amplification and plate reader readout

Cas12a reactions shown in **Figure 3.1E** were performed at 37°C for 1hr. We maintained a total activator solution concentration of 100 nM but tuned the ratio between the blocked and single stranded activator. We then added combined 20 nM Cas12a-gRNA complex and 100nM

fluorogenic reporter to the well and measured the final fluorescence intensity using plate reader with filter set (Ex/Em = 540/590 nm for reporter channel) during 1hr of enzyme activity.

3.6.7 Human platelet handling and Ethics agreement

Blood was collected by Emory Hospital, anticoagulated with sodium citrate or EDTA. The sample was then centrifuged for 12 min at 140 g (with 0.02U Apyrase). Then platelets rich plasma was separated and centrifuged for 5 min at 700 g with 3 μM PGE-1 and 0.02 U Apyrase. The platelets were then resuspended in Tyrodes buffer with 3uM PGE-1 and centrifuged for 5 min at 700 g. Finally, platelets were resuspended in Tyrodes buffer. It is worth noting that apyrase is important in the platelets purification process to prevent hemolysis caused platelets aggregation. Platelets counts were determined on a Sysmex XP- 300 automated hematology analyzer.

Ethics Human samples: This project has approval from the Emory University Ethics Committee to obtain samples from the participants and these ethical regulations cover the work in this study. Written informed consent was obtained from all participants

3.6.8 Cell culture

NIH/3T3 fibroblasts were cultured according to ATCC guidelines. Briefly, cells were cultured in DMEM supplemented with 10% fetal bovine serum (v/v) and penicillin/streptomycin. Cells were passaged every 2-3 days as required.

3.6.9 Mechano-Cas12a assisted tension sensor

MCATS assay was performed on the prepared biotin surface as described in the surface preparation section. First, hybridized concealed activator probes were incubated on biotin surface in 1x PBS buffer for 1hr. The wells were washed with 1x PBS. Then, cells were added onto the cRGDfK-labelled duplex surfaces for 1hr to promote cell adhesion with DMEM supplemented with 1% serum for NIH/3T3 cells or Tyrodes buffer with 10 μM ADP for platelets. Surfaces with exposed activator were imaged directly with fluorescence microscopy for high resolution characterization and quantification. Subsequently, 10mM of Mg^{2+}, gRNA/Cas12a complex and reporter DNA were mixed and added to the well to initiate the Cas12a amplification reaction with mechanically exposed activator. After 1hr of incubation, fluorescence intensities on 96 well plates were measured with a Bio-Tek® Synergy H1 plate reader (Ex/Em = 540/590 nm for reporter channel).

3.6.10 Dose-dependent inhibition of receptor mediated tension

For dose-dependent inhibition of experiments, the cell density of 3T3 fibroblasts was first characterized with a hemocytometer. Same number of 3T3 cells (25000) in cell culture medium were then incubated with different concentrations of inhibitor in the cell culture incubator for 30 minutes before plating onto 96 well plates. Afterwards, cells were incubated for 1hr to promote cell adhesion. Then the MCATS protocol was followed to achieve amplification and quantification.

For platelet MCATS measurements, human platelets were purified and incubated at room temperature for at least 30 min before beginning experiments. Platelets were then treated with drugs for 30 min before seeding onto 96 well-plates. 10 mM ADP was added to promote cell

adhesion. Then platelets were incubated at room temperature for 1hr. The same MCATS protocols were followed to achieve amplification and quantification for platelets.

3.6.11 Microscopy imaging

For MCATS experiments, Images were acquired on a Nikon Eclipse Ti microscope, operated by Nikon Elements software, a 1.49 NA CFI Apo 100x objective, perfect focus system, and a total internal reflection fluorescence (TIRF) laser launch with 488 nm (10 mW), 561 nm (50 mW), and 638 nm (20 mW). A reflection interference contrast microscopy (RICM) (Nikon: 97270) cube and a Chroma quad cube (ET-405/488/561/640 nm Laser Quad Band) were used for imaging. Imaging was performed on 96 well plates and glass coverslips using DMEM as cell imaging media for 3T3 cells and Tyrode's buffer for platelets. All imaging data was acquired at room temperature.

3.6.12 Statistics and reproducibility

P-values were determined by Student's t-test using GraphPad Prism8. Mechano-IC_{50} is calculated by fitting plot to a standard dose-response function: Signal=Bottom + (Top-Bottom)/(1+([drug]/IC50) using GraphPad Prism8. MCATS readout is typically replicated with 2 or 3 wells on the same plate within the same experiment. For CPB patient tension signal, all data are acquired along with positive control to adjust platelets tension signal to same positive level.

3.7 Acknowledgement

I thank the remarkable contributions from Dr. Roman Sniecinski in the clinical studies with MCATS. I thank Fania Szlam for running TEG and aggregometry experiments to validate MCATS results. I thank Dr. Renhao Li and Dr. Wenchun Chen for their extraordinary insights on human platelets experiment.

3.8 Appendix

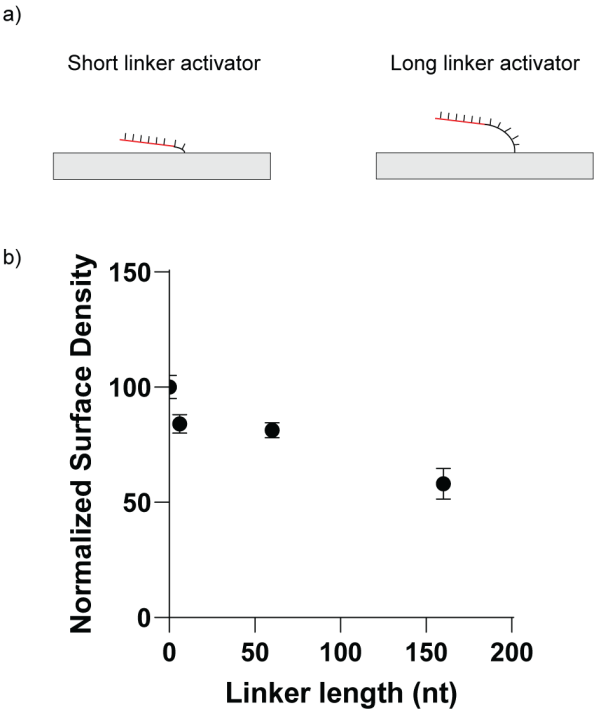

Figure 3.5. Comparison of surface density with different length of linkers. A) Scheme of different activators on the surface. B) Plots of normalized surface density vs linker length. All activators are incubated on surface for 1hr at 100nM. Surface density is normalized to activator without linker. Error bar represents S.E.M from five independent surfaces.

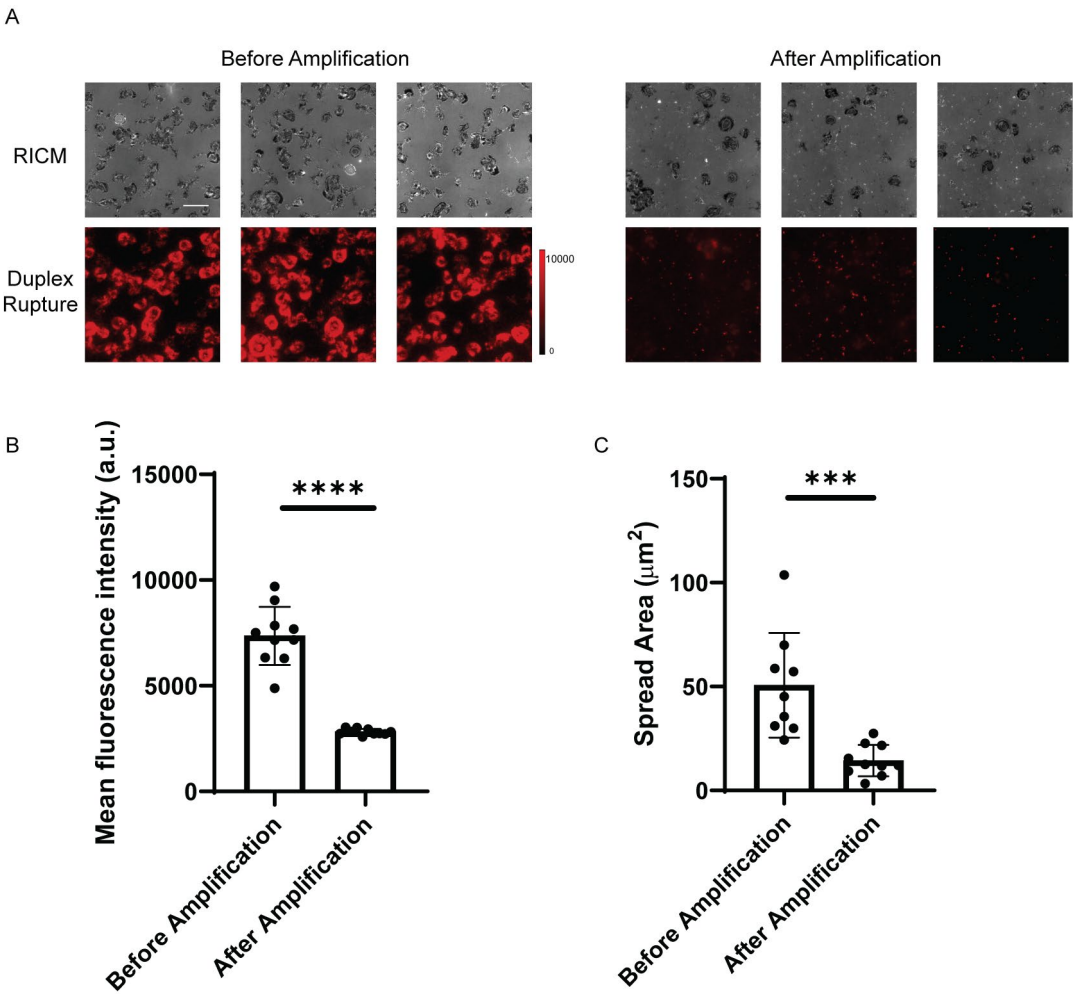

Figure 3.6. Cas12a auto-cleavage before and after amplification. A) Representative RICM, and duplex rupture (red) fluorescence images after platelets were incubated on concealed activator surface. The images compare the RICM cell spread area and duplex rupture signals before and after Cas12a/gRNA and reporter DNA were added for 1hr. Scale bar = 12 μm. B) Plot of mean fluorescence beneath platelets individual before and after amplification. Significance is calculated with Student T test, $P<0.0001$. Value is not background subtracted. Error bar represents S.D from 10 individual platelets C) Plot of spread area beneath individual platelets determined from RICM before and after amplification. Significance is calculated with Student T test, $P<0.001$. Error bar represents S.D from 10 individual platelets

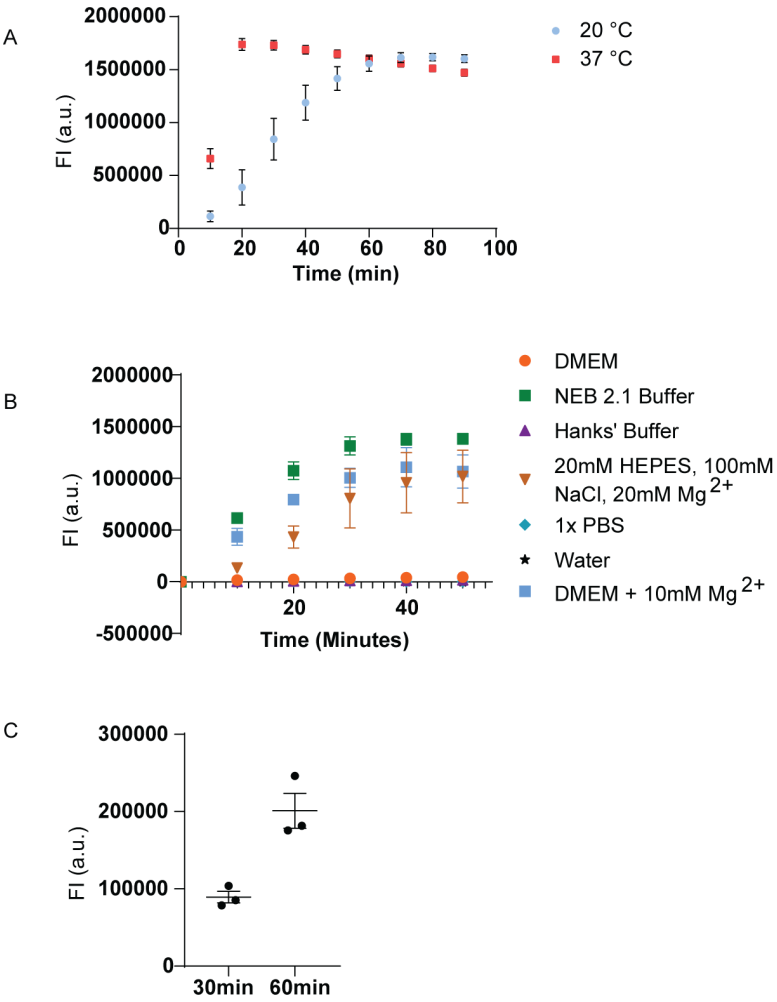

Figure 3.7. Optimization of MCATS parameters of temperature, buffer, and reaction time. A) Plot showing time-dependent fluorescence for Cas12a mediated hydrolysis of reporter DNA at 20 and 37 °C. The reaction was run with 100 nM soluble activator, 20 nM gRNA/Cas12a complex, and 100 nM reporter DNA. Results show that Cas12a activity is greater at 37 °C. Error bar represents S.E.M. obtained from three independent experiments. B) Plots of Cas12a activity in different buffers. We found that Cas12a is markedly less active in standard cell culture media compared to that of NEB buffer 2.1 which is likely due to decreased Mg ion concentration in cell media. Spiking cell culture media with 10 mM Mg^{2+} rescued Cas12a activity. Error bar represents S.E.M. obtained from three independent experiments. C) Plots of fluorescence signal at 30 and 60 min after triggering MCATS with Cas12a and reporter determined from human platelets (2*10^6). Error bar represents S.E.M. obtained from three independent experiments. Results indicate that 1hr amplification provides improved signal in cell experiments.

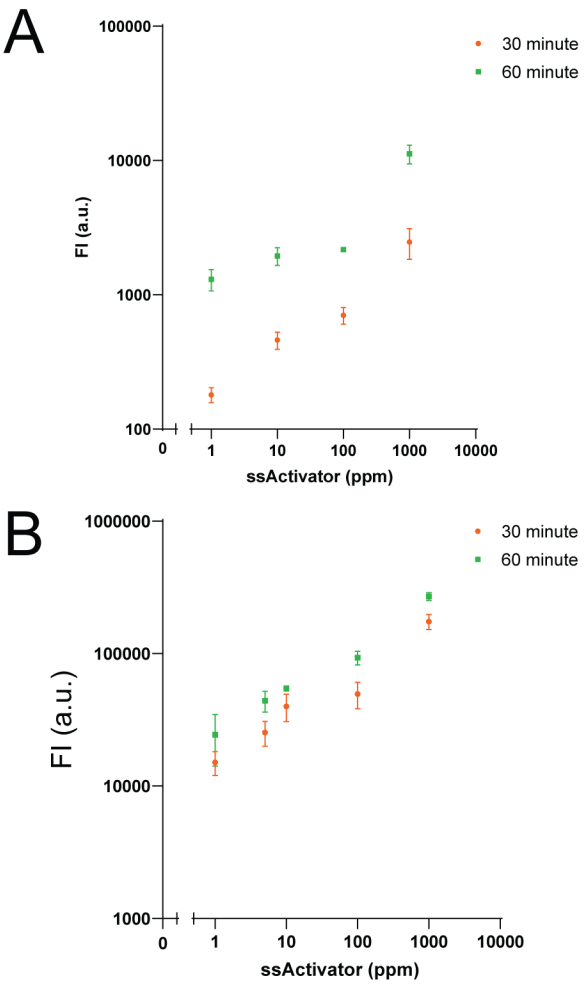

Figure 3.8. Comparing MCATS with two fluorogenic ssDNA substrates. A) 20 nM Cas12a-gRNA complex and 100 nM reporter DNA (/5ATTO565N/TT ATT /3BHQ_2/) of was added to 100nM ssDNA and concealed activator in solution, plot of fluorescence intensity-ssActivator concentration. S/N = 46. Error bar represents S.E.M. obtained from three independent experiments. B) 20 nM Cas12a-gRNA complex and 100 nM reporter DNA (/56-FAM/TT ATT /3IABkFQ/) of was added to 100 nM ssDNA and concealed activator in solution, plot of fluorescence intensity-ssActivator concentration. S/N = 19. Error bar represents S.E.M. obtained from three independent experiments.

A

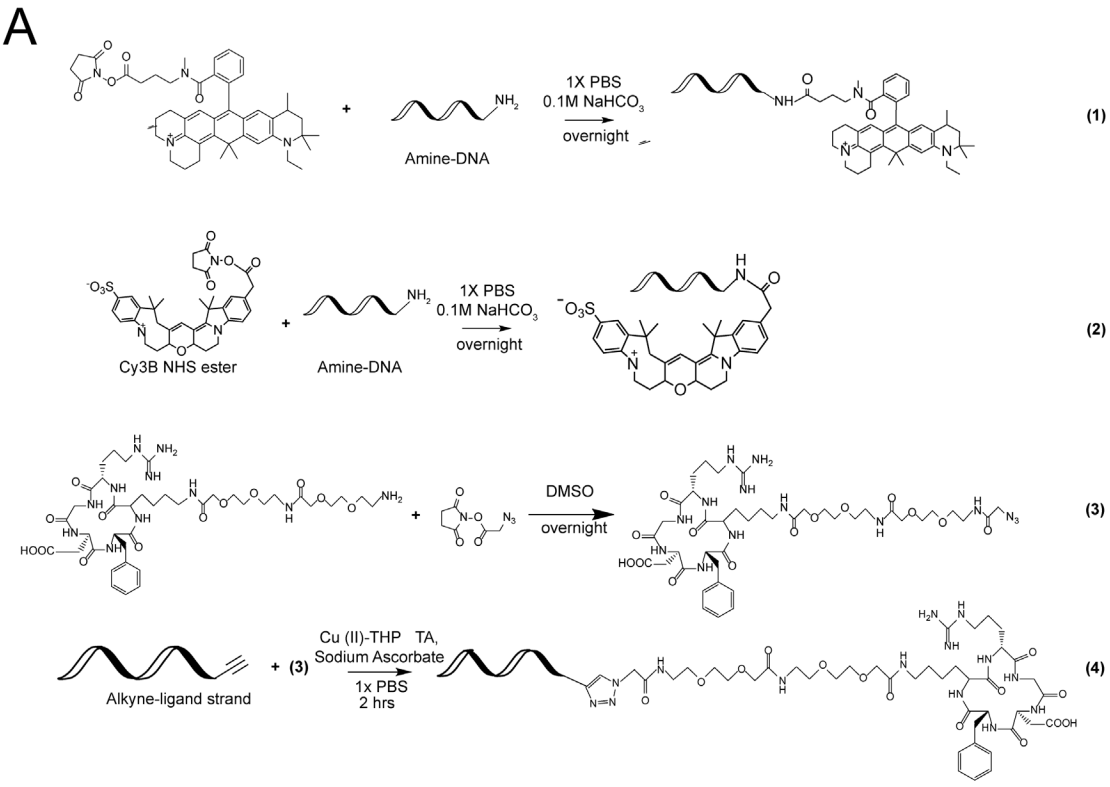

B

Strand Name	Expected Mass	Measured Mass
Cy3B 60T Cas12a Btm Strand	26059.7	26059.3
ATTO 647N 60T Cas12a TGT Btm Strand	26145.7	26143.3
cRGDfk BHQ2 Cas12a Top Strand	8514	8514.7
Cy3B 6T Cas12a Btm Strand	9633.2	9632.8
Cy3B No Spacer Cas12a Btm Strand	7808	7807.5

Figure 3.9. Characterization of modified oligonucleotides. A) Chemical structures and reactions of oligonucleotides, dye NHS esters and cRGDfk peptides. B) ESI-MS of DNA oligos used in the study and compared against that of expected mass.

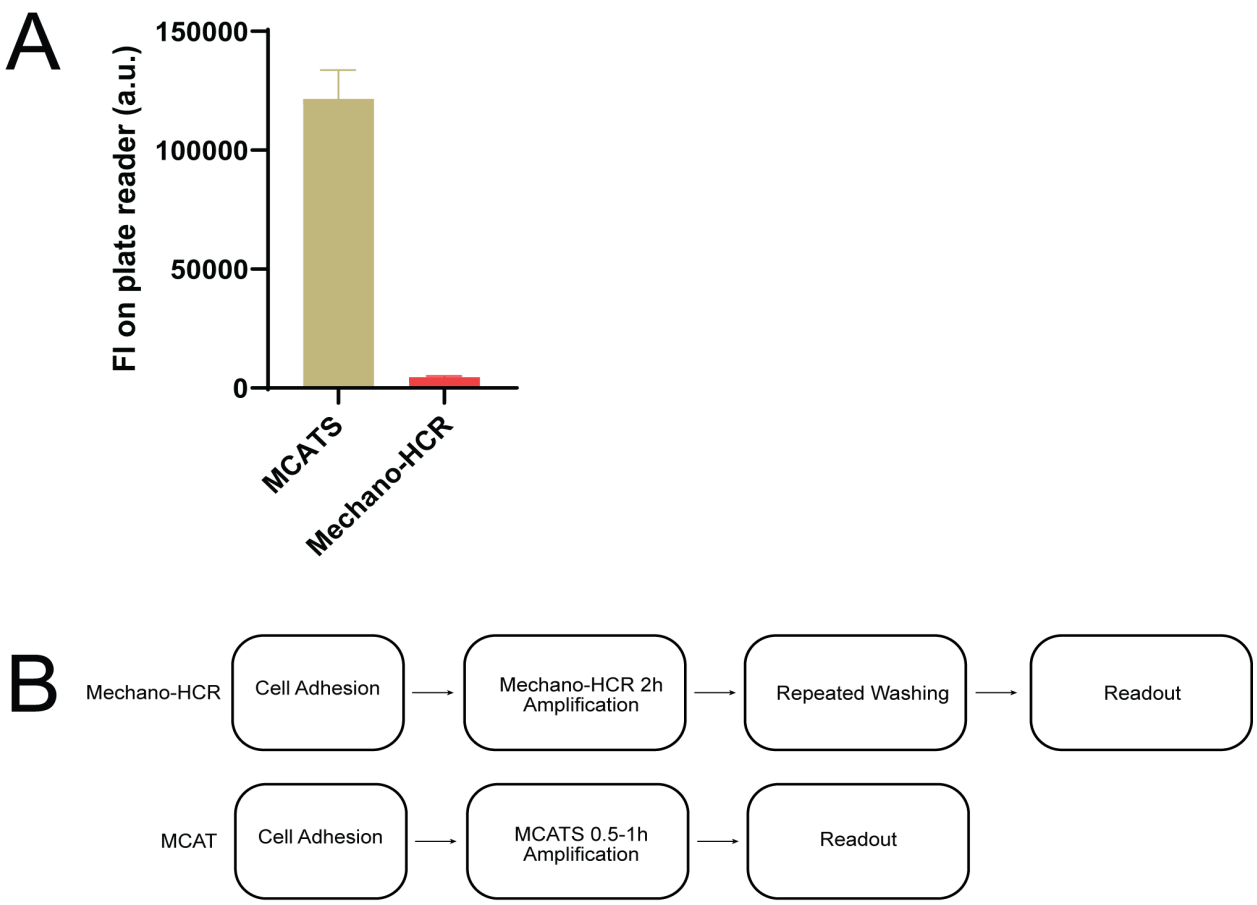

Figure 3.10. Comparison between MCATS and Mechano-HCR. A) Comparison of fluorescent signal of MCATS and Mechano-HCR amplified tension signal in the same day experiment with same number of cells (20000 NIH/3T3) incubating on the same surface and measured from same plate reader. B) Comparison of workflow of MCATS and Mechano-HCR. MCATS requires less steps in sample handling and less incubation time.

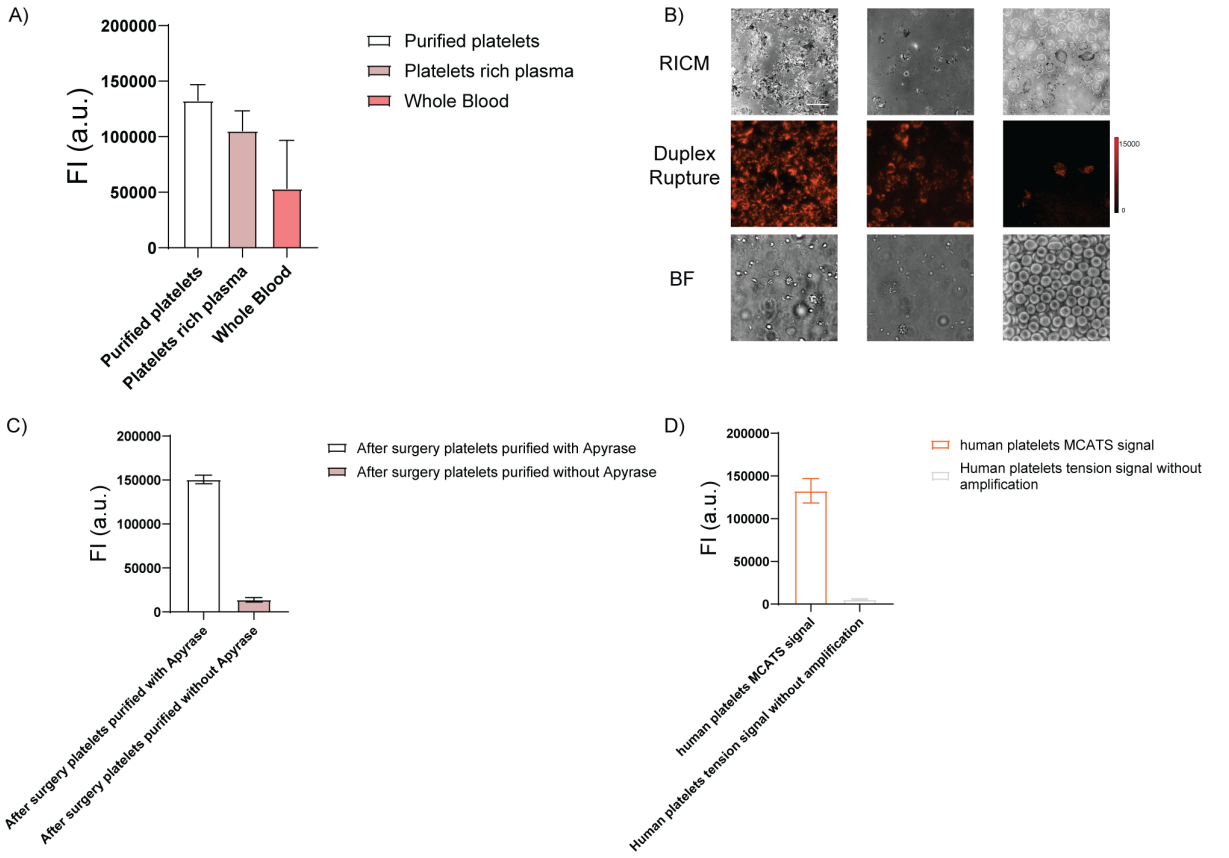

Figure 3.11. Platelets handling optimization. A) Comparison of MCATS signal using purified platelets, platelets rich plasma and whole blood. Error bar represents S.D from three wells with same patient sample. B) Representative of RICM, duplex rupture (red) fluorescence images and bright field images of tension signal when incubating different samples on concealed activator surface. Scale bar = 12 μm. C) Comparison of MCATS signal in one experiment with platelet purification with/without Apyrase. In some post-surgery samples, patients' blood showed hemolysis during centrifugation, which required Apyrase to prevent platelets aggregation during purification. Error bar represents S.D from three wells with same patient sample. D) Comparison of MCATS and non-amplified duplex rupture signal using plate reader, indicating MCATS amplification is crucial for detecting platelets tension signal. Error bar represents S.E.M. from three independent experiments.

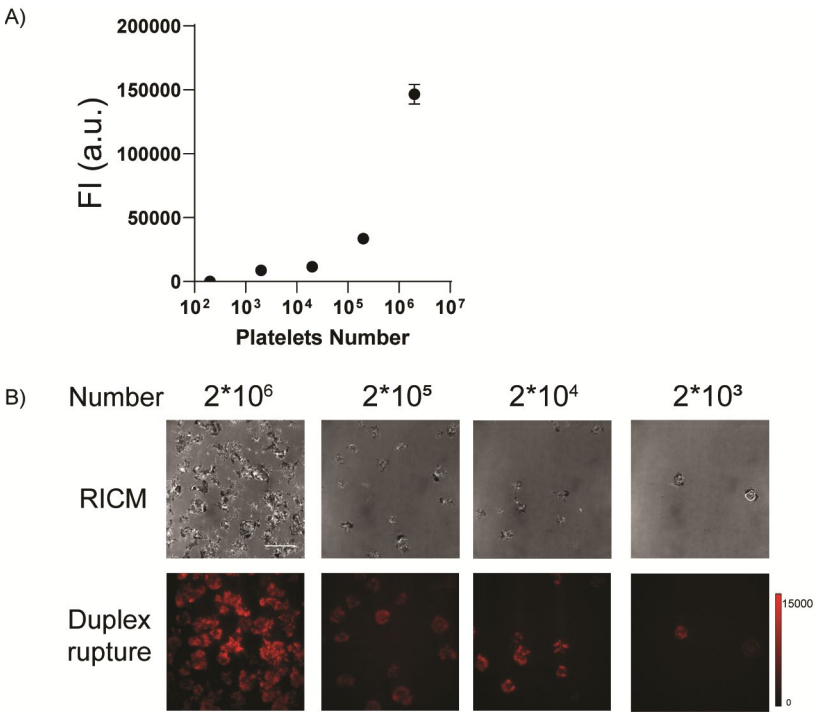

Figure 3.12. Testing MCATS with different number of platelets on surface. A) Comparison of MCATS signal using purified platelets, platelet rich plasma, and whole blood. Error bar represents S.E.M. from three independent experiments. B) Representative of RICM, duplex rupture (red) fluorescence images and bright field images of tension signal when incubating different samples on concealed activator surface. Scale bar = 10 μm

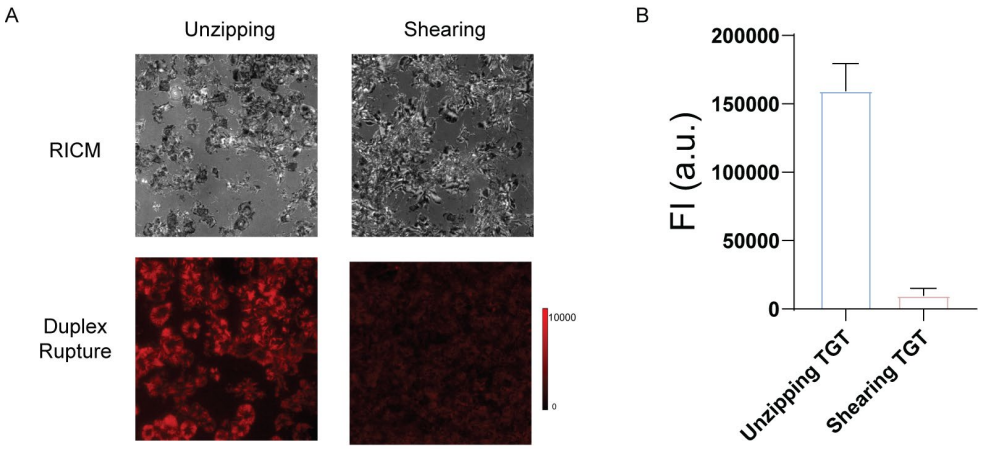

Figure 3.13: Shearing and unzipping probe with human platelets. A) Representative RICM and fluorescence images of cells cultured on T_{tol}= 12 pN and T_{tol}= 56 pN surfaces for 1hr. Scale bar = 12 μm. The red color is emission from Atto647N tagging the activator. The intensity bar next to each fluorescence image shows the absolute signal intensity for each image. B) Bar graph shows MCATS signal of same number of cells incubated on T_{tol}= 12 pN and T_{tol}= 56 pN surfaces. Error bars represent S.E.M. from n=3 independent experiments.

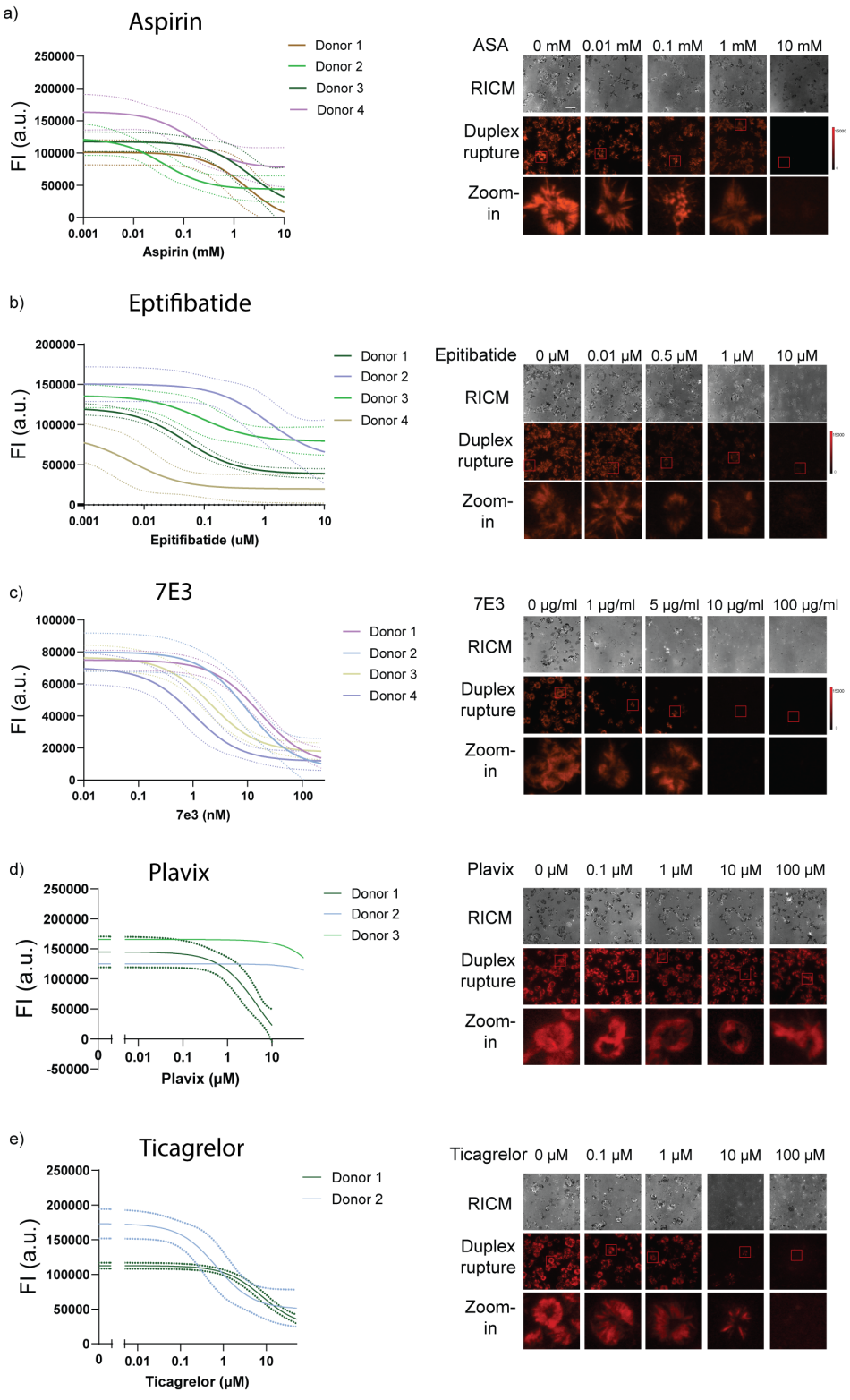

Figure 3.14: MCATS in measuring dose-response curves for inhibitors of platelets. A-E) Plots of [Aspirin], [Eptifibatide], [7E3], [Plavix], [Ticagrelor] vs MCATS signal for different donors. Representative RICM, duplex rupture fluorescence (red) and zoom-in fluorescence images for one

donor with drug concentration ranging from 0 mM to 10mM. Scale bar = 10 μm. Mechano-IC50 for each donor was calculated by fitting plot to a standard dose-response function: Signal=Bottom + (Top-Bottom)/(1+([drug]/IC50). Solid line represents the fitting and dashed line represents 95% CI.

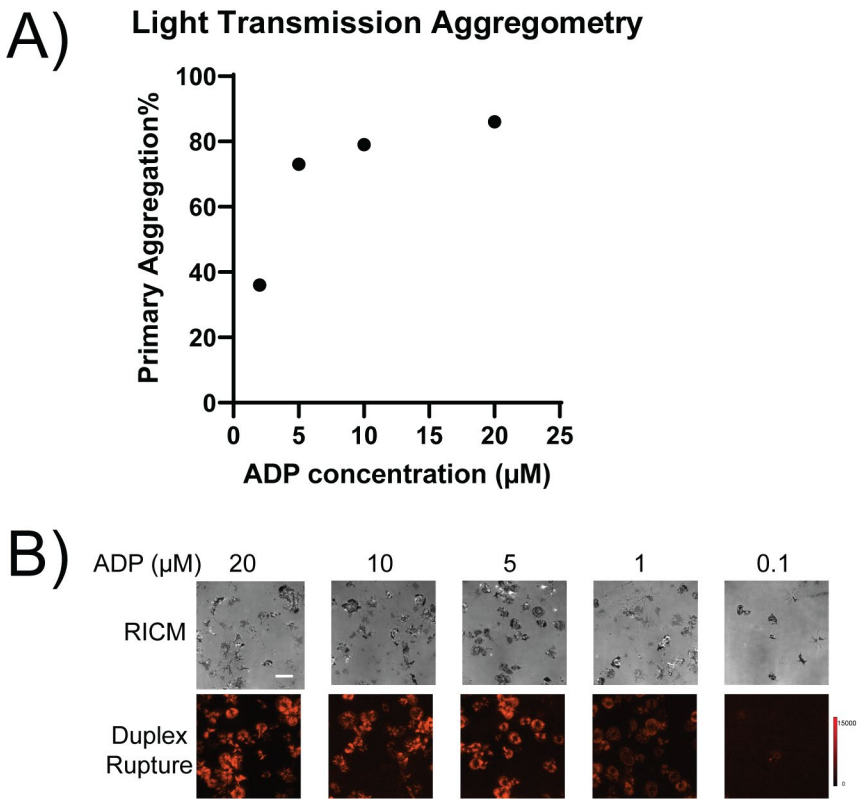

Figure 3.15: LTA data for ADP agonist test. A) Light Transmission aggregometry data for PA value against different concentration of ADP. B) Representative RICM, duplex rupture fluorescence (red) images for one donor with ADP concentration ranging from 0.1 mM to 20mM. Scale bar = 10 μm.

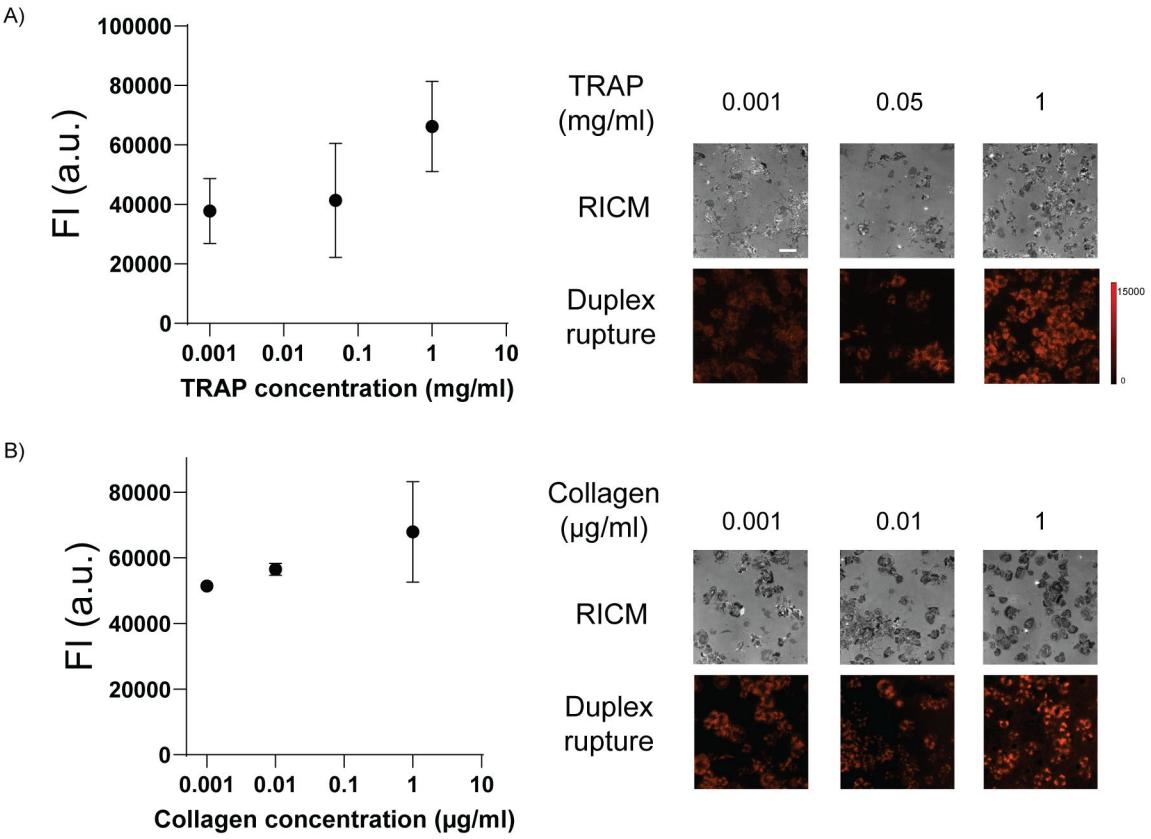

Figure 3.16: TRAP and collagen agonist test. A) Plots of MCATS signal against different concentration of TRAP. Representative RICM, duplex rupture fluorescence (red) images for one donor with TRAP concentration ranging from 0.001 mg/ml to 1mg/ml. Scale bar = 10 µm. B) Plots of MCATS signal against different concentration of Collagen. Representative RICM, duplex rupture fluorescence (red) images for one donor with TRAP concentration ranging from 0.001 µg/ml to 1µg/ml. Scale bar = 10 µm.

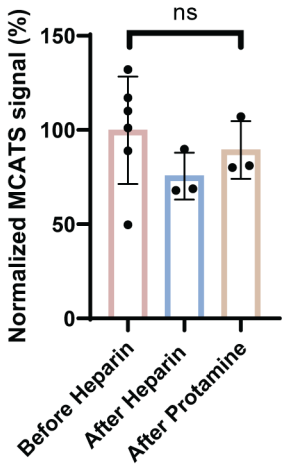

Figure 3.17: Heparin and protamine influence on platelet tension. Plots of normalized MCATS signal for purified platelets from non-heparin treated blood, purified platelets from 2h heparin (0.25U/ml) treated blood, and purified platelets from heparin treated and protamine neutralized (1mg/100U) blood. Results indicating heparin influence on platelets was fully reversed after protamine addition. Error bar represents SEM from n=3 independent experiments.

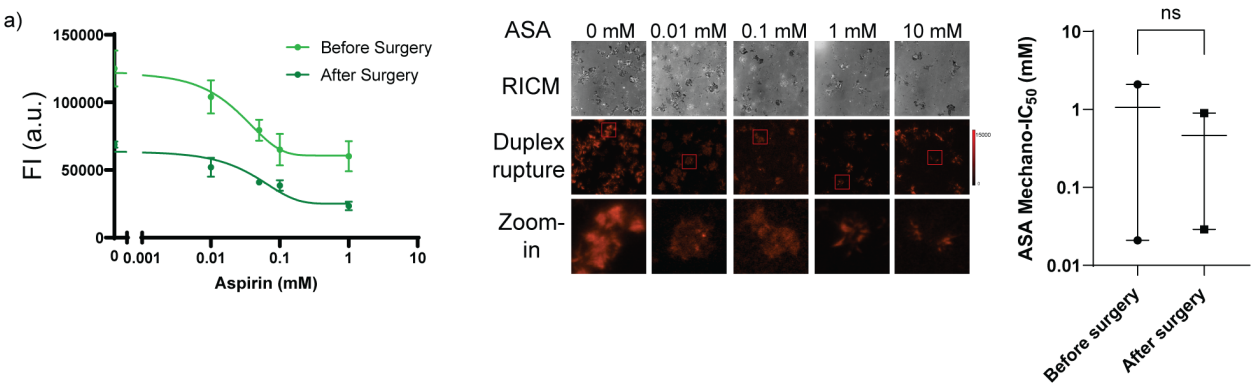

Figure 3.18: Mechano-IC50 of Aspirin for patients before and after surgery. Plots of [Aspirin] vs MCATS signal for patient 1 before and after Surgery. Error bar represents three replicate wells in the same day experiment. Representative RICM, duplex rupture fluorescence (red) and zoom-in fluorescence images for one donor with drug concentration ranging from 0 mM to 10mM. Scale bar = 10 μm. Mechano-IC50 for each donor was calculated by fitting plot to a standard dose-response function: Signal=Bottom + (Top-Bottom)/(1+([drug]/IC50). Plots of calculated IC50 before and after surgery for two patients. Non- significance is calculated with Student T test, P>0.05.

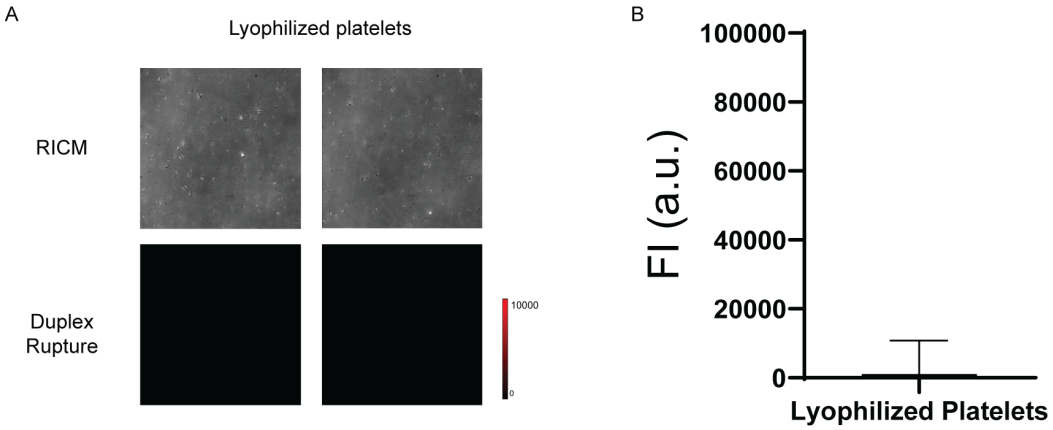

Figure 3.19: Testing lyophilized platelets. A) Representative RICM, duplex rupture fluorescence (red) images for lyophilized platelets on tension probes. Plots of MCATS signal. Results indicating lyophilized platelets have no active mechanical signal.

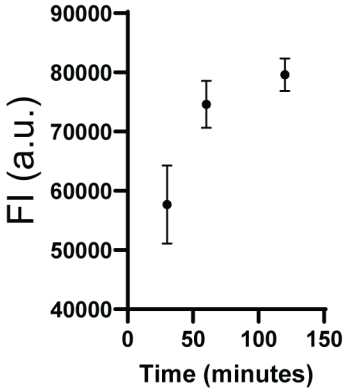

Figure 3.20: Amplification time influence on MCATS signal. Plots of MCATS signal at different time of amplification. Error bar represents SEM of three independent experiments.

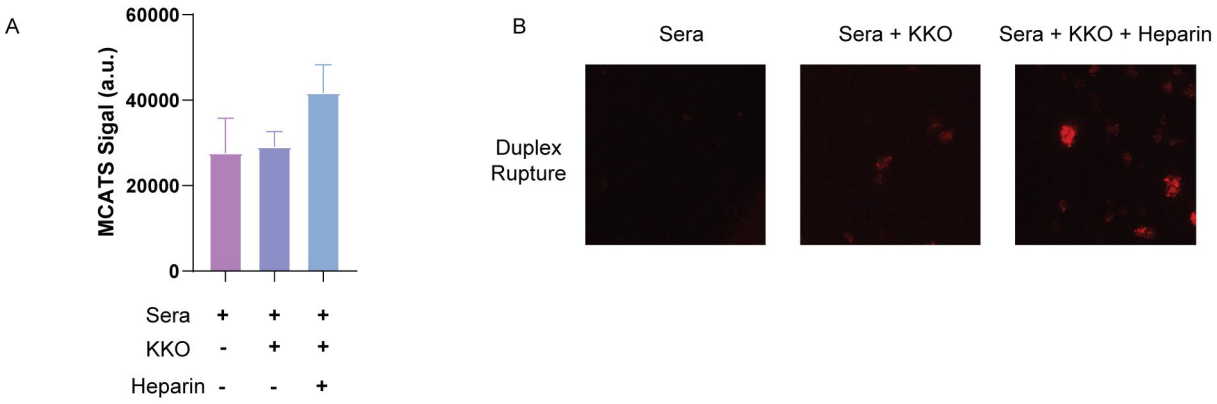

Figure 3.21: Antibody activating platelets detected by MCATS. A) Plots of MCATS signal for Platelets in sera, platelets in sera adding 80µg/ml KKO and platelets in sera adding 80µg/ml KKO and 0.1U/ml heparin. Results indicating MCATS may be used to detect antibody activated platelets. B) Representative duplex rupture fluorescence (red) images.

Table 3.2: Demographics, laboratory values, TEG data and surgery note for CPB patients

	Patient 1	Patient 2	Patient 3	Patient 4	Patient 5
Age	61	22	66	25	68
Sex	F	M	M	F	M
Operation	MVR/TVR	PVR	CABG_ablation	Nephrectomy	Bentall
Hematology*					
Platelet count (cells mcL-1)	322	264	167	482	168
Medication*					
Aspirin	Y	Y	Y	N	N
ADPI	N	N	Y	N	N
TEG6S MA (mm)	68.6	69	63.7	66	63
Operation Note					
CPB time (min)	314	84	229	204	182
Blood Products Transfused in Operation					
RBC in OR	3	0	1	18	0
PLT in OR	3	1	1	5	0
FFP in OR	4	0	3	19	0
Cryo in OR	15	5	10	50	0

3.9 References

1. Orr, A.W., Helmke, B.P., Blackman, B.R. & Schwartz, M.A. Mechanisms of mechanotransduction. *Dev. Cell* **10**, 11-20 (2006).
2. Zhang, Y. et al. Platelet integrins exhibit anisotropic mechanosensing and harness piconewton forces to mediate platelet aggregation. *Proc. Natl. Acad. Sci. U.S.A.* **115**, 325-330 (2018).
3. Ma, R. et al. DNA probes that store mechanical information reveal transient piconewton forces applied by T cells. *Proc. Natl. Acad. Sci. U.S.A.* **116**, 16949-16954 (2019).
4. Ramey-Ward, A.N., Su, H. & Salaita, K. Mechanical Stimulation of Adhesion Receptors Using Light-Responsive Nanoparticle Actuators Enhances Myogenesis. *ACS Appl. Mater. & Interfaces* **12**, 35903-35917 (2020).
5. Wang, X. & Ha, T. Defining single molecular forces required to activate integrin and notch signaling. *Science* **340**, 991-994 (2013).
6. Gaudet, C. et al. Influence of type I collagen surface density on fibroblast spreading, motility, and contractility. *Biophys. J.* **85**, 3329-3335 (2003).
7. Zhang, Y., Ge, C., Zhu, C. & Salaita, K. DNA-based digital tension probes reveal integrin forces during early cell adhesion. *Nat. Commun.* **5**, 1-10 (2014).
8. Doudna, J.A. & Charpentier, E. The new frontier of genome engineering with CRISPR-Cas9. *Science* **346**, 1258096 (2014).
9. Kaminski, M.M., Abudayyeh, O.O., Gootenberg, J.S., Zhang, F. & Collins, J.J. CRISPR-based diagnostics. *Nat. Biomed. Eng.* **5**, 643-656 (2021).
10. Chen, J.S. et al. CRISPR-Cas12a target binding unleashes indiscriminate single-stranded DNase activity. *Science* **360**, 436-439 (2018).

11. Broughton, J.P. et al. CRISPR–Cas12-based detection of SARS-CoV-2. *Nat.Biotechnol.* **38**, 870-874 (2020).

12. Xiong, Y. et al. Functional DNA regulated CRISPR-Cas12a sensors for point-of-care diagnostics of non-nucleic-acid targets. *J. Am. Chem. Soc.* **142**, 207-213 (2019).

13. Mannino, R.G. et al. Smartphone app for non-invasive detection of anemia using only patient-sourced photos. *Nat. Commun.* **9**, 1-10 (2018).

14. Ting, L.H. et al. Contractile forces in platelet aggregates under microfluidic shear gradients reflect platelet inhibition and bleeding risk. *Nat. Commun.* **10**, 1-10 (2019).

15. Cuisset, T. et al. Relationship between aspirin and clopidogrel responses in acute coronary syndrome and clinical predictors of non response. *Thrombo. Res.* **123**, 597-603 (2009).

16. Neira, H.D. & Herr, A.E. Kinetic analysis of enzymes immobilized in porous film arrays. *Anal. Chem.* **89**, 10311-10320 (2017).

17. Duan, Y. et al. Mechanically Triggered Hybridization Chain Reaction. *Angew. Chem. Int. Ed.* **60**, 19974-19981 (2021).

18. Glazier, R. et al. DNA mechanotechnology reveals that integrin receptors apply pN forces in podosomes on fluid substrates. *Nat. Commun.* **10**, 1-13 (2019).

19. Sahai, E., Ishizaki, T., Narumiya, S. & Treisman, R. Transformation mediated by RhoA requires activity of ROCK kinases. *Curr. Biol.* **9**, 136-145 (1999).

20. Davidson, B.L. et al. Bleeding Risk of Patients With Acute Venous Thromboembolism Taking Nonsteroidal Anti-Inflammatory Drugs or Aspirin. *JAMA Intern. Med.* **174**, 947-953 (2014).

21. Campo, G. et al. Poor response to clopidogrel: current and future options for its management. *J Thromb Thrombolysis* **30**, 319-331 (2010).

22. Awtry, E.H. & Loscalzo, J. Aspirin. *Circulation* **101**, 1206-1218 (2000).

23. Phillips, D.R. & Scarborough, R.M. Clinical pharmacology of eptifibatide. *J. Am. Coll. Cardiol.* **80**, 11B-20B (1997).

24. Tcheng, J.E. et al. Pharmacodynamics of chimeric glycoprotein IIb/IIIa integrin antiplatelet antibody Fab 7E3 in high-risk coronary angioplasty. *Circulation* **90**, 1757-1764 (1994).

25. Sassoli, P.M. et al. 7E3 F (ab') 2, an effective antagonist of rat αIIbβ3 and αvβ3, blocks in vivo thrombus formation and in vitro angiogenesis. *Thromb. Haemost.* **85**, 896-902 (2001).

26. Abe, M. & Ozawa, Y. Y. Uda, Y. Morimitsu, Y. Nakamura, T. Osawa,"A novel labdane-type trialdehyde from myoga (zingiber mioga roscoe) that potently inhibits human platelet aggregation and human 5-lipoxygenase". *Biosci. Biotechnol. and Biochem* **70**, 2494-2500 (2006).

27. Wang, X. et al. Comparative analysis of various platelet glycoprotein IIb/IIIa antagonists on shear-induced platelet activation and adhesion. *J. Pharmacol. Exp. Ther.* **303**, 1114-1120 (2002).

28. Dyke, C. et al. Universal definition of perioperative bleeding in adult cardiac surgery. *J. Thorac. Cardiovasc. Surg.* **147**, 1458-1463. e1451 (2014).

29. Greiff, G. et al. Prediction of bleeding after cardiac surgery: comparison of model performances: a prospective observational study. *J. Cardiothorac. Vasc. Anesth.* **29**, 311-319 (2015).

30. Bartoszko, J., Wijeysundera, D.N. & Karkouti, K. Comparison of two major perioperative bleeding scores for cardiac surgery trials: universal definition of perioperative bleeding in cardiac surgery and European coronary artery bypass grafting bleeding severity grade. *Anesthesiology* **129**, 1092-1100 (2018).

31. Kaufmann, C.R., Dwyer, K.M., Crews, J.D., Dols, S.J. & Trask, A.L. Usefulness of thrombelastography in assessment of trauma patient coagulation. *J. Trauma.* **42**, 716-720; discussion 720-712 (1997).

32. Moenen, F.C. et al. Screening for platelet function disorders with Multiplate and platelet function analyzer. *Platelets* **30**, 81-87 (2019).

33. Barton, C.A. et al. Thromboelastography with platelet mapping: Limited predictive ability in detecting preinjury antiplatelet agent use. *J. Trauma Acute Care Surg.* **91**, 803-808 (2021).

34. Kondo, C. et al. Platelet dysfunction during cardiopulmonary bypass surgery. With special reference to platelet membrane glycoproteins. *Asaio j.* **39**, M550-553 (1993).

35. Choi, J.-L., Li, S. & Han, J.-Y. Platelet Function Tests: A Review of Progresses in Clinical Application. *BioMed Res. Int.* **2014**, 456569 (2014).

36. Ranucci, M. et al. Platelet function after cardiac surgery and its association with severe postoperative bleeding: the PLATFORM study. *Platelets* **30**, 908-914 (2019).

37. Wang, T.Y. et al. Cluster-randomized clinical trial examining the impact of platelet function testing on practice: the treatment with adenosine diphosphate receptor inhibitors: longitudinal assessment of treatment patterns and events after acute coronary syndrome prospective open label antiplatelet therapy study. *Circ. Cardiovasc. Interv.* **8**, e001712 (2015).

38. Dhakal, B. et al. Disease burden, complication rates, and health-care costs of heparin-induced thrombocytopenia in the USA: a population-based study. *Lancet Haematol.* **5**, e220-e231 (2018).

39. Arepally, G. et al. Characterization of a murine monoclonal antibody that mimics heparin-induced thrombocytopenia antibodies. *Blood* **95**, 1533-1540 (2000).

40. Liu, Y. et al. DNA-based nanoparticle tension sensors reveal that T-cell receptors transmit defined pN forces to their antigens for enhanced fidelity. *Proc. Natl. Acad. Sci.* **113**, 5610-5615 (2016).

Chapter 4. Investigate T cell Mechanics with Reversible Tension Probe MCATS (RT-MCATS)

4.1 Abstract

T cells constantly sense and exert forces through their surface receptors. These forces influence the recognition, activation, and function of T cells in immune response. However, these forces are diminishingly weak, and infrequent. Hence, they are challenging to detect and investigate. Here, we report a MCATS assay that are based on reversible DNA tension probes. We optimize the probes with a strain-free design to further increase the S/N. With reversible tension probe MCATS, we can achieve high-throughput detection of T cell receptor mediated tension, detect different potency of altered peptide ligands, and test the influence of Latrunculin B on T cell Mechanics. The RT-MCATS assay may serve as a powerful tool in the development of cancer immunotherapy by measuring T cell mechanics in a rapid manner.

4.2 Introduction

T cell is a type of blood cell that play essential roles in immune response. T cells use their T cell receptors (TCRs) to search antigens on antigen-presenting cells (APCs) and trigger antigen-specific immune responses. Different mechanisms such as serial engagement and kinetic proofreading have been discussed about how TCRs can distinguish different antigenic peptide-bound major histocompatibility complexes (pMHCs).[1] Recently, it is reported that mechanical forces play an important role in regulating this specific and sensitive recognition between T cell receptors and antigenic peptide-bound major histocompatibility complexes (pMHCs).[2-4] However, forces applied by T cell receptors are highly transient (ms to 1s) and weak (1-20pN).[5-8] Therefore, studying the interplay between mechanical forces and chemical signaling in T cells is still

challenging. Our lab previously developed reversible DNA tension probe that can map the pN forces exerted by live cells.[9] As is discussed in Chapter 1, these tension probes revealed the importance of pN forces in T cell receptor triggering and decreased activation level was observed when force transmission was terminated.[10] Further development in using a locking strand for mechanical information storage also indicates mechanical sampling is correlated with antigen potency.[4] Together, a robust and convenient way to measure TCR-pMHC forces may provide great opportunity to identifying immunogenic antigens and T cells that can recognize them. However, the transient mechanical event between TCR and its target makes imaging methods challenging and limited signal from reversible tension probes requires a high-end fluorescent microscope to quantify. As a result, current methods to detect T cell forces depend on microscope and are low throughput, making it challenging to use TCR-pMHC mechanics in the development of cancer immunotherapy.

Accordingly, we apply MCATS technology to reversible DNA tension probes to address this challenge. MCATS is an ultrasensitive fluorescence-based assay to detect the molecular forces generated by cells. In reversible tension probe MCATS (RT-MCATS), the activator is located and hidden on the DNA hairpin probe within the stem region. (**Figure 4.1**) This hairpin probe is immobilized on a surface via hybridization to a surface anchor strand. Another strand hybridized to the other end of the hairpin tension probes contains biotin to conjugate with ligands or antibodies via biotin-streptavidin interaction for TCR engagement. Without active tension from T cell, the hairpin will stay closed and therefore can not active Cas12a because there is not a PAM sequence on the hairpin stem. This strategy is similar to what we've described in Chapter 3. When cells are seeded on the surface, T cell receptor would bind to anti-CD3ε antibody or pMHC and exert

tension to the tension probe. Forces that exceed that mechanical tolerance $F_{1/2}$ of the hairpin would lead to the opening of DNA hairpin and expose the single stranded activator sequence to trigger Cas12a/gRNA nuclease activity. Once activated, Cas12a will collaterally cleave single stranded DNA reporter. As a result, RT-MCATS will generate massive fluorescence signal and can be measured directly with conventional plate reader for high throughput readouts.

4.3 Results and Discussion

4.3.1 Design of MCATS with reversible DNA tension probe

We first designed a reversible DNA hairpin tension probe that can be mechanically opened by T cell generated forces. For reversible DNA hairpin tension probe, the $F_{1/2}$ (the force that leads to a 50% probability of hairpin unfolding) can be tuned by adjusting the GC content and length of the stem-loop structure.[11, 12] These DNA hairpin tension probes consist of three strands: a top strand with a ligand (anti-CD3Ɛ or pMHC in our case) and a fluorophore (Cy3B), a bottom strand with a quencher (BHQ2) and an anchoring functional group (DBCO), and a hairpin strand that is hybridized to the other 2 strands. **(Figure 4.1A)** The dye labeling and surface chemistry is described in the method section. Originally, we adopted the hairpin design from previous publication with $F_{1/2}$=4.7 pN which has shown to be able to detect pN forces applied by TCR.[9] However, in this design, the stem region is only 9 base pairs while CRISPR-Cas12a gRNA needs at least 18bp and ideally 20 or 21 bp complementary region for their activators. [13, 14] Therefore, we had to include single stranded region in the hairpin loop in the activator sequence design. However, this partially concealed activator sequence design led to an increased background leakage without cell tension because of the high affinity between the Cas12a/gRNAand its target. This would unfold the hairpin and therefore couldn't be used in T cell experiments. (**Figure 4.5**)

To address this issue, we elongated the stem region of the DNA hairpin to 20 base pairs to suppress the background leakage from the Cas12a/gRNA interacted with the DNA hairpin. Based on the length and GC content of the DNA, we estimated that the $F_{1/2} \sim 6$ pN of this DNA hairpin probe which TCR forces could open. [10, 11] In the case, the activator sequence is completely concealed in

stem region and can only activate Cas12a/gRNA complex upon being mechanically unfolded by TCR force.

To test whether the newly designed hairpin tension probe can detect live-cell TCR mechanics and whether it can be used for MCATS amplification, we seeded T cells on surfaces fully covered with our DNA hairpin tension probes presenting anti-CD3Ɛ antibodies. We observed the increased fluorescent tension signal, indicating the opening of the hairpin probe by TCR mediated tension as is shown in **Figure 4.1B**. After adding Cas12a/gRNA complex and single stranded reporter DNA to the system for 1 hr at 37 ℃, we were able to detect the amplified fluorescent signal using a conventional plate reader which showed significantly higher tension in T cell on hairpin probes group comparing with negative control groups. (**P=0.03, figure 4.1C**)

However, we noticed that even after amplification, the signal from RT-MCATS on T cell experiment is still significantly lower compared with positive control group (**Figure 4.6**) where we change the sequence of the other half of hairpin stem to make it constantly open. We believe there could be a few reasons behind the limited signal in T cell experiments. First, T cell mechanical events are weaker and less frequent compared with integrin mediated platelet forces. As a result, the signal would be low even after amplification. Second, the hairpin-based tension probe hasn't been fully optimized, such as the linker length, and therefore requires further investigation as is described in Chapter 3. Last but not least, in reversible tension probe design, the hairpin strand is constantly under force (F>6pN) in the experiment which is different from irreversible DNA duplex design. This force stretched behavior could limited the Cas12a targeting and cleavage activity as is recently reported by Rueda and colleagues.[15]

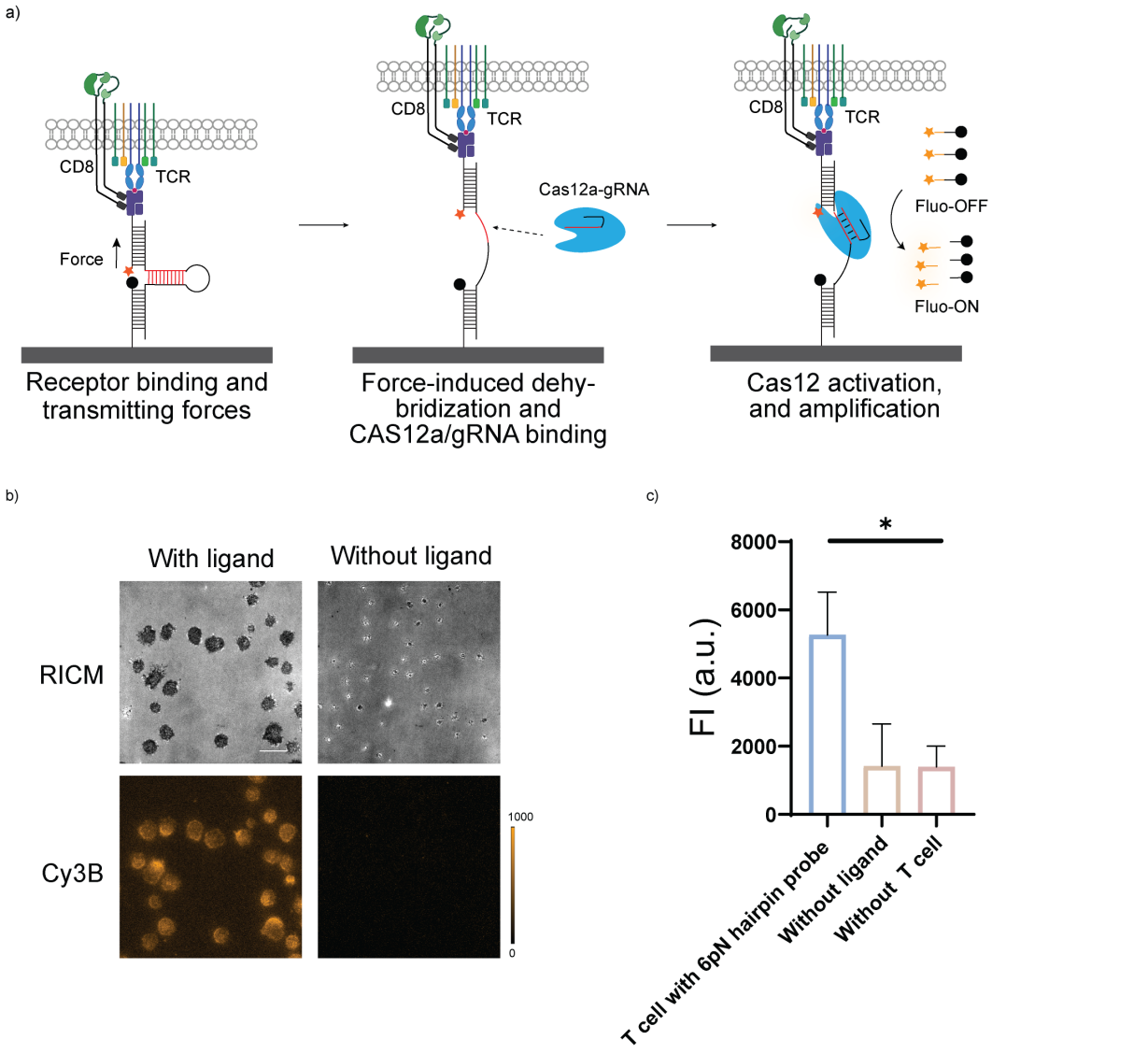

Figure 4.1: Scheme and T cell experiment of RT-MCATS. a-b) Schematic showing RT-MCATS T cell assay. Cellular forces would reveal an activator (Red) that activates Cas12a to cleave reporter strands in solution. In our work, the activator is tagged with Cy3B while the reporter DNA is tagged with Atto565N and BHQ2. b) Representative RICM and duplex rupture (orange) fluorescence images of T cell on 6pN hairpin tension probes. Scale bar = 10 μm. Calibration bar shows absolute value of fluorescent intensity. c) Plot showing plate reader can detect RT-MCATS signal with T cells. Error bar represents S.E.M. from 3 independent experiments. Significant value is calculated from student T test with p=0.03.

4.3.2 Optimization of RT-MCATS design with strain-free strategy and rapid detection of TCR forces with altered peptide ligands.

Since the force stretched hairpin may hinder the activation and nuclease activity of Cas12a, we designed a force-free reversible hairpin probe to further increase the sensitivity of our assay. To achieve this goal, we combined the ligand strand and surface anchor strand and linked them with a single stranded T rich linker. This linker is designed to be longer than the opened hairpin stem but shorter than the hairpin opened stem-loop structure. Therefore, when cellular forces are applied to the hairpin, the force will mechanically unfold the stem region since the linker is longer than the stem, the opening will not be influenced by the linker. After the hairpin is fully unfolded, because the linker is shorter than the stem and loop together, the force will be beard on the ligand-surface strand and therefore free the strain from hairpin to activate Cas12a. (**Figure 4.2A**) The detailed sequence of oligonucleotides used in this chapter can be found in **table 4.1.**

Next, we tested T cell experiment with strain-free reversible tension probe MCATS. By seeding the T cell ($2*10^6$) on the surface with strain-free hairpin probes and adding Cas12a/gRNA complexes and reporter DNA for 1hr, we noticed a twice increase in signal to noise ratio compared with traditional hairpin probe design. (**Figure 4.2B**) These results indicate that strain did inhibit Cas12a activity on traditional hairpin design. Considering that strain-free RT-MCATS had significantly higher signal to noise ratio, we next used this design for all the following experiments with reversible tension probes. It is also worth noting that we expect the activated Cas12a will be released from the surface as is suggested by T cell detached from surface after amplification. (**Figure 4.7**)

We next applied strain-free RT-MCATS to detect T cell mechanics with different cognate ligands. TCR–pMHC interaction is highly specific, which allows T cells to discriminate between even single amino acid mutants of pMHC despite their similar affinity.[16] It has been reported that TCR-pMHC force is related to antigen immunogenicity.[4] We tested OT-1 cell mechanics with pMHC N4 (SII**N**FEKL) and well-characterized altered peptide ligands (APL) pMHC V4 (SII**V**FEKL), as well as anti-CD3**Ɛ**. We found that RT-MCATS can rapidly detect TCR-ligand mechanics with a conventional plate reader. The results showed that pMHC N4 lead to a much higher tension signal compared with pMHC V4, which is consistent with previous report of TCR apply weaker force to pMHC V4 because of its low potency (**Figure 4.2 C, Figure 4.8**). It is also interesting to note that the V4 only show slightly weaker signal than antiCD3Ɛ. This may be due to the fact that while TCR exerted weaker tension with V4 than anti-CD3Ɛ, TCR has a higher mechanical sampling frequency with V4 than anti-CD3Ɛ, which is reported in the literature.[4]

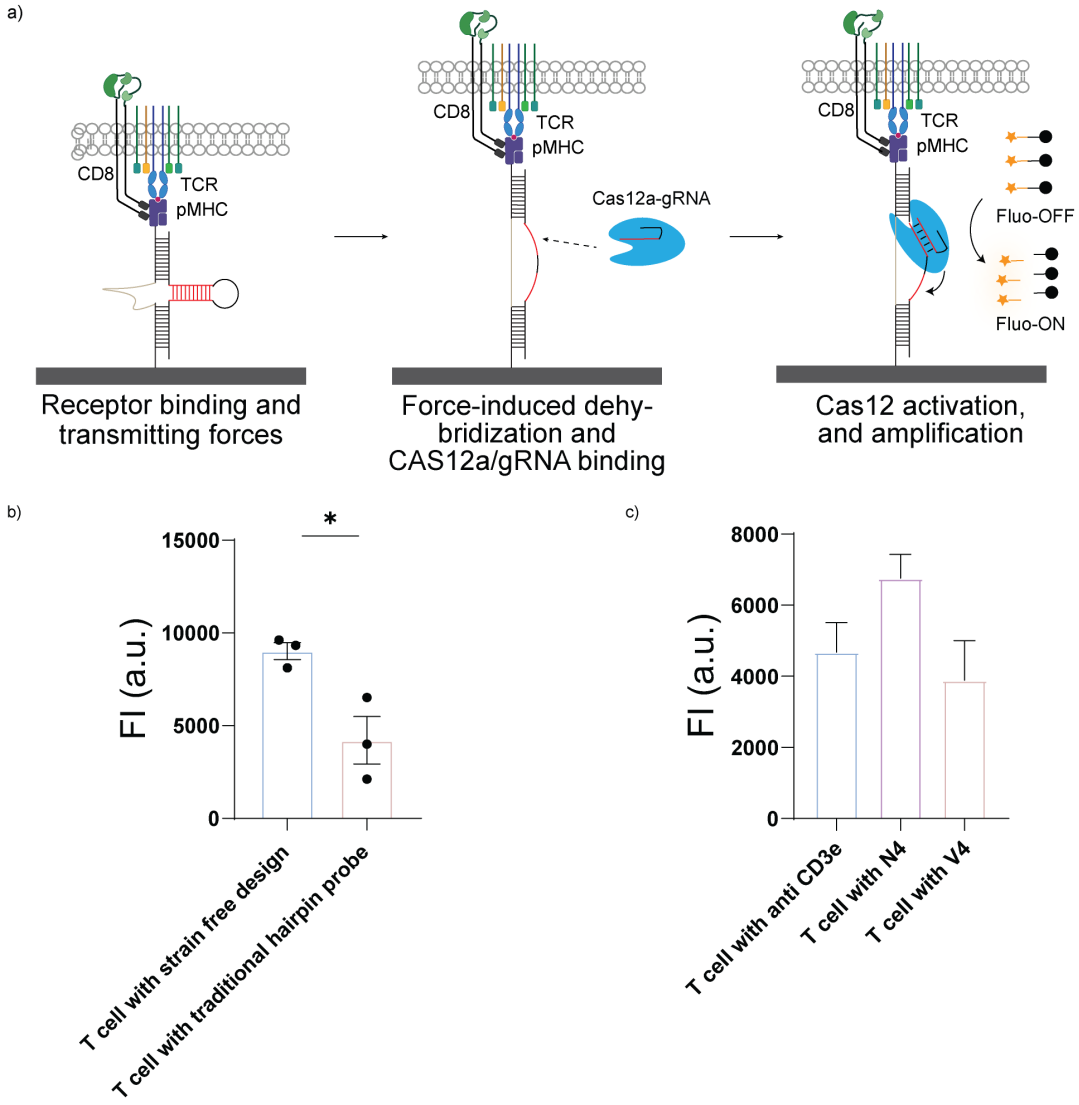

Figure 4.2: Strain-free RT-MCATS and detect of T cell mechanics with different cognate ligands. a-b) Schematic showing strain-free RT-MCATS T cell assay. Grey color represents single stranded linker that is longer than hairpin stem but shorter than hairpin stem and loop. b) Plot showing plate reader detected RT-MCATS signal with strain free or traditional hairpin probe design. Error bar represents S.E.M. from 3 independent experiments. Significant value is calculated from student T test with p=0.01. c) Plot showing plate reader detected RT-MCATS signal with anti CD3Ɛ, pMHC N4 and pMHC V4. Error bar represents S.E.M. from 3 independent experiments. Significant value is calculated from student T test with p=0.01.

4.3.3 Rapid detection of mechanics modulating drug's effect on T cell

We next applied RT-MCATS to test function of small molecules that target cell mechanics. We first investigated Latrunculin B (LatB) which can inhibit actin polymerization and therefore dampen forces transmitted by TCR. We pretreated naïve OT-1 cells ($2*10^6$) with a range of LatB concentrations (0-5 μM) for 10 min.[17] The drug-treated T cells were then plated on 96 well plates with the strain-free hairpin tension probe for 30 min, which was followed by RT-MCATS amplification and detection. We found that the RT-MCATS signal showed a dose-dependent reduction in fluorescence as a function of increasing LatB inhibitor concentration (**Figure 4.3**), indicating that plate-reader based RT-MCATS can be used to screen drugs that targets T cell mechanics. By fitting the plate reader data to a standard dose-response inhibition function [Signal=Bottom + (Top-Bottom)/(1+([drug]/IC50)], we found that the mechano-IC_{50} for LatB of T cells = 17.9 nM, which is similar to the reported IC_{50} 60 nM.[18]

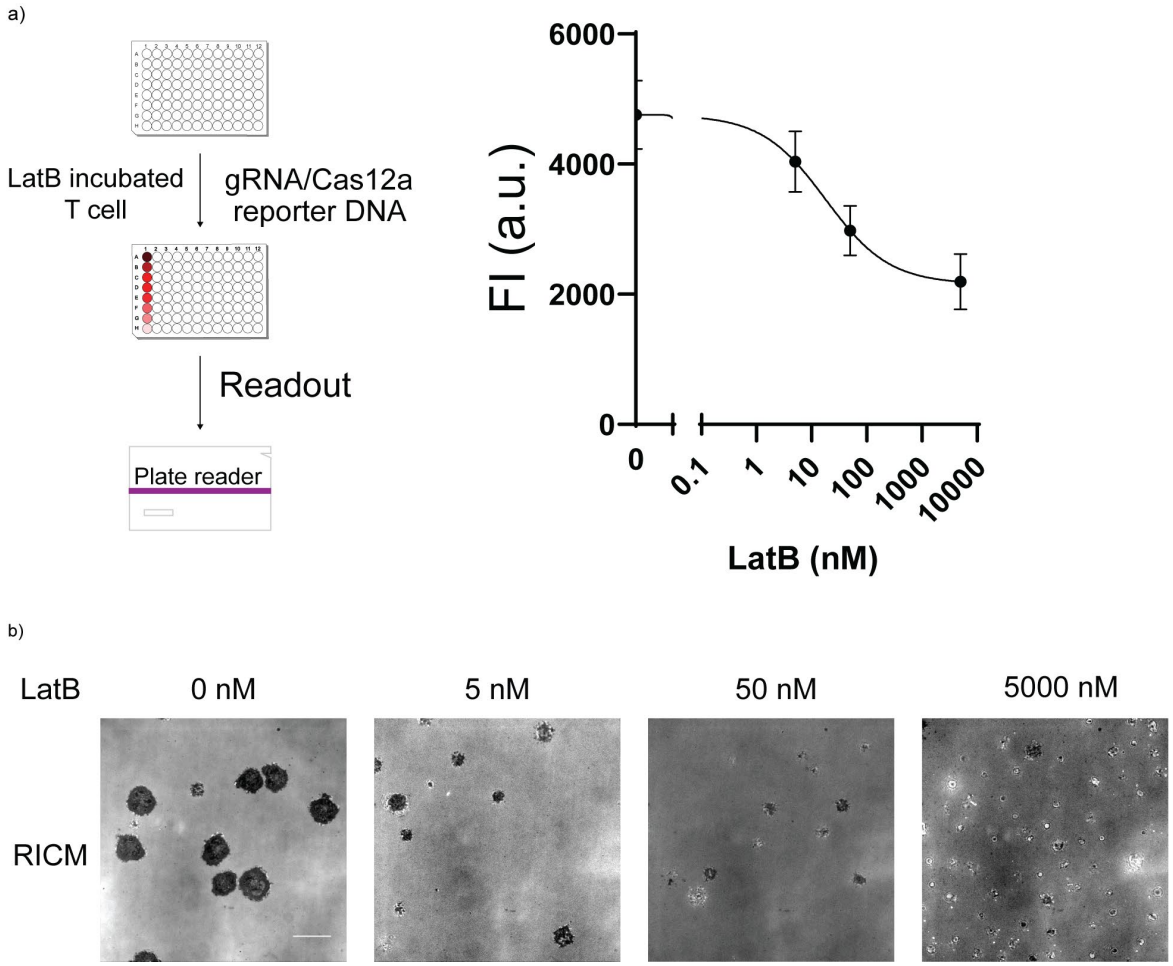

Figure 4.3: Rapid detection of LatB inhibition of T cell mechanics. a) Schematic and plot of plate reader measured RT-MCATS signal as a function of LatB concentration. Drug was incubated for 10 min prior to seeding. Error bar represents S.E.M. from 3 independent experiments. Mechano-IC50 was calculated by fitting plot to a standard dose-response function: Signal=Bottom + (Top-Bottom)/(1+([drug]/IC50). D) Representative RICM mages from wells used in dose-response measurement. Scale bar = 10 μm.

4.4 Conclusion

In this Chapter, we take advantages of MCATS assay and further expand MCATS system with reversible DNA tension probes to detect weak T cell receptor forces in a high-throughput manner. We optimize the system by designing a new strain-free hairpin probe that links the ligand strand and surface anchor strand with a proper length linker. This optimization doubles the S/N for RT-MCATS system. We applied the optimized system to detect TCR mechanics using 96 well plates and conventional plate reader. We found that TCR show higher tension signal with pMHC N4 compared with pMHC V4. We also detect the dose dependent inhibition of T cell mechanics with drugs such as LatB. These development and applications showed the great potential of applying MCATS system into different area of biomedical research and clinical applications

4.5 Materials and Methods

4.5.1 Chemicals and oligonucleotides

Cy3B-NHS ester (PA63101) was purchased from GE Healthcare Life Sciences (Pittsburgh, PA). Streptavidin (S000-01) was purchased from Rockland-Inc (Pottstown, PA). μ-Slide VI0.4 6-channel slides (80606) and 25 mm x 75 mm glass coverslips (10812) were purchased from Ibidi (Verona, WI). ProPlate® Microtiter (204969) are purchased from Thermo-Fisher Scientific. N-hydroxyl succinimide-5 kDa PEG-biotin (NHS-PEG-biotin, HE041024-5K) was purchased from Biochempeg (Watertown, MA). (3-Aminopropyl) triethoxysilane (APTES, 440140, 99% purity) was purchased from Sigma-Aldrich, Adenosine 5‘-diphosphate (ADP, A2754, 95% purity), Ethanol (459836), hydrogen peroxide (H1009), bovine serum albumin (10735078001), latruculin B (L5288, >80%), and Hank’s balanced buffer (H1387) were purchased from Sigma Aldrich (St. Louis, MO). Polystyrene beads (2μm in diameter, QDIGP-20-2) was purchased from ProSciTech. Biotinylated anti-mouse CD3ε (Cat# 13-0031-82), were purchased from eBioscience (San Diego, CA). Biotinylated pMHC ovalbumin (SIINFEKL) and Biotinylated pMHC ovalbumin mutants (SIIVFEKL) was obtained from the NIH Tetramer Core Facility at Emory University. All DNA oligonucleotides are listed in Table 4.1 and purchased from Integrated DNA Technologies (Coralville, IA); crRNA was purchased from Dharmacon Inc. (Lafayette, CO). All other reagents and materials (unless otherwise stated) were purchased from Sigma-Aldrich and used without purification. All buffers were prepared with 18.2 MΩ nanopure water.

Table 4.1: List of Oligonucleotides

Name	Sequence (5' to 3')
4.7pN Hairpin probe	GTG AAA TAC CGC ACA GAT GCG TTT GTA TAA ATG TTT TTT TCA TTT ATA CTT TAA GAG CGC CAC GTA GCC CAG C
6pN Hairpin Probe	GTG AAA TAC CGC ACA GAT GCG TTT GAA TTT ATT TTT TAA AAT TAT TTT TTT AAT TTT AAA AAA TAA ATT TTT AAG AGC GCC ACG TAG CCC AGC
Ligand strand	/5AmMC6/ - CGC ATC TGT GCG GTA TTT CAC TTT - /3Bio/
Surface Anchor strand	/5-DBCON/ - TTT GCT GGG CTA CGT GGC GCT CTT - /3BHQ_2/
DBCO Strain-free Strand	/5DBCON/ TTT GCT GGG CTA CGT GGC GCT CTT TTT TTT AAT CAA TTT TCA ATA CCT TAT ATT ATT ATA CAT CTA CCG GTT TTT CGC ATC TGT GCG GTA TTT CAC TTT /3bio/
Dig TGT strand	5DiGN/TTTTTTGCAATGTTGTTCCTTGAGGAGG/3BHQ_2/
Btm TGT strand	/5AmMC6/ CCT CCT CAA GGA ACA ACA TTG C TT TTT TTT TTT TTT TTT TTT TTT TTT TTT TTT TTT TTT TTT TTT TTT TTT TTT TTT T/3Bio/
ATTO 565N Reporter DNA	/5ATTO565N/TT ATT /3BHQ_2/
4.7pN crRNA	

	UAA UUU CUA CUA AGU GUA GAU UGA AAA AAA CAU UUA UAC AA
6pN crRNA	UAA UUU CUA CUA AGU GUA GAU UAU AUA UAU AUA UAU AUA UAC
TGT crRNA	UAA UUU CUA CUA AGU GUA GAU GCA AUG UUG UUC CUU GAG GA

4.5.2 Instruments

We used a Nikon Eclipse Ti microscope, operated by Nikon Elements software, using a 1.49 numerical aperture (NA) CFI Apo ×100 objective, perfect focus system, a TIRF laser launch, a Chroma quad cube (ET-405/488/561/640 nm Laser Quad Band) and an RICM (Nikon: 97270) cube for this work. Bulk fluorescence measurements were conducted using a Synergy H1 plate reader (Bio-Tek) using fluorescence filter sets. Microfluid device was built with Fisherbrand™ Single Syringe Pump. (Kd Scientific) All ultrapure water was obtained from a Barnstead Genpure pro water purifying system (Thermo Fisher) that indicated a resistivity of 18.2 MΩ. Nucleic acid purification was performed using a high-performance liquid chromatography (HPLC, Agilent 1100) equipped with a diode array detector. Microvolume absorbance measurements were obtained using a Nanodrop 2000 UV-Vis Spectrophotometer (Thermo Scientific). Mass identification of product was performed with an Exactive™ Plus Orbitrap Mass Spectrometer.

4.5.3 Surface preparation method

MCATS surface preparation method was modified from previously published protocols.[10, 19] Briefly, rectangular glass coverslips (25 x 75 mm, Ibidi) were rinsed with water and sonicated for 20 minutes in water and 20 minutes in ethanol. The glass converslips were then cleaned with piranha solution. The piranha solution was prepared using a 1:3 mixture of H_2O_2 and H_2SO_4. WARNING: Piranha solution becomes very hot upon mixing and is highly oxidizing and may explode upon contact with organic solvents. Then, slides were washed 6 times in beakers with ultrapure water, followed by 4 successive washes using ethanol. In a separate beaker of ethanol, slides were reacted with 3% v/v APTES at room temperature for 1 h. Coverslips were then washed 6 times with ethanol, baked in oven for 20 minutes at 80 °C. Procedure are different for different experiments after this step.

For T cell experiment, slides were then reacted with 10 mg/mL of NHS-PEG4-azide (Click Chemistry Tools) in 0.1 M NaHCO3 (pH = 9) for 1 h. The slides were then washed with water, dried with N_2 and sticked to Proplate 96 well plates. The surfaces were further blocked with 0.1% BSA in 1X PBS for 30 min and washed with 1X PBS and ~50 µL of solution was kept inside the well to prevent drying. Subsequently, the hairpin tension probes were assembled in 1M NaCl by mixing the Cy3B labeled A21B strand (220 nM), quencher strand (220 nM) and hairpin strand (200 nM) in the ratio of 1.1: 1.1:1. The mixture was heat annealed at 95 ℃ for 5 min and cool down to 25 ℃ for 30 min. ~50 µL of the assembled probe was added to the channels (total volume = ~100 µL) and incubated overnight at room temperature. This strategy allows for covalent immobilization of the tension probes on azide-modified substrates via strain-promoted cycloaddition reaction.

On the next day, the unbound DNA probes were removed with 3X PBS washes. Then 10 μg/mL of streptavidin was added to the channels and incubated for 45 min at RT. The surfaces were cleaned with 3X PBS washes. Next, 10 μg/mL of pMHC ligand was added to the surfaces, incubated for 45 min r.t. and washed thrice with 1X PBS. Surfaces were buffer exchanged with HBSS before imaging.

4.5.4 DNA hybridization and gRNA/Cas12a binding

DNA oligonucleotides were hybridized at 100 nM in a 0.2 μL PCR tube. DNA was firstly heated to 90°C and then cooled at a rate of 1.3°C per min to 35°C. gRNA and Cas12a were incubated for 10min at 37 °C at 20nM in a 0.2 μL PCR tube just before adding on surface and stored on ice for maximum preservation of activity.

4.5.5 Oligo dye/ligand coupling and purification

All sequences of DNA strands used in this work are provided in **Table 4.1**. Labeling of dye is conduct with the following protocol: 10 nmole Amine labelled strands were reacted overnight with a 20x excess of Cy3B-NHS dissolved in 10 μL DMSO. The total volume of the reaction was 100 μL, composed of 1x PBS supplemented with 0.1M $NaHCO_3$. Then P2 size exclusion gel was used to remove unreacted dye. The product was then purified by reverse phase HPLC using Agilent Advanced oligo column (Solvent A: 0.1M TEAA, Solvent B: acetonitrile; starting condition: 90% A + 10 % B, 1%/min gradient B, Flow rate: 0.5 mL/min). Concentrations of purified

oligonucleotide conjugates were determined by measuring their A260 absorption value on a Nanodrop 2000 UV-Vis Spectrophotometer (Thermo Scientific). ESI- mass spectrometry was performed to confirm the successful ligation.

4.5.6 T cell handling

In this chapter, OT-1 transgenic mice were housed and bred in the Division of Animal Resources Facility at Emory University with approval from the Institutional Animal Care and Use Committee. Naïve OT-1 T cells that express the CD8 co-receptor and specifically recognize chicken ovalbumin epitope 257–264 (SIINFEKL) were isolated and enriched from the spleen of a sacrificed mouse using MACS separation with the CD8+ T cell isolation kit according to the manufacturer's instructions. The purified CD8+ naïve OT-1 cells were kept in HBSS buffer at 4 °C before imaging.

4.5.7 MCATS assay with reversible tension probes.

MCATS assay was performed on the prepared surface as described in the surface preparation section.

For MCATS with T cell. First, T cells (2*10) was seeded on to surface with hairpin tension probes for 30 min. Surfaces with exposed activator were imaged directly with fluorescence microscopy for high resolution characterization and quantification. Subsequently, 10mM of Mg^{2+} was added to the wells and gRNA/Cas12a complex and reporter DNA were mixed and added to the well to initiate the Cas12a amplification reaction with mechanically exposed activator. After 1h of

incubation, fluorescence intensities on 96 well plates were measured with a Bio-Tek® Synergy H1 plate reader (Ex/Em = 540/590 nm for reporter channel).

4.5.8 Dose-dependent inhibition of receptor mediated tension

For dose-dependent inhibition of experiments, the cell density of OT-1 naïve T cells was first characterized with a hemocytometer. 2000000 T cells were then incubated with different concentrations of inhibitor (LatB) for 10 minutes before plating onto 96 well plates. Afterwards, cells were incubated for 30min. Then the MCATS protocol was followed to achieve amplification and quantification.

4.5.9 Microscopy imaging

For T cell and flow based MCATS experiments, Images were acquired on a Nikon Eclipse Ti microscope, operated by Nikon Elements software, a 1.49 NA CFI Apo 100x objective, perfect focus system, and a total internal reflection fluorescence (TIRF) laser launch with 488 nm (10 mW), 561 nm (50 mW), and 638 nm (20 mW). A reflection interference contrast microscopy (RICM) (Nikon: 97270) cube and a Chroma quad cube (ET-405/488/561/640 nm Laser Quad Band) were used for imaging. Imaging was performed on 96 well plates and glass coverslips using HBSS for T cell and PBS for flow-based assay. All imaging data was acquired at room temperature.

4.5.10 Statistics and reproducibility

P-values were determined by Student's t-test using GraphPad Prism. Mechano-IC_{50} is calculated by fitting plot to a standard dose-response function: Signal=Bottom + (Top-Bottom)/(1+([drug]/IC50) using GraphPad Prism8. MCATS readout is typically replicated with 2 or 3 wells on the same plate within the same experiment.

4.6 Acknowledgement

I thank Yuesong Hu for his help in purifying T cell and his great insights in T cell experiments.

4.7 Appendix

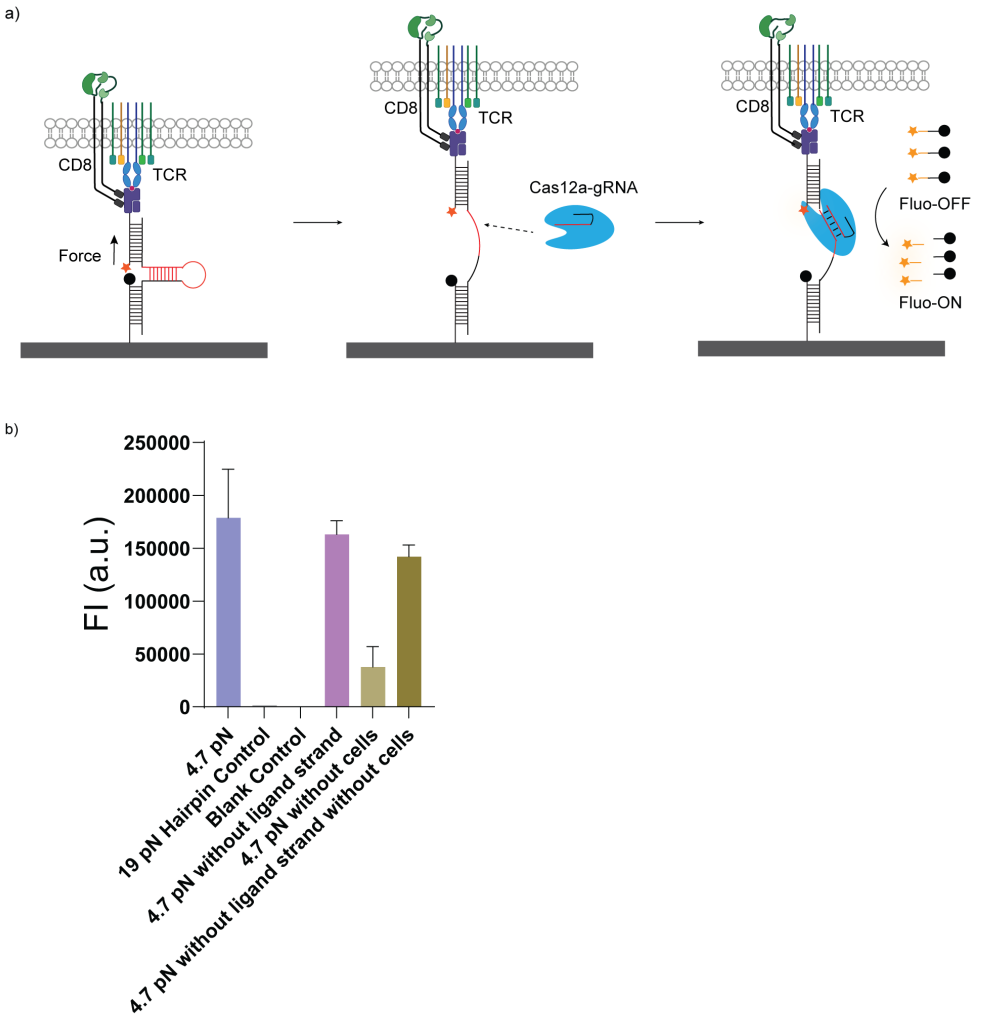

Figure 4.5: Scheme and RT-MCATS with 4.7 pN hairpin tension probes. a) Schematic showing RT-MCATS with 4.7 pN hairpin tension probes. Due to the length of stem, part of the stem and complementary region was designed to be the activator. b) plot of MCATS signal with 4.7pN hairpin probe and T cells and negative controls (no ligand group, no cell group, blank control and 19pN hairpin control). Results indicating that not fully concealed activator led to significant background amplification and can't be used in T cell tension detection. Error bar represents S.E.M. from n=3 independent experiment.

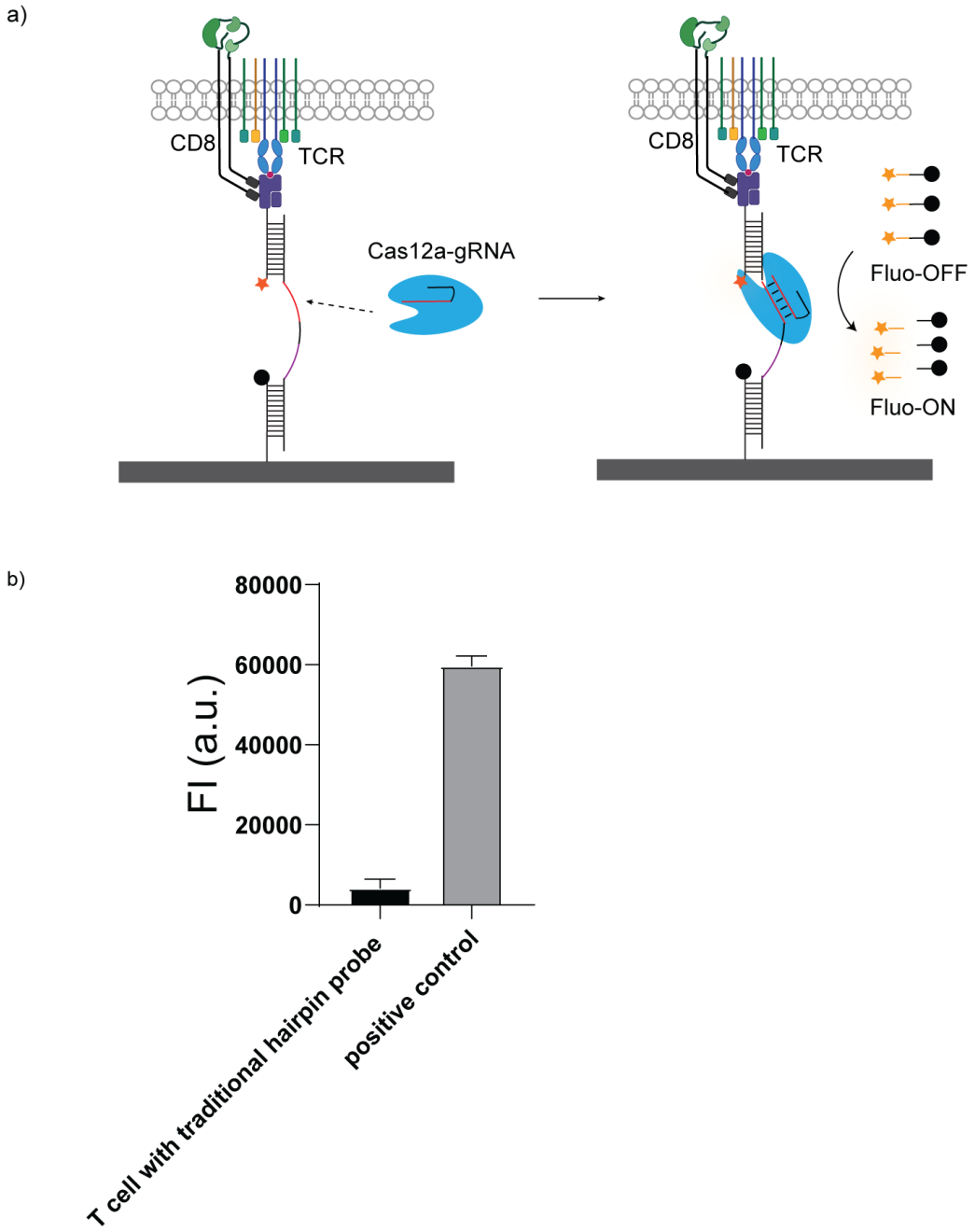

Figure 4.6: Scheme and RT-MCATS with partially scrambled hairpins. a) Schematic showing design of positive control hairpin with sequence of complementary region (purple) to activator (red) scrambled. b) plot of MCATS signal with 6pN hairpin probes and positive hairpin control. Error bar represents S.E.M. from n=3 independent experiment.

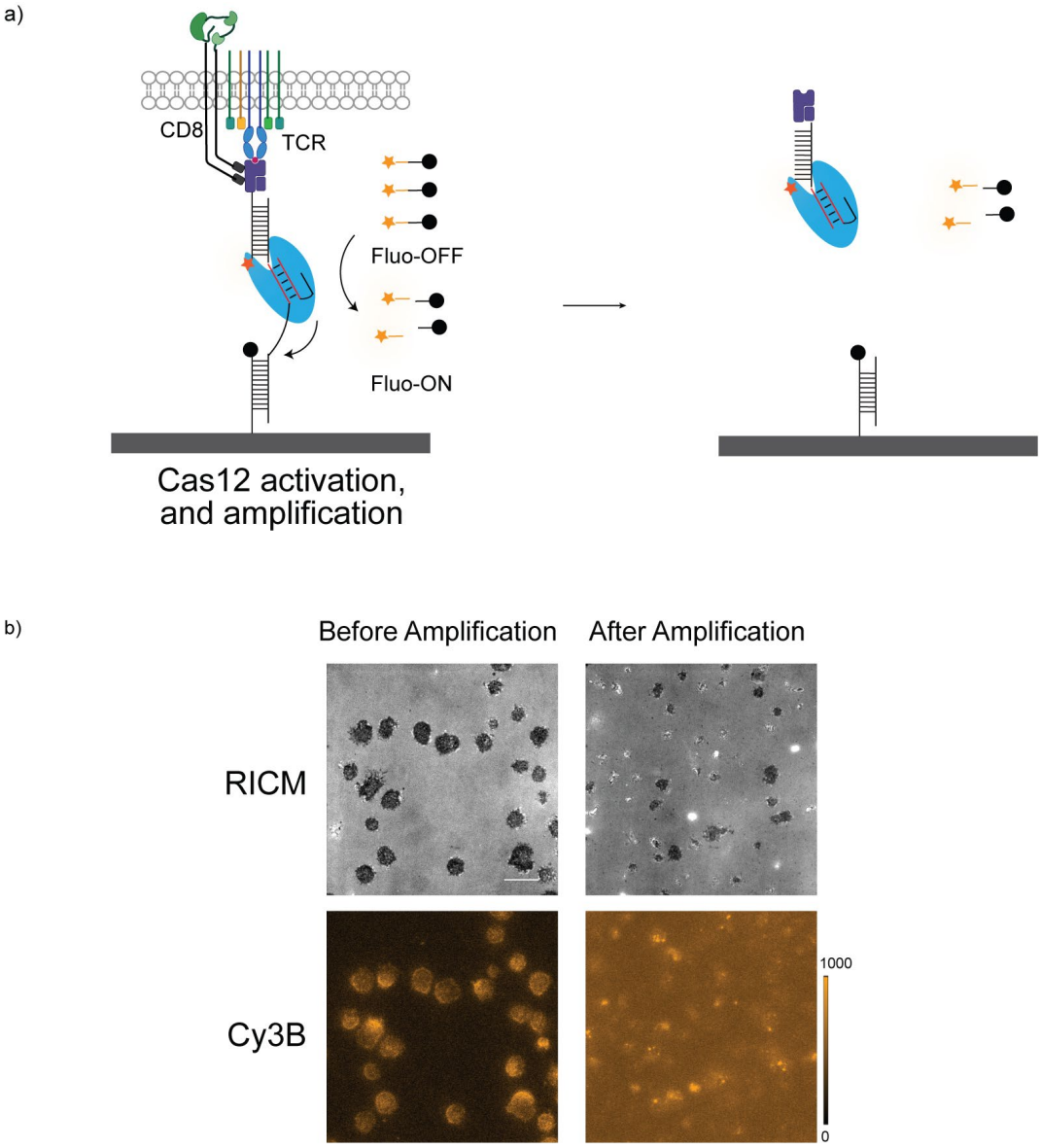

Figure 4.7: Scheme and representative images after MCATS amplification. a) Schematic of self-cleavage activity of RT-MCATS. b) Representative RICM and Cy3B fluorescence images showing that T cells are detached after MCATS amplification. Scale bar = 10 μm. The intensity bar next to each fluorescence image shows the absolute signal intensity for each image.

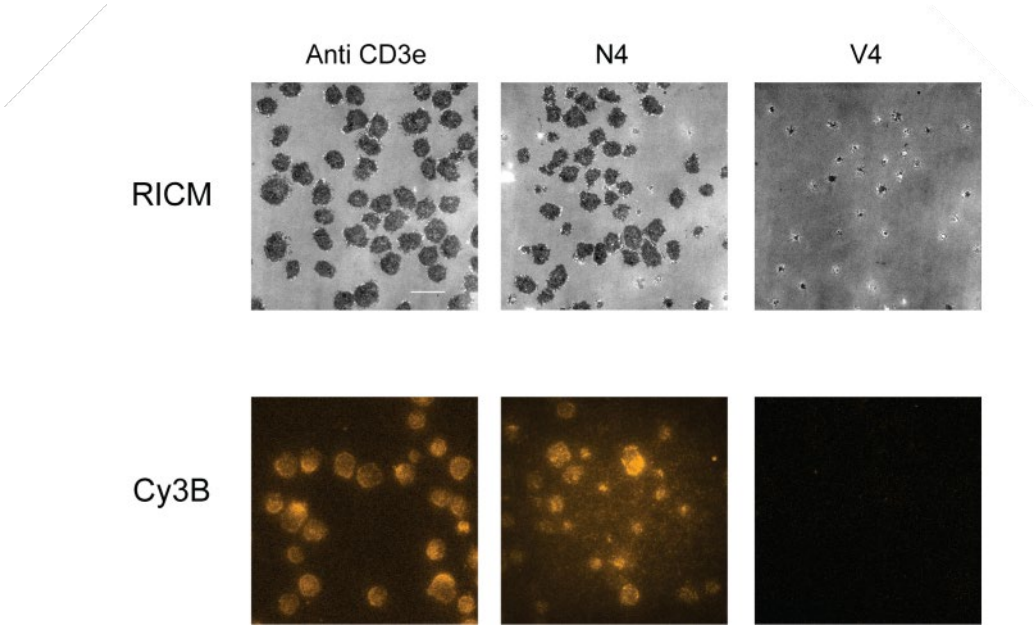

Figure 4.8: Representative RICM and fluorescence images for T cell interact with different cognate ligands. Scale bar = 10 μm.

4.8 References

1. Harrison, D.L., Fang, Y. & Huang, J. T-Cell Mechanobiology: Force Sensation, Potentiation, and Translation. *Front. Phys.* **7** (2019).
2. Purbhoo, M.A., Irvine, D.J., Huppa, J.B. & Davis, M.M. T cell killing does not require the formation of a stable mature immunological synapse. *Nat. Immunol.* **5**, 524-530 (2004).
3. Alam, S.M. et al. T-cell-receptor affinity and thymocyte positive selection. *Nature* **381**, 616-620 (1996).
4. Ma, R. et al. DNA probes that store mechanical information reveal transient piconewton forces applied by T cells. *Proc. Natl. Acad. Sci. U.S.A.* **116**, 16949-16954 (2019).
5. Liu, B., Chen, W., Evavold, B.D. & Zhu, C. Accumulation of dynamic catch bonds between TCR and agonist peptide-MHC triggers T cell signaling. *Cell* **157**, 357-368 (2014).
6. Sibener, L.V. et al. Isolation of a structural mechanism for uncoupling T cell receptor signaling from peptide-MHC binding. *Cell* **174**, 672-687. e627 (2018).
7. Das, D.K. et al. Force-dependent transition in the T-cell receptor β-subunit allosterically regulates peptide discrimination and pMHC bond lifetime. *Proc. Natl. Acad. Sci. U.S.A.* **112**, 1517-1522 (2015).
8. Hong, J. et al. A TCR mechanotransduction signaling loop induces negative selection in the thymus. *Nat. Immunol.* **19**, 1379-1390 (2018).
9. Zhang, Y., Ge, C., Zhu, C. & Salaita, K. DNA-based digital tension probes reveal integrin forces during early cell adhesion. *Nat. Commun.* **5**, 5167 (2014).
10. Liu, Y. et al. DNA-based nanoparticle tension sensors reveal that T-cell receptors transmit defined pN forces to their antigens for enhanced fidelity. *Proc. Natl. Acad. Sci. U.S.A.* **113**, 5610-5615 (2016).

11. Woodside, M.T. et al. Nanomechanical measurements of the sequence-dependent folding landscapes of single nucleic acid hairpins. *Proc. Natl. Acad. Sci. U.S.A.* **103**, 6190-6195 (2006).

12. Blakely, B.L. et al. A DNA-based molecular probe for optically reporting cellular traction forces. *Nat. Methods* **11**, 1229-1232 (2014).

13. Li, S.-Y. et al. CRISPR-Cas12a-assisted nucleic acid detection. *Cell Discov.* **4**, 20 (2018).

14. Zhang, L. et al. Conformational Dynamics and Cleavage Sites of Cas12a Are Modulated by Complementarity between crRNA and DNA. *iScience* **19**, 492-503 (2019).

15. Losito, M., Smith, Q.M., Newton, M.D., Cuomo, M.E. & Rueda, D.S. Cas12a target search and cleavage on force-stretched DNA. *Phys. Chem. Chem. Phys.* **23**, 26640-26644 (2021).

16. Huang, J. et al. The kinetics of two-dimensional TCR and pMHC interactions determine T-cell responsiveness. *Nature* **464**, 932-936 (2010).

17. Glazier, R. et al. DNA mechanotechnology reveals that integrin receptors apply pN forces in podosomes on fluid substrates. *Nat. Commun.* **10**, 1-13 (2019).

18. Wakatsuki, T., Schwab, B., Thompson, N.C. & Elson, E.L. Effects of cytochalasin D and latrunculin B on mechanical properties of cells. *J. Cell Sci.* **114**, 1025-1036 (2001).

19. Duan, Y. et al. Mechanically Triggered Hybridization Chain Reaction. *Angew. Chem. Int. Ed.* **60**, 19974-19981 (2021).

Chapter 5. Summary and Perspective

5.1 Summary

Due to the weak, transient, and sparse nature of cellular forces, researchers in mechanobiology typically utilize highly sophisticated techniques such as traction force microscopy, single molecule force microscopy or molecular tension probes to study the interaction between mechanical cues and chemical signaling of cells. Considering that most of these methods require dedicated instruments and well-trained scientists for data collection and analysis, the field of mechanobiology is mostly studied in a few labs in the US and around the world. In this dissertation, we developed mechanically triggered catalytic amplification reactions based on DNA tension probes that can achieve ultrasensitive molecular tension detection without any dedicated instruments. These reactions and assays are robust, rapid, and hands-on, which can lower the barrier for adopting mechanobiology methods in any cell biology research labs or clinical applications.

In **Chapter 2**, we described the development of mechanically triggered hybridization chain reaction (mechano-HCR), which can trigger an isothermal and enzyme-independent amplification of tension signal when a cell receptor mechanically denatures a duplex to reveal a cryptic initiator. Importantly, we show that mechano-HCR offers one-order of magnitude enhancement in S/N when compared to directly quantification of DNA duplex rupture. Therefore, mechano-HCR enables rapid readout of pN forces on a 96 well plate with a conventional plate reader. We characterized the kinetics of surface-initiated HCR and applied mechano-HCR to investigate integrin receptor forces in fibroblasts and platelets. Finally, we leverage the ability to readout cellular forces using a conventional plate reader to measure the IC_{50} for three different anti-platelet drugs in a rapid manner, thus providing a convenient readout of platelet functions.

When we developed mechano-HCR, however, we found out that toehold mediated strand displacement reaction-based HCR showed a limited reaction rate. As a result, the slow kinetics limit the sensitivity of this assay in cell-experiment. The recent advancement in CRISPR-Cas based assay inspired us to developing a more sensitive and rapid technique using this technology.

Next in **Chapter 3**, we developed mechano-Cas12a assisted tension sensor (MCATS). MCATS is currently our most sensitive force detection assay that can detect tension generated from as few as 50 cells on surface. MCATS is developed by designing a concealed activator without PAM sequence. When a cell mechanically ruptures the DNA tension probe, the exposed activator triggers Cas12a/gRNA trans-nuclease activity and produces massive fluorescent signal. Because of the efficient and robust amplification of the Cas12a system, we can achieve a high-throughput detection of cellular tension in 30 mins using a plate reader. MCATS can serve as a platform technology for many cell types and different receptors. In this chapter, we demonstrate its power by using it to study the integrin mediated tension with human platelets. Due to the sensitivity of MCATS, we only need 5ul of blood for each measurement, which allow us to finish a personalized drug sensitivity profile with only one blood draw. (~1ml). We showed that we can determine the IC_{50} of a full panel of anti-platelet FDA-approved drugs including aspirin, eptifibatide(integrilin®), 7E3(Reopro®), and the inhibitors Plavix® and Brelinta® with 1ml of blood. Next, we show that detecting platelet tension with MCATS can be used to predict blood transfusion needs for patients undergoing CPB surgery. These results validate that a rapid cell tension detection method such as MCATS could democratize studies of cell mechanobiology and explore the potential of using cellular forces as a diagnostic marker in the clinic.

Furthermore, we expanded the utilities of MCATS in **Chapter 4** by developing reversible tension probe- based MCATS (RT-MCATS). By designing a strain-free reversible DNA tension probe that can trigger Cas12a nuclease activity upon mechanical unfolding, we are able to screen T cell mechanics in a rapid manner. We show that RT-MCATS can be used to detect the TCR- mediated forces and detect the potency of different pMHC ligands. We can also apply RT-MCATS to screen dose-dependent inhibition of drugs inhibiting T-cell mechanics.

Taken together, this dissertation aimed to address the sensitivity and instrument limitation of DNA tension probes to democratize the basic studies of mechanobiology as well as open the door for "mechanopharmacology" and "mechanodiagnostics". We utilize the advantages of catalytic amplification reactions to develop two new types of mechanically triggered reactions that can detect receptor mediated forces in a robust and high-throughput manner. We envision that these ultrasensitive tension sensors would allow more researchers and clinicians to investigate and understand cell mechanics and utilize them as diagnostic markers.

5.2 Perspective

The development and optimization of mechano-HCR and MCATS has offered novel opportunities to study mechanobiology and detect molecular forces without any dedicated instruments. While these methods are robust, rapid, and sensitive, an idealized tension detection method should have a few traits that we have not fully accomplished due to a due to limited time and expertise. For example, an idealized tension sensor should be versatile, meaning it could be used with any protein of interest and be used with any cell type. Ideally, this sensor should be as fast as possible, and provide results within minutes. Additionally, this sensor should have a high enough sensitivity to detect mechanics of single cells in addition to being highly specific for the protein of interest. If possible, the method should be automated to limit human error and improve efficiency. Fortunately, new developments in science and technology have allowed us to further improve our assays. Here, I would like to envision some future directions for further development and applications of mechanically triggered catalytic amplification reactions.

5.2.1 Further development of mechano-HCR and MCATS

5.2.1.1 Optimization of assay running time and sensitivity

Considering we are using catalytic amplification reactions to boost signal from the mechanical events, and the rate limiting step in cellular force detection is the amplification reaction, the high sensitivity and slow running times are tradeoffs in these assays.[1] Increasing the kinetics of amplification steps could help us improve sensitivity and running time simultaneously. As is described in **Chapter 1**, there has been numerous developments in both HCR and CRISPR-Cas technology that can help us achieve this goal.

For mechano-HCR, recent developments in branched HCR[2] or controlled HCR[3] can be used to achieve a high magnitude of amplification by simply redesigning the sequence of initiator and hairpins and therefore increasing the sensitivity of mechano-HCR assays. (**Figure 5.1**) For MCATS, there have been reports of many other types of Cas proteins including Cas14 and CasΦ protein, which have different sizes and gRNA design principles than Cas12a.[4, 5] A physically smaller Cas12a with a shorter gRNA sequence could potentially decrease the steric hindrance and further increase the kinetics of MCATS. The development of new protein engineering techniques and directed evolution could also provide Cas12a with faster target searching and trans-cleavage activity to further optimize the MCATS assay. [6, 7]

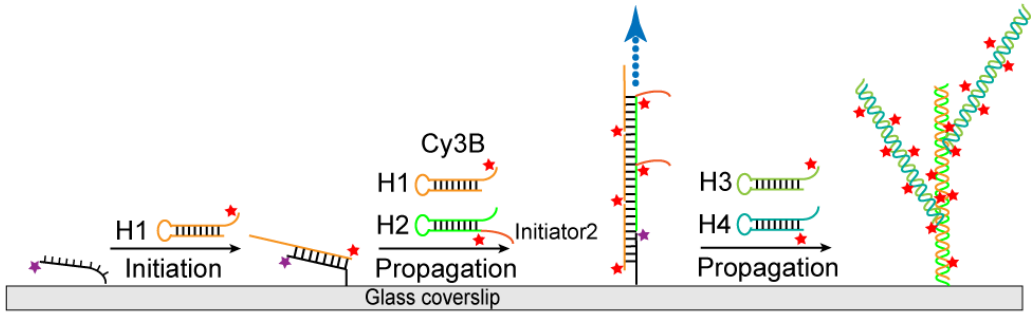

Figure 5.1: Schematic of using branched HCR to increase mechano-HCR sensitivity.

In addition to the strategy that focus on the amplification reaction themselves, the DNA tension probe also provides a good platform to increase the sensitivity of these assays. Better amplification can be achieved by simply putting DNA tension probes in a series connection, therefore increasing the number of reactions with the same number of mechanical events. Also, combining HCR and Cas12a by introducing an activator sequence into HCR hairpins could potentially increase the sensitivity of detection.

5.2.1.2 Increasing the versatility of the assays

One limitation of the DNA tension probe is that it is vulnerable to DNase activity. This limitation is particularly problematic when these ultrasensitive tension sensors are used with cancer cells.[8] Modified oligonucleotide such as peptide nucleic acid (PNA) have been used to tackle this problem. By combing HCR or Cas12a with modified oligonucleotide, we may be able to create a nuclease-resistant ultrasensitive tension sensor for additional applications.

Also, in this current method, we have only used fluorescent-based methods to detect tension signal. Chemiluminescence[9], colorimetry,[10] surface plasmon resonance (SPR),[11] and surface-enhanced Raman scattering (SERS)[12] have previously been used as detection methods for HCR and Cas12a. Cooperating these methods with MCATS or mechano-HCR can potentially support additional applications including point-of-care diagnostics.

5.2.1.3 Standardizing and simplifying the experimental procedure

As an assay with the goal of being widely used in any lab or hospital setting around the world. The mechano-HCR or MCATS assays require further engineering and development to simplify the experimental procedure and automate the process. For mechano-HCR, the current protocol requires washing excess fluorophore from the wells. These washing steps may add additional error and increase the reaction time. Applying strategies such as FRET HCR can address this issue (**Figure 5.2**).[13] The only steps in the MCATS assay are the addition of different reagents to wells at different times during the experiment. By using a liquid handling robot combined with an automated plate reader, it is possible to develop a fully automated tension sensor assay that can help to reduce human error and increase the throughput of cellular tension detection.

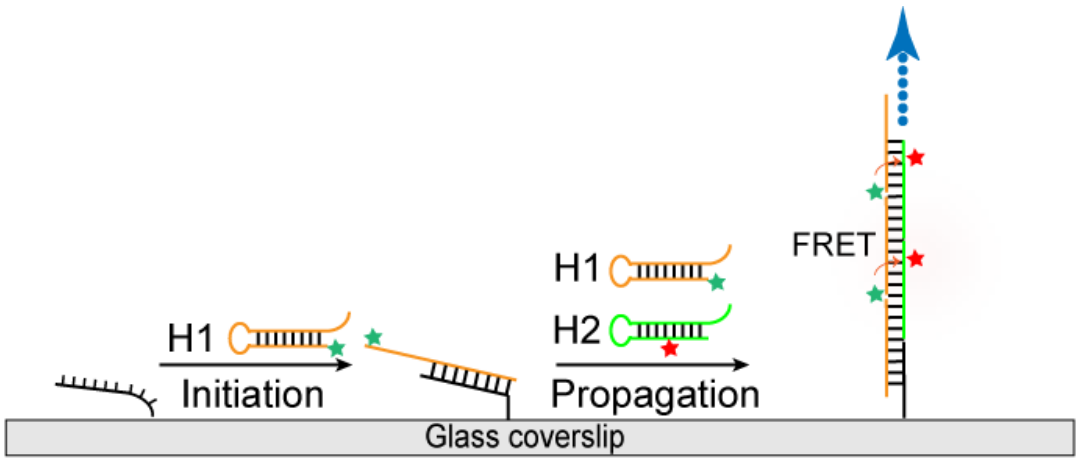

Figure 5.2: Schematic of using FRET HCR to simplify the mechano-HCR procedure.

5.2.2 Future applications for ultrasensitive tension sensors

5.2.2.1 Detection of platelets mechanics and clinical applications

In Chapter 2 and Chapter 3, we mainly applied MCATS and mechano-HCR to the detection of integrin αIIbβ3- mediated forces of platelets. However, GP1b is also an essential receptor that senses and transduces force through von willebrand factor (VWF) to mediate platelets activation. By conjugating VWF to tension probes, we can detect GP1b-VWF forces and may gain a better understanding of platelet forces under shear flow.

Also, diseases such as Glanzmann's thrombasthenia has linked to abnormalities in the integrin αIIbβ3.[14] Detecting platelet tension mediated by these abnormal receptors could potentially serve as a useful diagnostic marker for different bleeding or thrombotic disorders.

5.2.2.2 Tension history profile with Exchange HCR

Because mechano-HCR is a real-time, live cell amplification strategy, in theory, the fluorescence intensity at a specific location could be used to back-calculate to the time of rupture and plot the tension history of cells from one HCR fluorescence images. However, it is challenging with the current design because the density of the HCR product is controlled by both time and the local concentration of exposed initiator sites. The strong HCR signal may also be due to accumulation of early mechanical events that produce longer HCR polymer products. In the future, it may be possible to perform an "Exchange-mechano-HCR assay" where the hairpin monomers are barcoded with different dyes and flowed into the sample periodically. (**Figure 5.3**) This way, we may be able to create a tension history profile with catalytic amplification reactions.

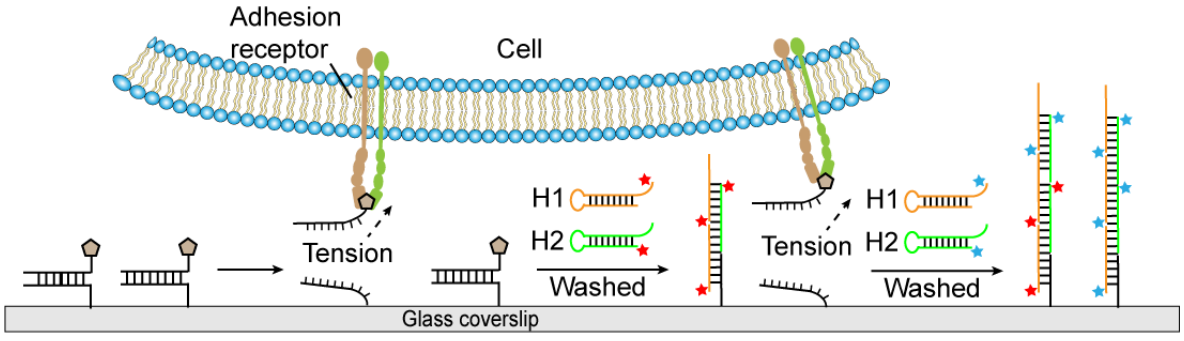

Figure 5.3: Schematic of exchange HCR to profile tension history.

5.2.2.3 Mechanical proofreading of interactions of target molecules with flow induced MCATS

Beyond its potential in rapid detection of cellular forces including T cell and platelet mechanics, MCATS can also be used in protein detection assays or to identify potent molecular interactions without cells. Over the past decades, numerous efforts have been made to detect these targets.[15, 16] Among them, Western Blotting and ELISAs are the gold standards and most commonly used techniques in the field of molecular biology.[17, 18] However, these methods typically require complex procedures such as carefully extracting protein, repetitive washing steps which increase the chance of error and limit the sensitivity of these assays.[19, 20] The use of optical method such as fluorescence and surface enhanced Raman scattering are also growing in popularity because of their high sensitivity and relatively straight-forward protocols.[21, 22] Nevertheless, the requirement for dedicated instruments hinder the widespread use of these methods.[23] Therefore, the development of a rapid, sensitive, and highly specific flow-based assay that detects molecular interactions is highly desired in the development of cancer immunotherapies, protein detection assays and other molecular diagnostics.[24-26]

The MCATS system provide a fast, ultrasensitive, and high-throughput assay with good mechanical selectivity. Inspired by fact that a T cell can detect single amino-acid mutations in the TCR-pMHC interaction by employing a mechanical selective process, we aim to develop a system that uses MCATS to recognize interactions between target molecules such as TCR-pMHC targets in a cell-free environment. To achieve this goal, we replaced cells with beads that were decorated with a protein of interest and applied flow to induce force on the beads. In this system, the beads that contain a ligand of interest that interacts with a target protein that is immobilized to the surface

with DNA tension probes. (**Figure 5.4A)** When shear flow is applied to the system therefore applying force to the beads, the force will mechanically rupture the DNA tension probe if the molecular interaction is strong enough (Mechanical proofreading). Because DNA tension probes are highly modular and tunable, this design could potentially detect a wide range of protein-ligand interaction and targets. Compared to other fluorescent- or SERS- based assay, the flow-induced MCATS assay offers a cost-effective, high-throughput and high-sensitivity method because of its utilization of mechanical selection process that can be developed for detecting proteins and potent molecular interaction. Therefore, this assay could potentially be used for application such selecting of SARS-Cov-2 aptamers and screening pMHC potency for engineering T cell-based immunotherapies.

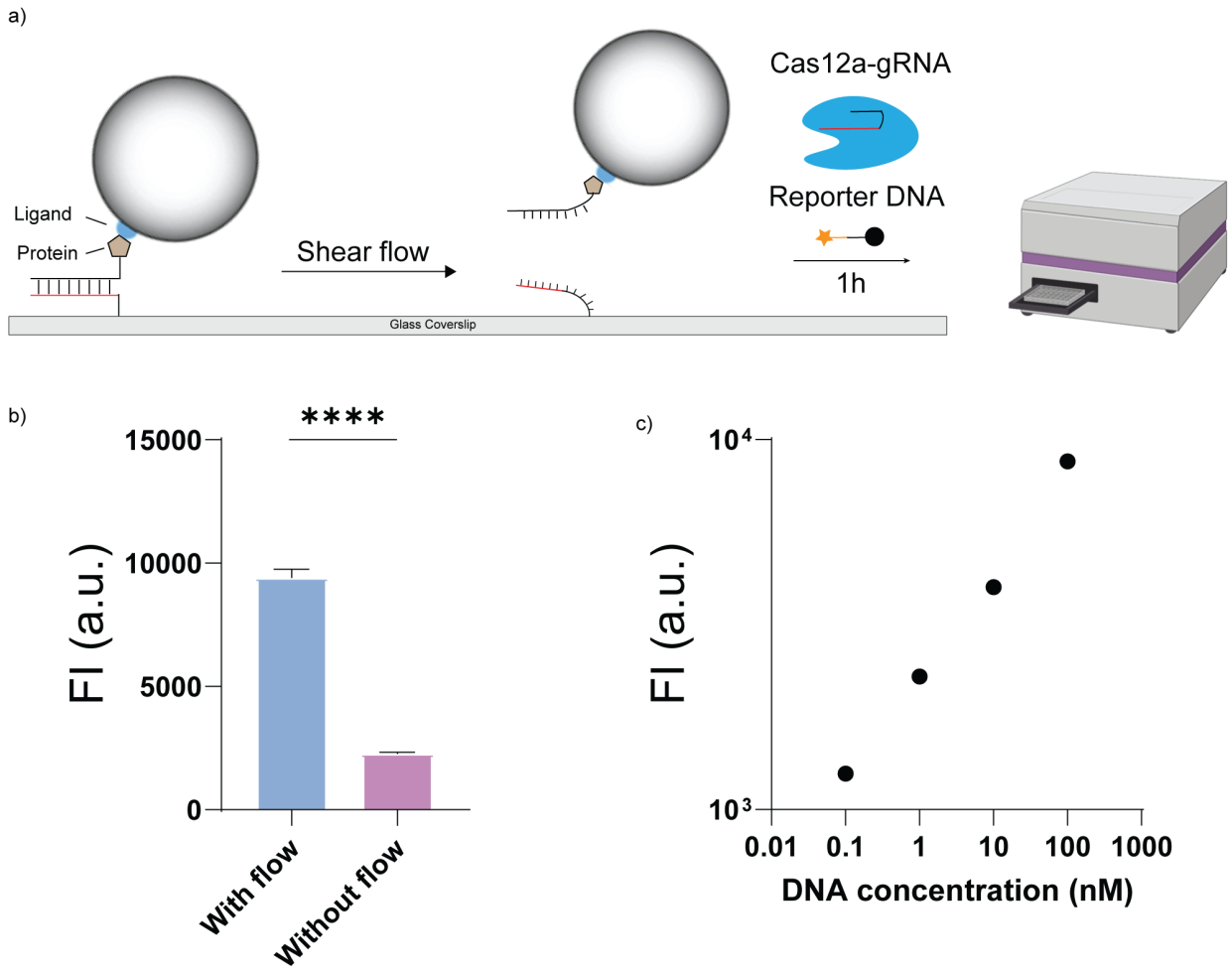

Figure 5.4: Flow induced MCATS for detection of Dig/anti Dig interaction. a) Schematic of flow induced MCATS. In this experiment, dig is immobilized on the surface and anti-dig is decorated on polystyrene beads. The flow experiment is conducted in a µ-Slide VI0.4 6-channel slide with a flow rate = 6 ml/min. b) Plots of MCATS signal for experiments with or without flow. Error bar represents S.E.M. from 3 independent experiments. D) Plots of MCATS signal for experiments using different concentrations of DNA strand incubated on the surface. Error bar represents S.E.M. from 3 independent experiments

In our proof-of principle experiment, we show that flow-induced MCATS can be used to detect Dig-labeled DNA strands when applying a shear flow on the bead-labeled tension probe. The oligonucleotides used in this application are listed in **table 5.1**. We immobilized irreversible DNA tension probes with a digoxigenin modification on surfaces that coated with biotin (methods

described in previous chapters) and incubated the probe with polystyrene beads (2µm in diameter, ProSciTech QDIGP-20-2) decorated with anti-dig. Typically, 10 µl of anti-Dig coated beads (0.1% W/V) were added to the ibidi channel and incubated for 1hr. Then the ibidi channel was connected to a Fisherbrand™ Single Syringe Pump to construct a home-made microfluidic device to apply shear flow (**Figure 5.5**). (Kd Scientific). A high flow rate at 6ml/min or a low flow rate at 0.12 ml/min was applied during the experiment. Then, 10mM of Mg^{2+} was added to the wells and the gRNA/Cas12a complex and reporter DNA were mixed and added to the well to initiate the Cas12a amplification reaction with mechanically exposed activator. After a 1hr incubation, surfaces with exposed activator were imaged directly with fluorescence microscopy and the solution was then transferred to 96-well plates to measure the fluorescent intensities with a Bio-Tek® Synergy H1 plate reader (Ex/Em = 540/590 nm for reporter channel).

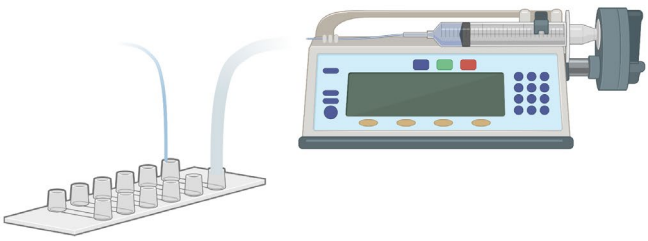

Figure 5.5: Schematic of flow induced MCATS fluidic device. The flow is generated with a syringe pump connected to an ibidi channel.

By applying flow (6ml/min) to the ibidi channel, we found that flow induced MCATS can detect amplified fluorescent signal from ruptured tension sensors and recognize the dig strand with anti-dig beads (**Figure 5.4 B, Movie 5.1**). We also noticed that a lower density of dig strand leads to lower MCATS signal. (**Figure 5.4 C, Figure 5.6)**. Interestingly, if we change the flow rate, lower flow rate that provide a drag force ~3pN led to a significantly lower MCATS signal, indicating that mechanical proofreading is very important to the system (**Figure 5.7).**

Table 5.1: List of Oligonucleotides for flow induced MCATS

Name	Sequence (5' to 3')
Dig TGT strand	5DiGN/TTTTTTGCAATGTTGTTCCTTGAGGAGG/3BHQ_2/
Btm TGT strand	/5AmMC6/ CCT CCT CAA GGA ACA ACA TTG C TT TTT TTT TTT TTT TTT TTT TTT TTT TTT TTT TTT TTT TTT TTT TTT TTT TTT T/3Bio/
ATTO 565N Reporter DNA	/5ATTO565N/TT ATT /3BHQ_2/
TGT crRNA	UAA UUU CUA CUA AGU GUA GAU GCA AUG UUG UUC CUU GAG GA

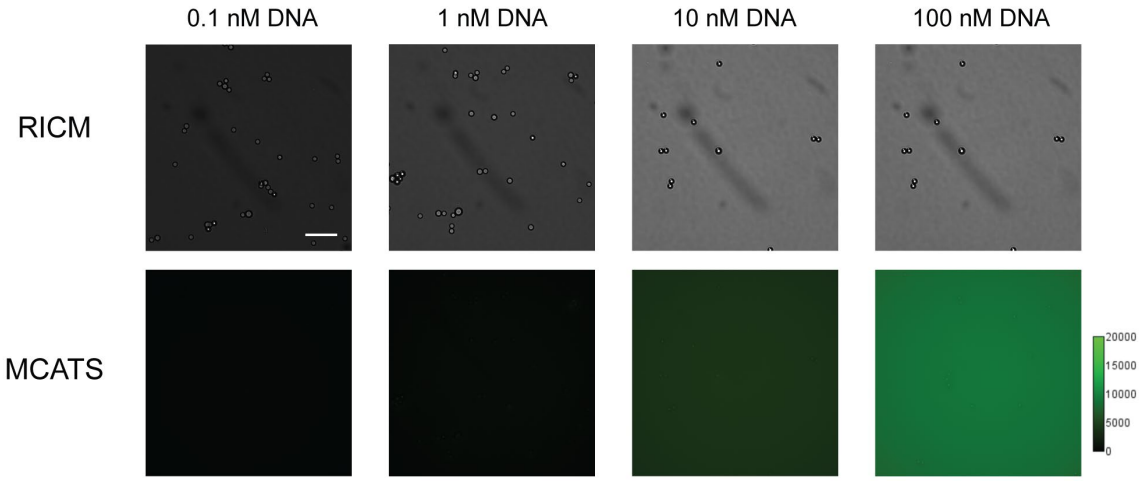

Figure 5.6: Representative images showing flow-induced MCATS with different densities of Dig-DNA on the surface. Representative RICM and fluorescence images showing that a higher density of DNA leads to higher MCATS signal with same number of beads. Scale bar = 10 μm. The intensity bar next to each fluorescence image shows the absolute signal intensity for each image.

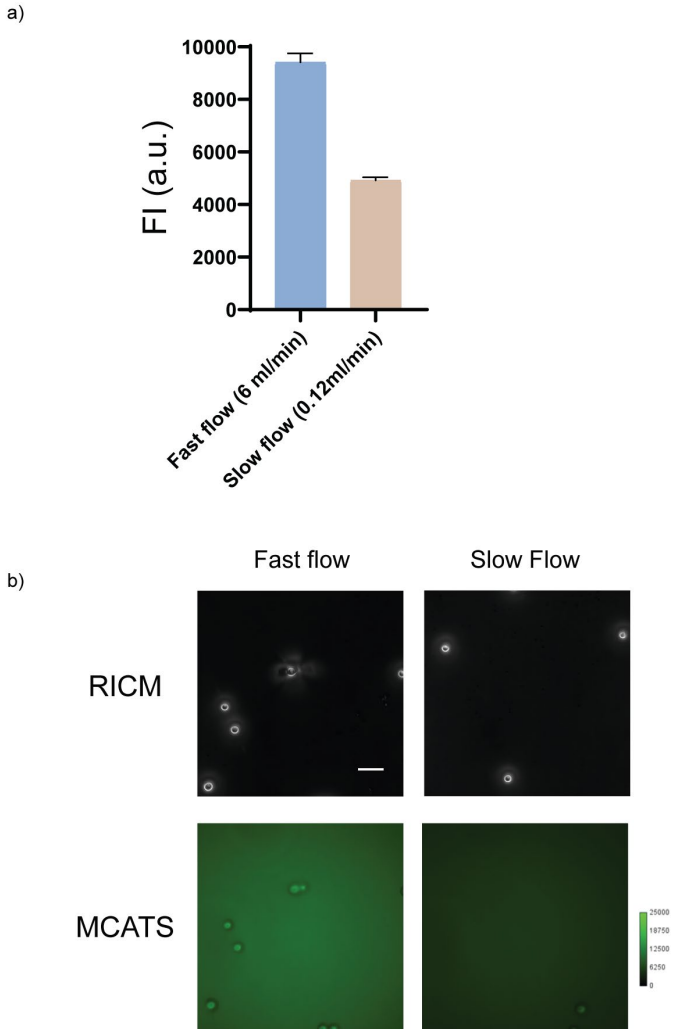

Figure 5.7: Fast and slow flow rates in flow induced MCATS. a) Graph showing the plate reader readout of MCATS signal for channels that run with fast flow rates (6ml/min ~ 150pN drag forces) or slow flow rates (0.12ml/min, ~3pN drag forces). Error bar represents S.E.M. from n=3 independent experiments. b) Representative RICM and fluorescence images showing that fast flow leads to higher tension signal. Scale bar = 10 μm.

Movie 5.1: Flow induced shearing of anti-dig beads with dig DNA strands. Raw timelapse of the RICM channels showing the beads are sheared at 5s.

5.2.2.3 Other applications

As a platform technology, MCATS and mechano-HCR can be used to detect tension of many different cell types and receptors. It has been reported that cardiomyocytes, cancer cells, and reactive astrocytes transmit forces to influence their maturation, migration, and contractility.[27-29] Rapid detection of tension using ultrasensitive tension sensors may provide a good opportunity to understand the biological process in cancer or neuronal healing. In recent years, aptamer-tethered HCR has been proposed for targeted drug delivery.[30] A mechanically triggered drug delivery process based on mechano-HCR may provide a high specificity and high drug payload capacity for targeted drug delivery.

5.3 Other Contributions

As a PhD student co-advised by Dr. Ke and Dr. Salaita, another "hobby" and significant part of my research was designing and developing different DNA origami structures for various applications. Although this work does not fit into the scope of this dissertation, more details of these projects can be found in the following papers.

Duan, Y*; Su, H*; Brockman, J*; Ke Y; Salaita, K. *"Massively Parallelized Molecular Force Manipulation with On-Demand Thermal and Optical Control"* Journal of the American Chemical Society *doi*:10.1021/jacs.1c08796. 2021

Brockman, J; Su, H; Blanchard, A; **Duan, Y**; Yonggang Ke; Salaita, K. *"Live-cell super-resolved PAINT imaging of piconewton cellular traction force"* Nature Methods doi:10.1038/s41592-020-0929-2. 2020

Bazrafshan, A; Meyer, T; Brockman, J; Blanchard, A; Piranej, S; **Duan, Y**; Yonggang Ke; Salaita, K. *"Tunable DNA Origami Motors Translocate Ballistically Over μm Distances at nm/s Speeds"* Angewandte Chemie International Edition doi: 10.1002/anie.20191628. 2020

Hui, L; Lu, Q; Zhou, K; **Duan, Y**; Ke, Y; Wang, R; Liu, H. "Deposition of DNA Nanostructures on Polymer Surfaces", manuscript submitted to Advanced Materials

5.4 Closing Remarks

The growth of modern biochemistry coincided with the advent of two enabling catalytic reactions: PCR and ELISA. These reactions allow one to easily measure the expression of nucleic acids and proteins in living systems. In the past few decades, researchers have found that mechanobiology is relevant to almost every disease and organ system. However, it has not yet been adopted by medical clinics. One reason behind this is that current mechanobiology research is mainly focused on the fundamental biology of cells and proteins and not on tissues and pathology. The other reason is because of a lack of tools that allow any lab or hospital to detect cellular forces easily and cost-effectively. We hope that our ultrasensitive tension sensors developed with catalytic amplification reactions can democratize mechanobiology and open the door for "mechanodiagnostics" and "mechanopharmacology".

5.5 References

1. Brockman, J.M. & Salaita, K. Mechanical Proofreading: A General Mechanism to Enhance the Fidelity of Information Transfer Between Cells. *Front. Phys.* **7** (2019).
2. Bi, S., Chen, M., Jia, X., Dong, Y. & Wang, Z. Hyperbranched Hybridization Chain Reaction for Triggered Signal Amplification and Concatenated Logic Circuits. *Angew. Chem. Int. Ed.* **54**, 8144-8148 (2015).
3. Figg, C.A., Winegar, P.H., Hayes, O.G. & Mirkin, C.A. Controlling the DNA Hybridization Chain Reaction. *J. Am. Chem. Soc.* **142**, 8596-8601 (2020).

4. Pausch, P. et al. CRISPR-CasΦ from huge phages is a hypercompact genome editor. *Science* **369**, 333-337 (2020).

5. Li, S.-Y. et al. CRISPR-Cas12a-assisted nucleic acid detection. *Cell Discov.* **4**, 20 (2018).

6. Wang, Y. et al. Directed evolution: methodologies and applications. *Chem. Rev.* **121**, 12384-12444 (2021).

7. Yang, K.K., Wu, Z. & Arnold, F.H. Machine-learning-guided directed evolution for protein engineering. *Nat. Methods* **16**, 687-694 (2019).

8. Wang, Y., Zhao, Y., Sarkar, A. & Wang, X. Optical sensor revealed abnormal nuclease spatial activity on cancer cell membrane. *J. Biophotonics.* **12**, e201800351 (2019).

9. Bi, S., Zhao, T., Luo, B. & Zhu, J.-J. Hybridization chain reaction-based branched rolling circle amplification for chemiluminescence detection of DNA methylation. *Chem. Commun.* **49**, 6906-6908 (2013).

10. Sun, J., Jiang, W., Zhu, J., Li, W. & Wang, L. Label-free fluorescence dual-amplified detection of adenosine based on exonuclease III-assisted DNA cycling and hybridization chain reaction. *Biosens. Bioelectron.* **70**, 15-20 (2015).

11. Li, X., Wang, Y., Wang, L. & Wei, Q. A surface plasmon resonance assay coupled with a hybridization chain reaction for amplified detection of DNA and small molecules. *Chem. Comm.* **50**, 5049-5052 (2014).

12. Zheng, J. et al. Universal surface-enhanced Raman scattering amplification detector for ultrasensitive detection of multiple target analytes. *Anal. Chem.* **86**, 2205-2212 (2014).

13. Guo, J., Mingoes, C., Qiu, X. & Hildebrandt, N. Simple, Amplified, and Multiplexed Detection of MicroRNAs Using Time-Gated FRET and Hybridization Chain Reaction. *Anal. Chem.* **91**, 3101-3109 (2019).

14. Nurden, A. & Caen, J. An abnormal platelet glycoprotein pattern in three cases of Glanzmann's thrombasthenia. *Br. J. Haematol.* **28**, 253-260 (1974).

15. Zhao, B., Wu, P., Zhang, H. & Cai, C. Designing activatable aptamer probes for simultaneous detection of multiple tumor-related proteins in living cancer cells. *Biosens. Bioelectron.* **68**, 763-770 (2015).

16. Sun, M. et al. Force-Coded Strategy for the Simultaneous Detection of Multiple Tumor-Related Proteins. *Anal. Chem.* **94**, 8992-8998 (2022).

17. Mahmood, T. & Yang, P.-C. Western blot: technique, theory, and trouble shooting. *N. Am. J. Med. Sci.* **4**, 429 (2012).

18. Clark, M.F., Lister, R.M. & Bar-Joseph, M. in Methods in enzymology, Vol. 118 742-766 (Elsevier, 1986).

19. Ghosh, R., Gilda, J.E. & Gomes, A.V. The necessity of and strategies for improving confidence in the accuracy of western blots. *Expert Rev. Proteomics* **11**, 549-560 (2014).

20. Onorato, J.M., Thorpe, S.R. & Baynes, J.W. Immunohistochemical and ELISA Assays for Biomarkers of Oxidative Stress in Aging and Disease a. *Ann. N. Y. Acad. Sci.* **854**, 277-290 (1998).

21. Kou, X., Zhang, X., Shao, X., Jiang, C. & Ning, L. Recent advances in optical aptasensor technology for amplification strategies in cancer diagnostics. *Anal. Bioanal. Chem.* **412**, 6691-6705 (2020).

22. Cheng, A., McDonald, N.A. & Connolly, C.N. Cell surface expression of 5-hydroxytryptamine type 3 receptors is promoted by RIC-3. *J. Biol. Chem.* **280**, 22502-22507 (2005).

23. Forouzanfar, S., Alam, F., Pala, N. & Wang, C. A review of electrochemical aptasensors for label-free cancer diagnosis. *J. Electrochem. Soc.* **167**, 067511 (2020).

24. Zhang, T. et al. Protein–ligand interaction detection with a novel method of transient induced molecular electronic spectroscopy (TIMES): experimental and theoretical studies. *ACS Cent. Sci.* **2**, 834-842 (2016).

25. Salentin, S., Schreiber, S., Haupt, V.J., Adasme, M.F. & Schroeder, M. PLIP: fully automated protein–ligand interaction profiler. *Nucleic Acids Res.* **43**, W443-W447 (2015).

26. Rossi, A.M. & Taylor, C.W. Analysis of protein-ligand interactions by fluorescence polarization. *Nat. Protoc.* **6**, 365-387 (2011).

27. Rashid, S.A. et al. DNA Tension Probes Show that Cardiomyocyte Maturation Is Sensitive to the Piconewton Traction Forces Transmitted by Integrins. *ACS Nano* **16**, 5335-5348 (2022).

28. Jaalouk, D.E. & Lammerding, J. Mechanotransduction gone awry. *Nat. Rev. Mol. Cell Biol.* **10**, 63-73 (2009).

29. Pérez, L.A. et al. An Outside-In Switch in Integrin Signaling Caused by Chemical and Mechanical Signals in Reactive Astrocytes. *Front. Cell Dev. Biol.* **9** (2021).

30. Zhu, G. et al. Self-assembled, aptamer-tethered DNA nanotrains for targeted transport of molecular drugs in cancer theranostics. *Proc. Natl. Acad. Sci. U.S.A.* **110**, 7998-8003 (2013).